Christine Peintner BSc

Investigations on artificial samples with different aggregates regarding rockburst proneness.

MASTER THESIS

for obtaining the academic title

Diplom-Ingenieurin

Mastercourse - Geotechnical and Hydraulic Engineering

submitted at the

Technical University Graz

Supervisors

O. Univ.-Prof. Dipl.-Ing. Dr. mont. Wulf Schubert

Institute for Rock mechanics and Tunneling

Technical University Graz

Dipl.-Ing. Angelika Klammer

Institute for Rock mechanics and Tunneling

Technical University Graz

Ass.Prof. Dipl.-Ing. Dr.techn. Manfred Blümel

Institute for Rock mechanics and Tunneling

Technical University Graz

Graz, May 2017

Eidesstattliche Erklärung

Affidavit

Ich erkläre an Eides statt, dass ich die vorliegende Arbeit selbstständig verfasst, andere als die angegebenen Quellen/Hilfsmittel nicht benutzt, und die den benutzten Quellen wörtlich und inhaltlich entnommenen Stellen als solche kenntlich gemacht habe. Das in TUGRAZonline hochgeladene Textdokument ist mit der vorliegenden Masterarbeit identisch.

I declare that I have authored this thesis independently, that I have not used other than the declared sources/resources, and that I have explicitly marked all material which has been quoted either literally or by content from the used sources. The text document uploaded to TUGRAZonline is identical to the present master‘s thesis.

Datum / Date

Unterschrift / Signature

Danksagung

An dieser Stelle möchte ich mich zuerst bei meiner Familie bedanken. Bei meinen Eltern, die mir dieses Studium überhaupt ermöglicht haben und besonderer Dank gilt auch meiner Schwester und meinen Großeltern, die mich immer moralisch unterstützt haben und für Abwechslung sorgten. Natürlich möchte ich mich auch bei meinen Freunden in Graz bedanken, ohne die die Studienzeit nur halb so lustig gewesen wäre.

Des weiteren bedanke ich mich bei Herrn O. Univ.-Prof. Dipl.-Ing. Dr. mont. Wulf Schubert für die durchgehende Betreuung während der Masterarbeit und meines gesamten Studium

Besonderer Dank gilt natürlich auch Herrn Dipl.-Ing. Manuel Lagger und vor allem Frau Dipl.-Ing. Angelika Klammer für die hervorragende Betreuung und tatkräftige Unterstützung bei der Durchführung der Versuche.

Ebenso bedanke ich mich bei Herrn Ass. Prof. Dipl.-Ing. Dr. techn. Manfred Blümel und Herrn Anton Kaufmann für die Unterstützung bei der Vorbereitung und Durchführung der Versuche. Ebenso möchte ich mich bei Herrn Dipl.-Ing. Michael Huß bedanken für die Hilfe bei der Materialherstellung.

Abstract

Rockburst is a sudden, violent brittle failure mechanism that can cause serious damage to men and equipment.
In this thesis the influence of the heterogenity of rock on the failure mechanism is examined. Therefore, artificial rock samples, made from Ultra high performance concrete, containing different aggregates were produced and tested. The aggregates were picked according to their stiffness. This had to be done twice because of big compacting pores that were unevenly distributed. The results were then compared according to their stress strain curves in regards to brittle behaviour. Parameters evaluating rockburst proneness, developed by various scientists were also used to determine the rockburst proneness of the rocks.

Results show how the heterogeneity of a rock can influence the rockburst proneness.

Kurzfassung

Bergschlag ist ein plötzliches, sprödes Versagen, welches schwere Schäden an Personen und Geräten verursachen kann. In dieser Masterarbeit wird der Einfluss von Heterogenität auf Kornebene auf Bergschlag untersucht. Zu diesem Zweck wurden künstliche Gesteinsproben hergestellt, welche aus hochfestem Beton mit verschiedenen Zuschlägen bestehen. An diesen Proben wurden Druck und Zugversuche durchgeführt. Zusätzlich wurden Akustische Sensoren während der Druckversuche angebracht um eine genaue Rissbildung darstellen zu können. Die Proben mussten ein zweites mal hergestellt werden, da große Verdichtungsporen entstanden waren, die die Ergebnisse beeinflussen würden. Die Ergebnisse wurden ausgewertet und verglichen. Zusätzlich zu den Spannungsdehnungsdiagrammen wurden Parameter welche das Bergschlagverhalten von Gesteinen beschreiben zur Auswertung der Bergschlaggefährdung herangezogen.

Die Ergebnisse zeigen sehr gut wie sich die Heterogenität eines Gesteins auf die Bergschlaggefährdung auswirken kann.

Inhaltsverzeichnis

Abbildungsverzeichnis

Tabellenverzeichnis

Abbreviations

UHPC	.....	Ultra high performance concrete
UCS	.....	Uniaxial compressive strength
E	.....	Young's modulus
E_{dyn}	.....	dynamic Young's modulus
V	.....	Deformation modulus
B	.....	Brittleness Index
BIM	.....	Brittlenessindex Modified
PES	.....	Potential of elastic strain
W_{ET}	.....	equivalent to index F - Energy storage index
H_cr	.....	minimum depth, rockburst can happen
E_s	.....	Unloading tangential modulus
$E_{0.5}$	.....	modulus taken at 50 % of UCS
E_s	.....	Tangential unloading modulus
D_{max}	.....	maximum grain diameter [mm]
D_{min}	.....	minimum grain diameter [mm]
AR	.....	Aspect ratio [-]

Symbols

σ_c	.....	compressive strength [MPa]
σ_t	.....	tensile strength [MPa]
ν	.....	Poisson ratio [-]
γ	.....	specific weight [kN/m^3]
ρ	.....	bulk density [kg/dm^3]

1 Introduction

A major problem in tunneling and mining at the present time is the prediction and prevention of rockburst. Rockburst is a phenomenon which describes a wide range of failures in rock mass, always occurring spontaneously and violently.

Rockbursts are the result of brittle fracturing of rock. Brittleness describes failure where no significant plastic deformation prior to peak occurs. Because rockburst happens very sudden and violent, it often causes injuries and damages equipment. As tunnels are dug deeper into the ground, rockbursts occur more often.

Rockbursts are often classified in three types (Kaiser, Kaiser)

- strainbursts or self-initiated rockbursts - occur near mine openings and are caused by high stress conditions in brittle rockmass. Strainbursts are also the most common rockbursts.
- pillar bursts - caused by mining operations
- fault-slip bursts - occur due to the existence of structural features

In this master thesis the main focus lies on strainbursts. This means a sudden, energy rich failure occurs, caused by highly stressed rock and the sudden release of stored strain energy.

1.1 Qbjective

This master thesis is part of a research project investigating rockburst proneness and the influence rock heterogenity at grain-scale has on this failure process. In this first part of the project artificial rock samples are produced to show various characteristics due to different aggregates.

For the failure process and the effect of rock heterogenity at grain-scale, various laboratory tests are performed on artificially produced rock samples, consisting of UHPC and coarse

rock grains. Those rock grains i.e. aggregates are added as a constant volumetric fraction and with a constant grain size. In addition, one sample set of pure UHPC is produced for comparison.

After suitable aggregates with different characteristics in stiffness and strength are found and artificial samples are produced, the samples are tested in the laboratory for various properties. In addition, parameters developed for predicting rockburst are examined and later used for a comparison between the different artificial samples regarding rockburst proneness.

In addition the samples are tested with acoustic emission sensors, but due to the time-consuming analysis, it is beyond the scope of this master thesis and will be evaluated at a later point of the project.

2 Parameters

Of all rockburst parameters developed and proposed in the last 50 years, five were chosen, which seemed the most reliable and also feasible with the laboratory equipment at hand. In chapter (letztes unten) parameters which depend not only on the rock parameters themselves but on the surrounding rock conditions as well are briefly introduced.

2.1 Laboratory Parameters

(Tang, 2000) proposed a differentiation between Parameters that are calculated from stress parameters, and those deriving also from strain Energy.

2.1.1 Stress Method

2.1.1.1 Brittleness Index (B)

With rockburst being a brittle failure, a brittleness indices are often used to describe rockburst hazard. The brittleness index describes the ratio between the uniaxial compressive strength and the uniaxial tensile strength. There are more ways to calculate Brittleness indices, but there are no comparative values to be found, so it was chosen to only elaborate on the one, most commonly used.(Wang & Park, 2001)

$$B = \frac{\sigma_c}{\sigma_t} \tag{2.1}$$

B ... Brittleness index [-]

σ_c ... uniaxial compressive strength [MPa]

σ_t ... uniaxial tensile strength [MPa]

The uniaxial compressive strength was determined by a uniaxial compression test and the uniaxial tensile strength was indirectly evaluated by a splitting tension test to avoid the time consuming direct uniaxial tensile test. According to (ÖNORM.3124**?**), the splitting tensile strength is recognised as the uniaxial tensile strength.

(Qiao, 2007)((Wang & Park, 2001)) developed a classification, derived from experimental study in a copper mine:

- B $>$ 40 - no rockburst
- 40 $\geq$ B $>$ 26.7 - weak rockburst
- 26.7 $\geq$ B $>$ 14.5 - strong rockburst
- B $\leq$ 14.5 - violent rockburst

The Brittleness index (B) is not to be confused with the ductility index Z, which although calculated the same way, describes brittleness and ductility regarding the detachability of rock. A distinction has to be made, because the brittleness index states, that the higher the tensile strength in relation to the UCS is, the more brittle a rock is. The ductility index, on the other hand, states the exact opposite. The brittleness index, therefore, states that because due to a higher tensile strength more energy can be stored and the higher is the rockburst hazard. The ductility index, on the other hand, argues that the lower the tensile strength is, the easier it is for a cutter to detach rock parts from the face. (Thuro, 1996)

(Masterarbeit Kluckner besagt allerdings dass auch Einfluss auf rockburst hab aber in seiner Quellenangabe nix derartiges gefunden)

2.1.2 Energy Method

2.1.2.1 Energy Storage Index (W$_{ET}$)

It was discussed, that rockburst tendency is based on the ability of rock to store elastic strain energy. This is reduced by the increase of plastic deformation under pressure. This index comes with quite a few different names, but whether it is called Index F (Wang & Park, 2001), Burst Proneness Index or Energy Storage Index W_{ET} (Neyman, 1972), it always comes down to comparing strain energy retained and strain energy dissipated while unloading.

$$\Phi_{st} = \Phi_c - \Phi_{sp} \tag{2.2}$$

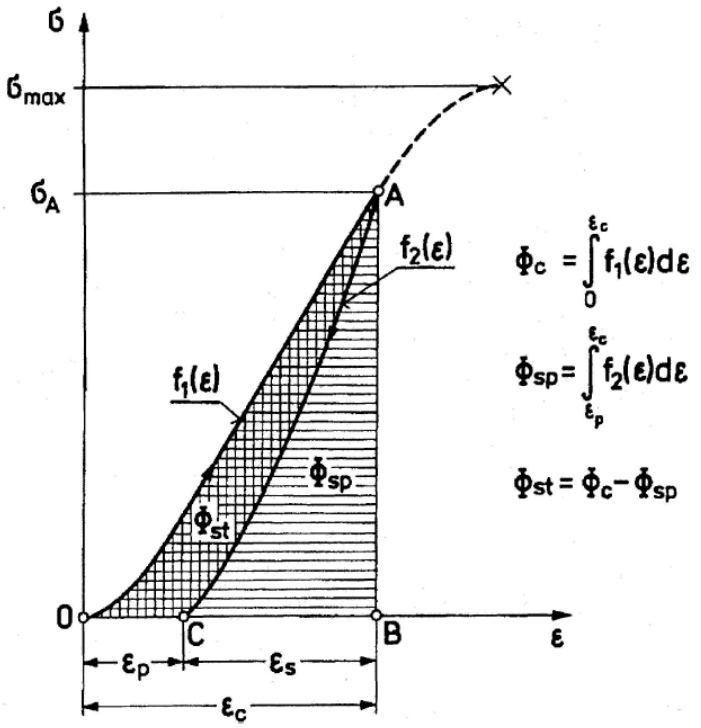

Abbildung 2.1: Schematic of energy calculation for W_{ET} (Wang & Park, 2001).

$$W_{ET} = \frac{\Phi_{sp}}{\Phi_{st}} \tag{2.3}$$

with

W_{ET} ... Energy Storage Index [-]

Φ_c ... total energy obtained while loading, i.e. equals the area under the primary loading curve [MPa]

Φ_{sp} ... elastic strain energy recovered during unloading, i.e. the area under the unloading curve [MPa]

Φ_{st} ... energy lost due to plastic deformation, heat dissipation and (decompaction), i.e. the difference between the primary loading and the unloading curve [MPa]

- $W_{ET} \geq 5.0$ - strong to violent shock
- $2.0 \leq W_{ET} < 5.0$ - medium shock
- $W_{ET} < 2.0$ - no shock

2.1.2.2 Potential Energy of Elastic Strain (PES)

As the W_{ET} index, the PES is based on the ability of rock to store elastic strain energy which influences rockburst behaviour. It was proposed by (Kwa´sniewski, 1994)(see (Wang & Park, 2001)) that the elastic strain energy stored in rock before peak stress is directly related to rockburst.

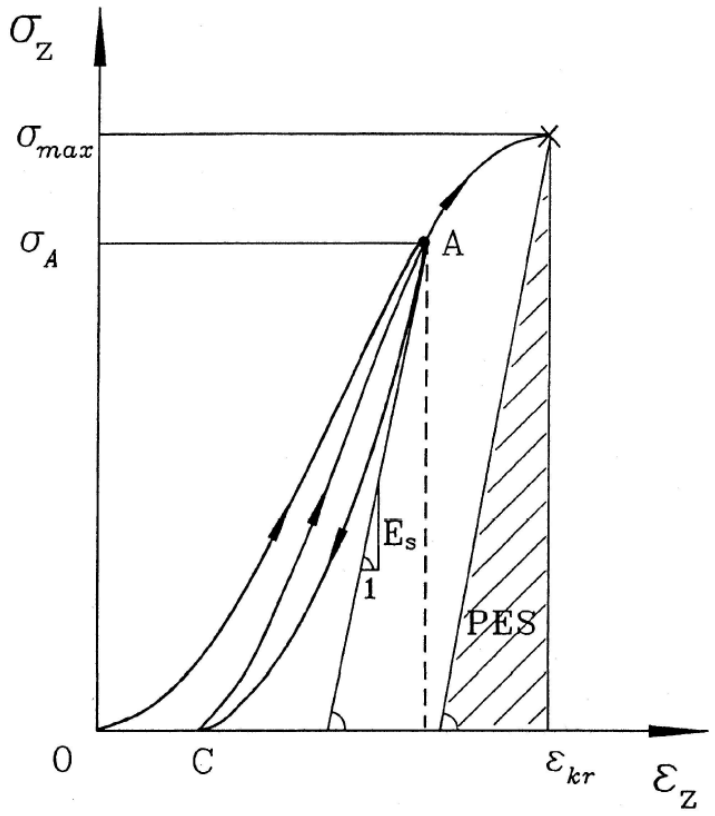

Abbildung 2.2: Schematic of potential energy of elastic strain (PES) (Wang & Park, 2001).

It can be calculated with:

$$PES = \frac{\sigma_c^2}{2 * E_s} \tag{2.4}$$

with

PES ... Potential energy of elastic strain $[kJ/m^3]$

σ_c ... uniaxial compressive strength [MPa]

E_s ... unloading tangential modulus [GPa]

(Wang & Park, 2001) defined the classification with:

- PES $\leq 50\ kJ/m^3$ - the rockburst hazard is very low.
- $50 <$ PES $\leq 100\ kJ/m^3$ - the rockburst hazard is low.
- $100 <$ PES $\leq 150\ kJ/m^3$ - the rockburst hazard is moderate
- $150 <$ PES $\leq 200\ kJ/m^3$ - the rockburst hazard is high
- PES $> 200\ kJ/m^3$ - the rockburst hazard is very high.

2.1.2.3 Brittleness Index Modified (BIM)

The W_{ET} index requires knowing beforehand the approximate uniaxial compressive strength of rock to achieve an unloading curve at about 70 - 90 of the uniaxial compressive strength. So the Brittleness Index Modified was proposed by (Aubertin, 1988)(see (Tang, 2000)).

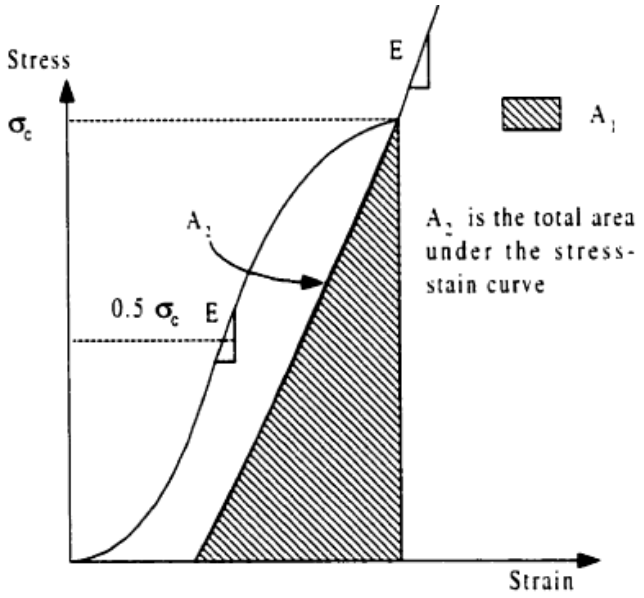

Abbildung 2.3: Schematic of determination of BIM from uniaxial compression test. (Aubertin, 1988)(see (Tang, 2000))

The Index calculated by

$$BIM = \frac{A_2}{A_1} \stackrel{!}{>} 1 \tag{2.5}$$

with

BIM ... Brittleness Index Modified [-]

A_2 ... fracture energy, i.e. the area under the loading curve of a uniaxial compression test up to the point of failure

A_1 ... area under the curve, corresponding to the deformation modulus of the rock at 50% of the uniaxial compressive strength

The categories regarding rockburst proneness were later set by (Aubertin, 1994)(see (Tang, 2000))

- $1.0 < \text{BIM} \leq 1.2$ - rockburst hazard is high
- $1.2 < \text{BIM} \leq 1.5$ - rockburst hazard is moderate
- $\text{BIM} > 1.5$ - rockburst hazard is low

2.1.2.4 critical depth (H_{cr})

The critical depth (H_{cr}) was proposed by (Hou, 1989)(see (Li, 2006)) and describes the minimal depth in which rockburst can occur. As the original paper was written in Chinese only secondary literature is available. Those give no information about the development of this parameter.

$$H_{cr} = \frac{0.318 * \sigma_c * (1 - \nu)}{(3 - 4 * \nu) * \gamma} \tag{2.6}$$

H_{cr} ... minimal depth for rockburst [m]
σ_c ... uniaxial compressive strength [kPa]
ν ... poisson ratio [-]
γ ... specific weight [kN/m^3]

2.1.3 InSitu - Parameters

Insitu Parameters that are commonly used include the Activity index, which describes the Verhältnis of the uniaxial compressive strength to the major principal stress and the stress coefficient, which compares the uniaxial compressive strength to the tangential stress in rock mass.

3 preparation of the samples

3.1 Selection of rocks

The artificial samples consist of a rock matrix and rock aggregates. Ultra-high performance concrete (UHPC) was chosen as the matrix because of a high uniaxial compressive strength and an inclination towards brittle failure. The maximum grain size of the constituents is 0.20 mm. In order to ensure that the rock aggregates are clearly identifiable the grain size was set to 1 - 2 mm diameter. 35 % per volume of aggregates were added.

Suitable rock types to gain distinct results had to be chosen. The Young's modulus was identified as the crucial parameter, for the rock grains would influence mostly the Young's modulus of the UHPC. Therefore, rocks with higher, lower and about the same Young's modulus as the initial UHPC were chosen. The next step was to find rocks with these characteristics which had to be also locally available.
The following rocks were chosen:

- Talc
- Marble
- Limestone
- Quartz

The properties of the chosen rocks are shown in table 3.1. The same limestone and marble have been tested before in the laboratory, so those properties were used and no additional tests performed. For talc, it was not possible to bore and cut a piece big enough to test, and because this is a common problem, no general properties could be obtained. Also for the quartz no specimen could be acquired, which was big enough to perform a uniaxial compression test, so general properties of quartz were chosen.

Tabelle 3.1: Mechanical Properties

		Talc	Limestone	Quartz	Marble
E	[GPa]	˜25	˜40	˜55	˜85
σ_c	[MPa]	not measurable	˜110	˜75	˜90
ν	[-]	not measurable	˜0.25	˜0.13	˜0.21
stiffness ratio		$E_T < E_{UHPC}$	$E_L \approx E_{UHPC}$	$E_Q \approx E_{UHPC}$	$E_M > E_{UHPC}$
ρ	[kg/dm^3]	2.78	2.70	2.80	2.65

Sieving and crushing of the rock aggregates

- Talc

  Talc is one of the softest rock materials and was provided by Imerys Talc in fractions of 0 to 25 mm in diameter. These had to be crushed to the desired size. Because talc is very soft, the grains were mainly sieved dry and afterwards washed very carefully by hand over a sieve. Then the grains were put into the oven, which was gradually heated up to 100 °C over the course of a day and then dried for two and a half days at a constant temperature of 100 °C.

Abbildung 3.1: Talc grains

Abbildung 3.2: Used crusher

- Marble

  Marble was picked up at a local masonry and was already crushed into rock fragments of 1 to 2 mm diameter. It was only washed to get rid of additional dust and dried in an oven at 60 °C for four days.

Abbildung 3.3: Marble grains

Abbildung 3.4: Used sieves

- Limestone

  A local mason provided a big block of limestone which was then broken into pieces about the size of a fist and afterwards also crushed into finer grains. At first, when the crushing plant (Brecher) was set quite coarse, small pieces in the desired size of 1 to 2 mm split of and could already be used. Later on it was discovered, that the grain form differed and showed more of an oblong shape with sharp edges, whereas the grains produced by finer settings were overall rounder and not unlike marble grains. Then the aggregates were sieved with water, and later on gradually heated up to 100 °C and dried for 2 days at a constant temperature of 100 °C.

Abbildung 3.5: Limestone grains

- Quartz

  The concrete department provided two bags of quartz grains, one bag containing grains from 0.6 to 1.2 mm and the other one grains from 1.6 to 2.4 mm. All grains were sieved wet and everything < 1 mm and > 2 mm was eliminated. It is worth mentioning that a lot more grains in the size 1 to 1.2 mm were present than grains in the size 1.6 to 2 mm. The washed and sieved grains were put in an oven by 60 °C for four days.

Abbildung 3.6: Quartz grains

The grain shape of the aggregates was determined by the aspect ratio (AR) and the results are portrayed in table 3.2. For a detailed description see 4.1. Although this shows the ellipticity and describes whether the grains are round or not, it does not describe whether the grains

portray as flat or rather as oblong. Therefore, this is noted separately. Assumable the grain shape of the aggregates also influences the results of the laboratory tests. The minimal and maximal diameter, especially from the quartz grains, should not be taken as average sizes because in general bigger grains were chosen for measurement.

Tabelle 3.2: Grain shape

		Talc	Marble	Limestone	Quartz
grain shape	[-]	flakey	$\overset{shape}{round}/\overset{edged}{elongated}$	round	round
D_{max} (mean|std)	[mm]	3.14|0.84	3.07|1.41	2.51|0.34	2.70|0.37
D_{min} (mean|std)	[mm]	0.75|0.38	1.21|0.23	1.55|0.20	1.37|0.15
AR	[-]	4.19	2.54	1.61	1.97

3.2 Sample preparation

The concrete recipe was developed by the concrete laboratory and the concrete was produced with their help. The mixer held 7 l, which was too little for the required size of the formwork, so for every formwork two batches were mixed. When the first batch was finished, it was stored in a plastic bucket and covered with a plastic sheet. The next batch took about 15 minutes to mix. After the second batch was finished both were put into the bucket and afterwards stirred until both batches were joined together. Then the concrete was poured into the formwork and compacted by vibration. After 2 days the formwork was removed, the concrete put in water and the samples including the water were put in an oven. The oven was slowly heated to 80 °C over the course of a day and then the temperature stayed consistent at 80 °C for another 4 days.

Abbildung 3.7: Concrete mixer

Concreting and required deviations of the rock matrix

- UHPC with Talc aggregates

  The first batch was by far to dry. All in all, 390 g of water and 20 g of concrete plasticizer were added and still the concrete was moldable. Because adding water when the mixing was already in progress did not work, the second batch was mixed with a higher water to cement ratio of 0.35 from the beginning, which increased the workability, and the concrete portrayed as very liquid.

Abbildung 3.8: First batch of concrete with talc

- UHPC with Marble aggregates

  The marble batch was produced according to the recipe, but it would have been better for the workability and the volume of pores if additional water would have been added.

- UHPC with Limestone aggregates

  For this batch, additional 50 g of water was necessary to get a better workability, still it was the driest batch. As is evident by the number and size of the pores appearing in the drilled out specimen.

- UHPC with Quartz aggregates

  The quartz was easily workable, everything was done exactly according to the recipe. Assumable it works very well because quartz is a commonly used aggregate for this type of concrete.

- Pure UHPC

  Due to the lack of aggregates, the initial recipe had to be slightly changed, for the matrix alone to be usable. For this quartz sand was used.

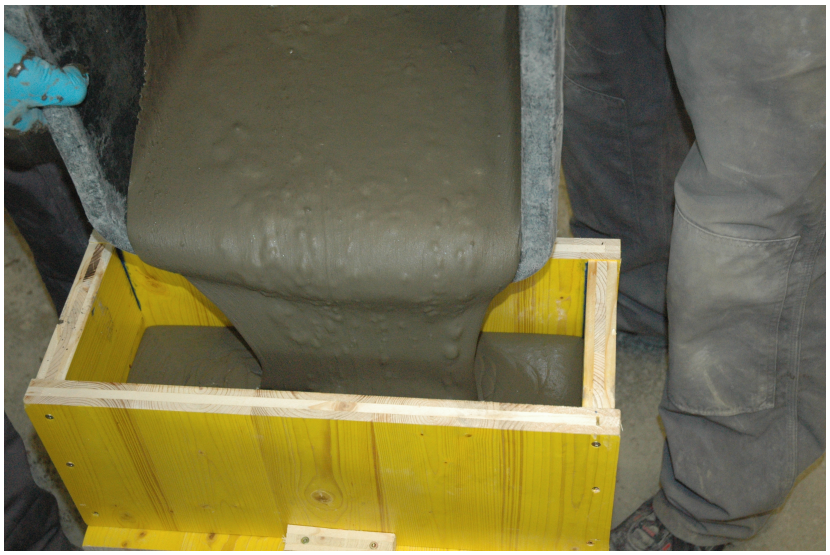

Abbildung 3.9: Desired consistency of mixed concrete

3.2.1 Results

Only after the cores were drilled, pores with up to 1 cm diameter were visible. Especially the limestone portrayed with pores up to 1 cm in diameter. It was theorized that due to the separate mixing of the two batches the first started to dry before any deaerating could take place which made the later vibration not as effective as it should have been. Also due to a fear of segregation (Entmischung) the formwork was kept on the vibrating table only for about 1 minute, which proofed not to be enough. Because of this it was decided to produce the samples again and make changes accordingly.

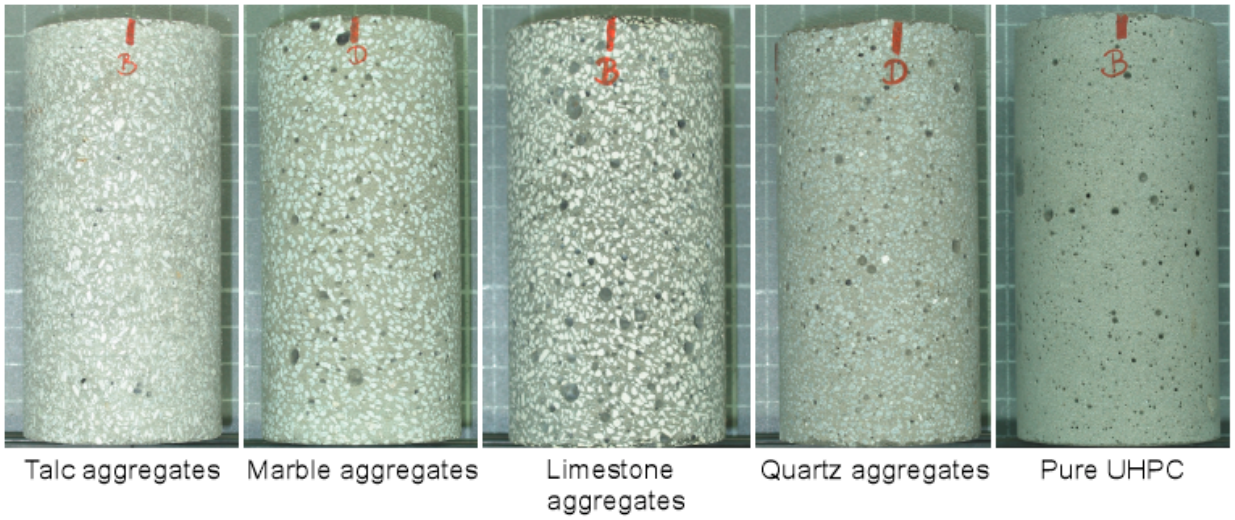

Abbildung 3.10: Drilled cores from the first series with big visible pores up to 1 cm on the artificial limestone sample

3.2.2 Sample preparation with updated recipe

In addition to a switch to a smaller formwork, also the water to cement ratio was increased and the amount of added rock grains was changed to 33 % per volume. In addition, the formwork was put on a vibrating table while pouring in the concrete and afterwards it was deaerated for another 3 - 4 minutes while still under vibration. After the drilling of the cores, compacting pores appeared to be reduced both in size and in quantity.
Only the talc samples showed slight segregation on the top and bottom of the sample. The problem was easily solved by using only the middle part of the specimens.

Concreting and required deviations of the rock matrix for the second series

- UHPC with Marble aggregates

  No changes to the original recipe had to be made. The workability was better than of the first batch, due to more water being added.

- UHPC with Talc aggregates

  Because the first time the WZ ratio was increased to 0.35, this time a WZ ratio of 0.30 was chosen, i.e. the WZ ratio was decreased opposed to the others, which all received an increase in the amount of water added. But to ensure the desired workability 175 ml water had to be added nonetheless.

- UHPC with Limestone aggregates

  Like at the first attempt, the initial mixture was too dry and 70 ml of water had to be added to the mix, still it again was the most malleable one.

- UHPC with Quartz aggregates

  No changes were made to the original recipe.

- Pure UHPC

  Again no changes were made, except the initial difference between this and the other recipes due to the lack of aggregates.

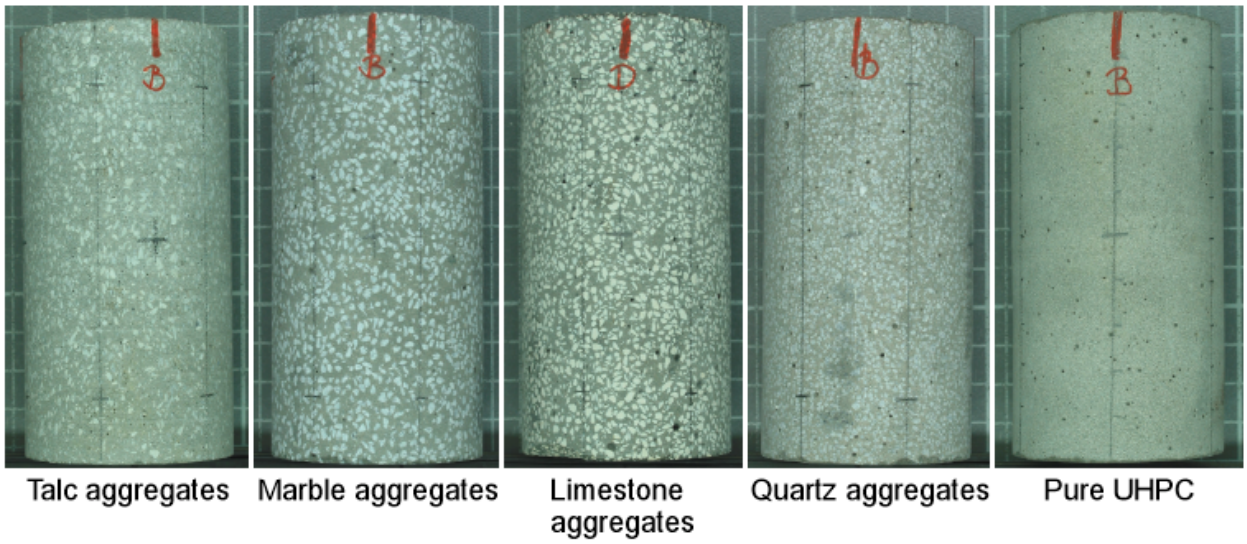

Abbildung 3.11: Drilled cores from the first series with a lot less visible pores

4 Laboratory-Tests

All tests were performed in cooperation with Dipl.-Ing. Angelika Klammer.

4.1 Rebound-test

Originally used in concrete technology, the compressive strength can be calculated from the rebound-value (R). To obtain a reliable mean value the test has to be done several times on one surface. Also, cracks and unsound parts should be avoided because this can lead to falsified results. The device calculates the mean value and the standard deviation. Also, it eliminates outliers. This test is mainly for rough estimates in the field. With the measured rebound-value the compressive strength can be determined by using different diagrams.

4.2 Dynamic Young's Modulus

Measuring with an ultrasonic unit is an easy, fast and non-destructive method to determine the dynamic Young's modulus of rock. It was measured axial and radial with two different attachments, one planar for the axial measurements and the other has a pointed end for the radial measurements.

Under the assumption of a plausible Poisson ratio ν the dynamic Young's modulus E_{dyn} can be calculated directly from the sonic wave velocity v.

After the uniaxial compression test is analysed the dynamic modulus is calculated again with the determined Poisson ratio. The sonic wave velocity is also very useful as a controlling value when using acoustic emission sensors on uniaxial compression tests.

4.3 Splitting Tension Test

Splitting tensile tests on two specimens from the first series and three from the second were conducted, with the specimens having a length of 25 mm and a length to width ratio of 1:2. From the Pressure applied on the specimens, the splitting tensile strength can be calculated. The splitting tensile strength is adopted as the uniaxial tensile strength. (ÖNORM.3124**?**)

4.4 Uniaxial Compression Test

Uniaxial compression tests were performed in a standard servo-hydraulic testing machine. With digital feedback control, the axial load and deformation are monitored.

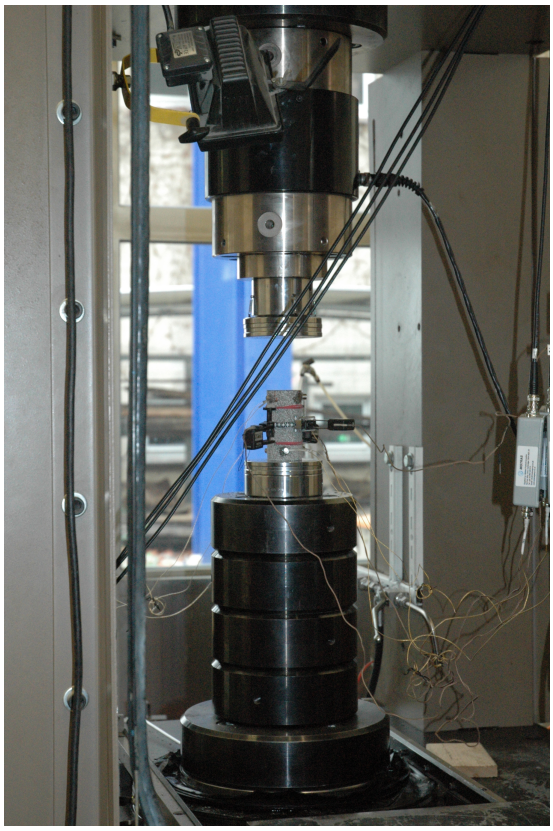

Abbildung 4.1: Testing machine with specimen to be tested

4.4.1 Preparation of the specimen

The cylindrical specimens used were drilled out of the manufactured concrete blocks with a core drilling machine. The specimens were 50 cm in diameter. The diameter to height ratio was 1:2. The end planes are ground to ensure a uniform loading of the specimen. Axial

and circumferential strain gauges were put onto the specimens in the middle, so end effects would not influence the measurements. Two axial gauges were put onto the specimens on opposite sides and unless one would portray incorrect measurements both would be used for the determination of the axial displacements.

4.4.2 Testing

Unloading/reloading loops were performed at first between 25 and 45 % for the determination of the Young's modulus, then at about 70 to 80 %, another loop was performed, which unloads to zero. This second loop was needed for the calculation of various rockburst parameters. During the process of the un- and reloading the load is applied continuously at a constant stress rate of 0.5 MPa/s. After the last loop unloaded to zero, a constant circumferential displacement of 0.05 mm/min was used to control the loading for the ongoing procedure.

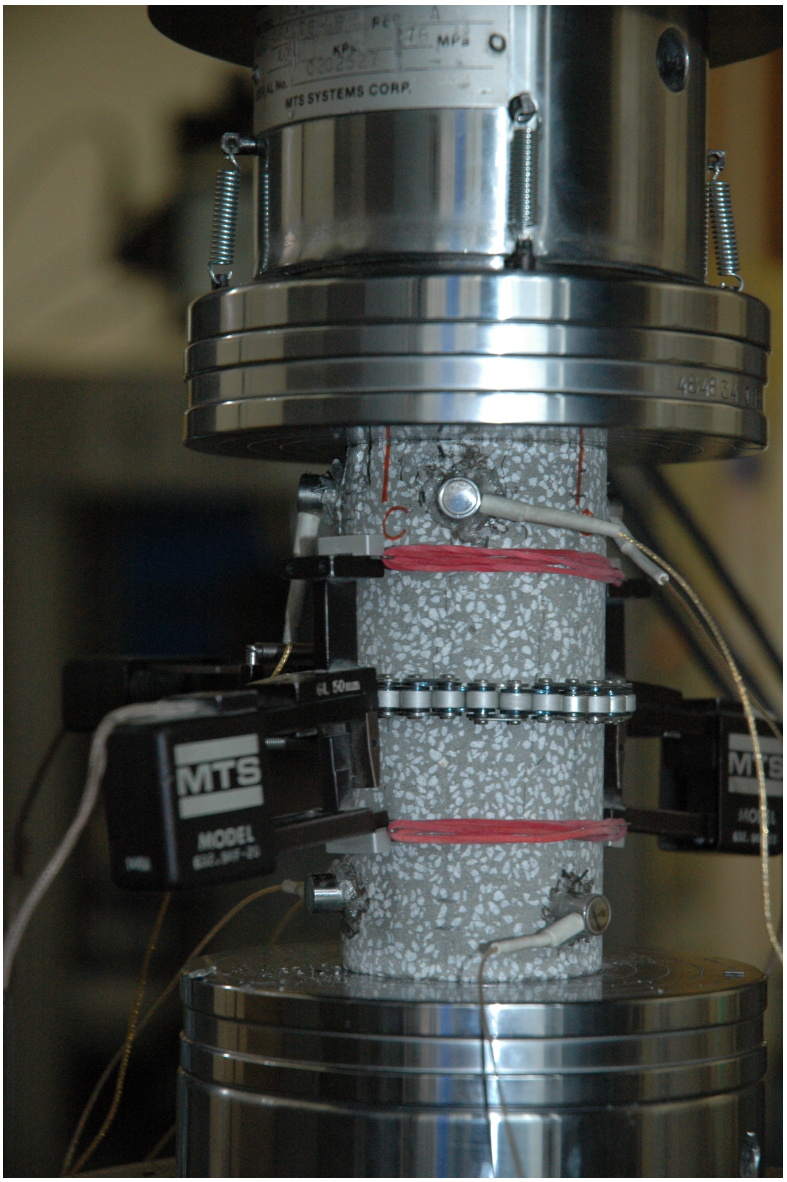

Abbildung 4.2: Specimen during testing

4.4.3 Processing of the Data

The data was evaluated with Mat lab to determine the uniaxial compressive strength (σ_c), the Poisson ratio (ν), the Young's modulus (E) and the deformation modulus (V). In addition, the total energy and the energy at various stages in the Post-Peak area were calculated.

4.4.4 Acoustic Emission Test

Applying acoustic emission sensors to standard laboratory tests allowed for more information to be obtained because the sensors detect microcracks that the strain gauges cannot receive.

4.4.4.1 Preparation of the specimen

The sensors first had to be clean and rubbed with alcohol, and adhesive is put on the specimen optimally in the pattern shown below in figure 4.3

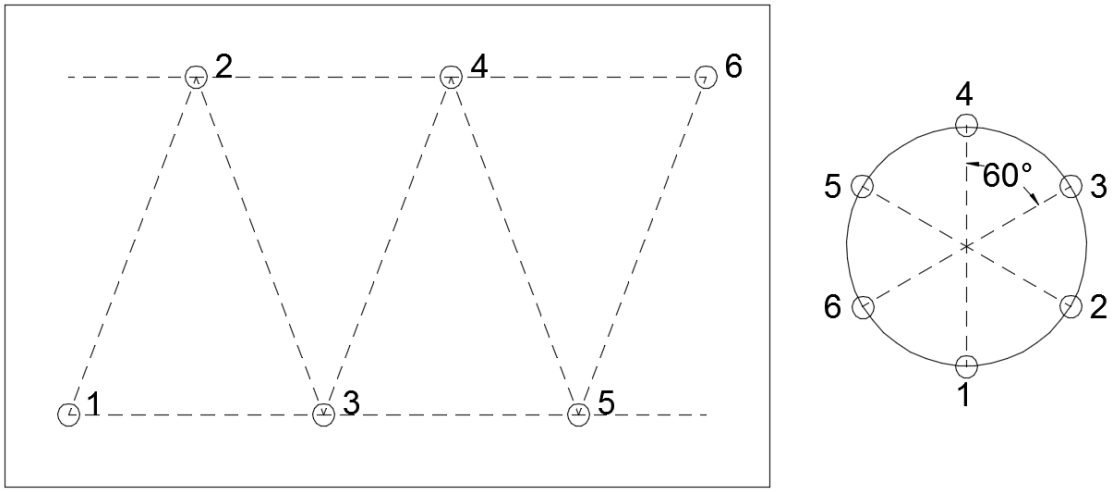

Abbildung 4.3: Schematic of the layout of acoustic emissions sensors

To get the best results the sensors were arranged so that they formed isosceles triangles and were best not too close to the top and bottom because of friction which might influence the data. It was also important to avoid that the sensors and the cables attached to them, to get in contact with the surrounding machinery, for this can also influence the results. The adhesive had to dry for about 10 minutes before the sensors were put onto the sample. When the adhesive had hardened sufficiently, they were tested if the sensors received information and if they were coupled together. Here it was important to make sure that each sensor was coupled consistently on every side. Also, localisation tests had to be done. For localisation of an event in the specimen, at least three sensors are required. Because of bigger cracks that can isolate a sensor from the others, or if the bond between the sensor, the specimen, and the adhesive is insufficient and a sensor cannot receive any more information or falls off completely, it is always preferable to work with more sensors than the minimum amount required.

Abbildung 4.4: a) Sensor not coupled after failure because totally isolated. b) Sensor still weakly coupled because of deep cracks on both sides.

4.4.4.2 Postprocessing

After the test had finished, the sensors had to be again checked if they were still coupled to each other. This was important for the correct analysis of the results. It was also vital to clean the sensors very meticulously because small pieces of dried adhesive can influence the future serviceability of the sensors.

4.5 Pore size and amount

4.5.1 Apparent density determination

The specific weight ρ was determined for all specimens from the uniaxial compressive tests.

4.5.2 Pycnometer Test

The pycnometer tests were done in accordance with (ÖNORM.1936**?**), and for the sample size in general between 19 and 20 g were taken. And exception had to be made for the UHPC

with marble aggregates of the first series, where the sample size was reduced to 10 g because it was not possible to finish a test without losing material during the vacuuming process. To determine the true density the rock pieces had to be dried in an oven at 105 °C. Then they had to be crushed and finely ground with mortar and pestle and in part with a pebble mill.

Abbildung 4.5: Concrete being ground up finely

Three samples for every rock type were done and the mean value was defined as the true density. The samples could only be considered when they differed maximally $\pm 0.005g$.

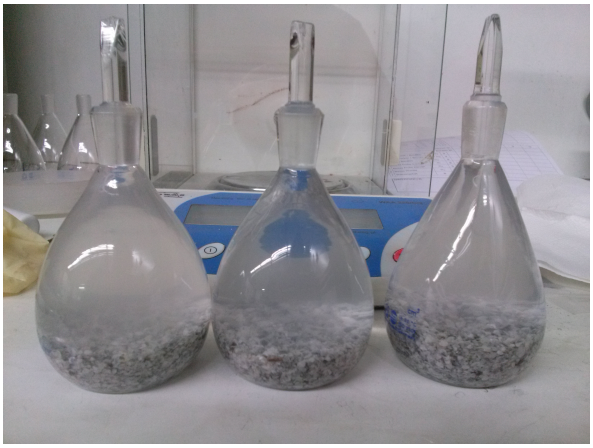

Abbildung 4.6: Pycnometers vacuumed and filled fully

4.5.3 Peintner-Gottsbacher Method (kleiner Scherz am Rande - ich weiss allerdings nicht wie ich des nennen soll)

Because of different reasons, explained previously, the pycnometer tests did not provide satisfying results, so another approach was pursued.

4.5.3.1 First ideas

The first attempt at tracing the pores from a rounded surface onto a piece of paper without distortion was to hatch with a soft pencil over a piece of paper. The problem was, that the pencil had to be pressed firmly onto the paper, which resulted in the rupture of the paper in the pores which defeated the purpose of showing the pores as white spaces left over. Experiments with paint and ink pads also proved ineffective, because the layers could not be applied thin enough for it not to ooze and change the size of the pores considerably and in some cases erasing smaller pores completely.

4.5.3.2 final Approach

After several attempts, the final solution was to draw on the specimen themselves with black/grey chalk (here Cretacolor grey chalk was used). After the excess powder had been dusted off, a strip of tape was put onto the surface. It was important to rub over the tape firmly so it could attach itself to the whole surface and slight irregularities were not traced over as pores in the end. The adhesive tape, considered suitable for this was „Magic Transparent Tape“ from the Scotch brand. A small disadvantage was that it is only available in a width of 19 mm. In order to not only consider a small part of the specimen, it was decided that four strips of tape would be used, spread evenly across the surface (see figure 4.7).

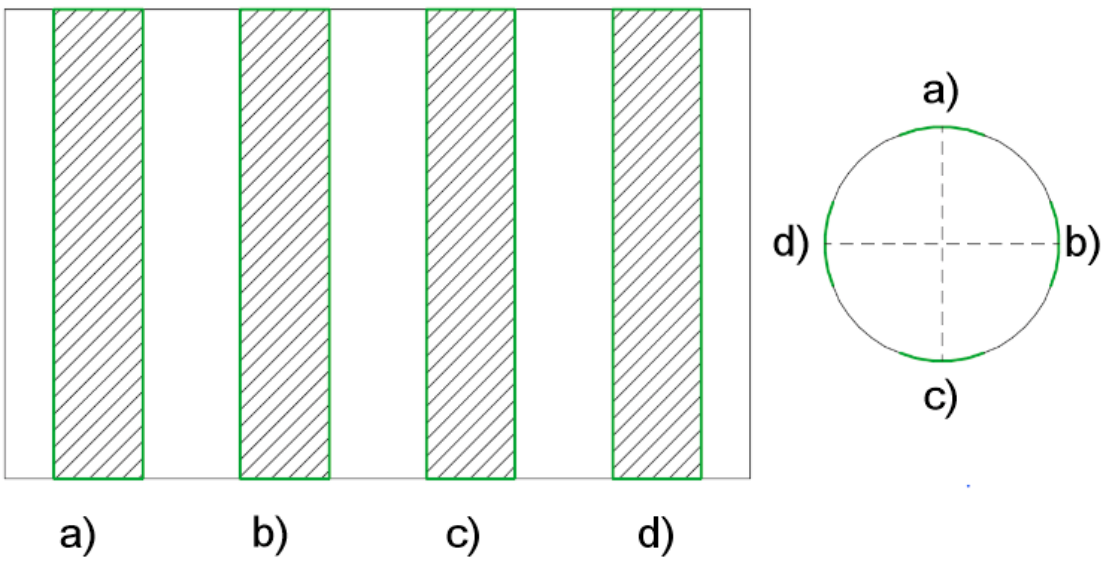

Abbildung 4.7: Schematic of how to place chalk and tape

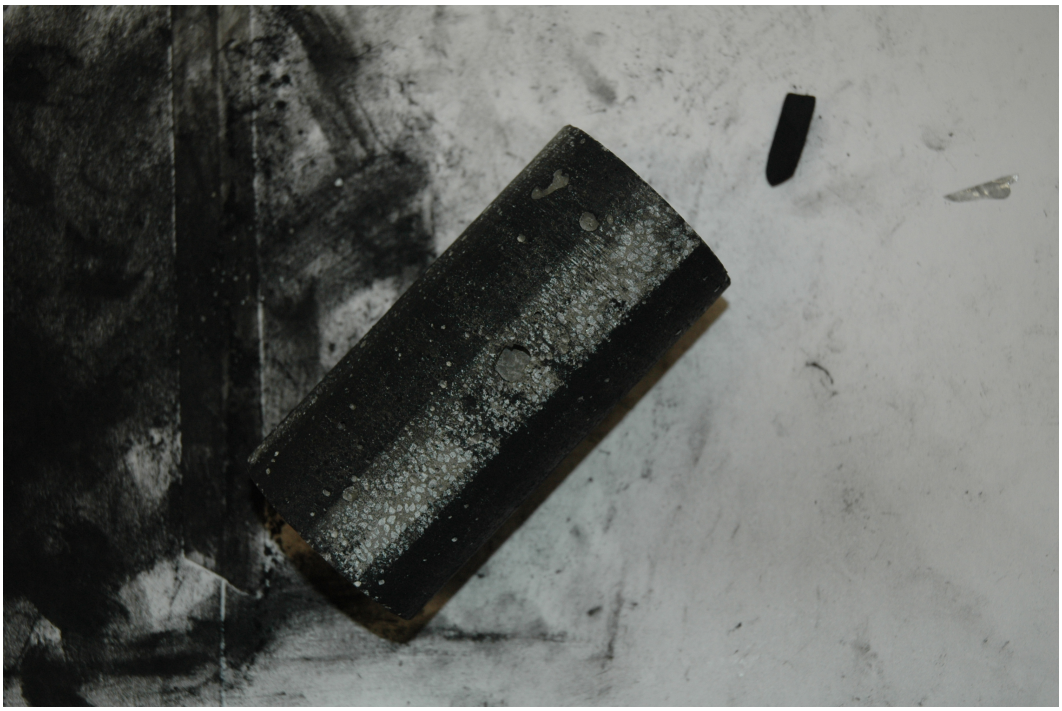

Abbildung 4.8: Work in progress

Then the tapes would be taken off the specimen and put flat on a piece of paper and scanned with a high resolution. The piece of tape with the chalk on it could be taped onto the paper with another strip of tape or weighed down with a book while scanning to flatten it completely and avoid shadows, which could lead to falsifications of the results. Then it was run through a Matlab code.
First, the strips of tape were considered separately and then put together for a mean value. If one is considerably different from the others then it will still be considered because this part of the specimen is as representative as the rest. Especially in the first series this can be observed and only shows how irregular the pores were distributed throughout the samples.

The disadvantages of this method are that only a very small part can be considered as well as it obviously can only be calculated in 2D. A big advantage, of course, is that the determination of the pores was quite simple and the actual task was not very time consuming, once the procedure was figured out and the Matlab code was written.

4.6 Grain shape

For every rock type, single grains were measured with a caliper. The maximal and minimal diameter was then used to calculate the aspect ratio (AR) which describes the ellipticity of the grains.

The aspect ratio was determined by

$$AR = \frac{D_{min}}{D_{max}} \tag{4.1}$$

with

AR ... Aspect ratio [-]
D_{min} ... minimal diameter [mm]
D_{max} ... maximal diameter [mm]

For every rock type, 10 grains were measured and the mean value and the standard deviation were calculated.

5 Results

If not specified in the graphs, the lighter colour in the background portrays the results from the first series, while the more prominent values in the front show the results from the second series.

5.1 Exemplary Solution

A detailed description of the performed calculations is shown in the following sections. As an example, a specimen of the second series with marble aggregates was used.

5.1.1 Mechanical properties of the specimen

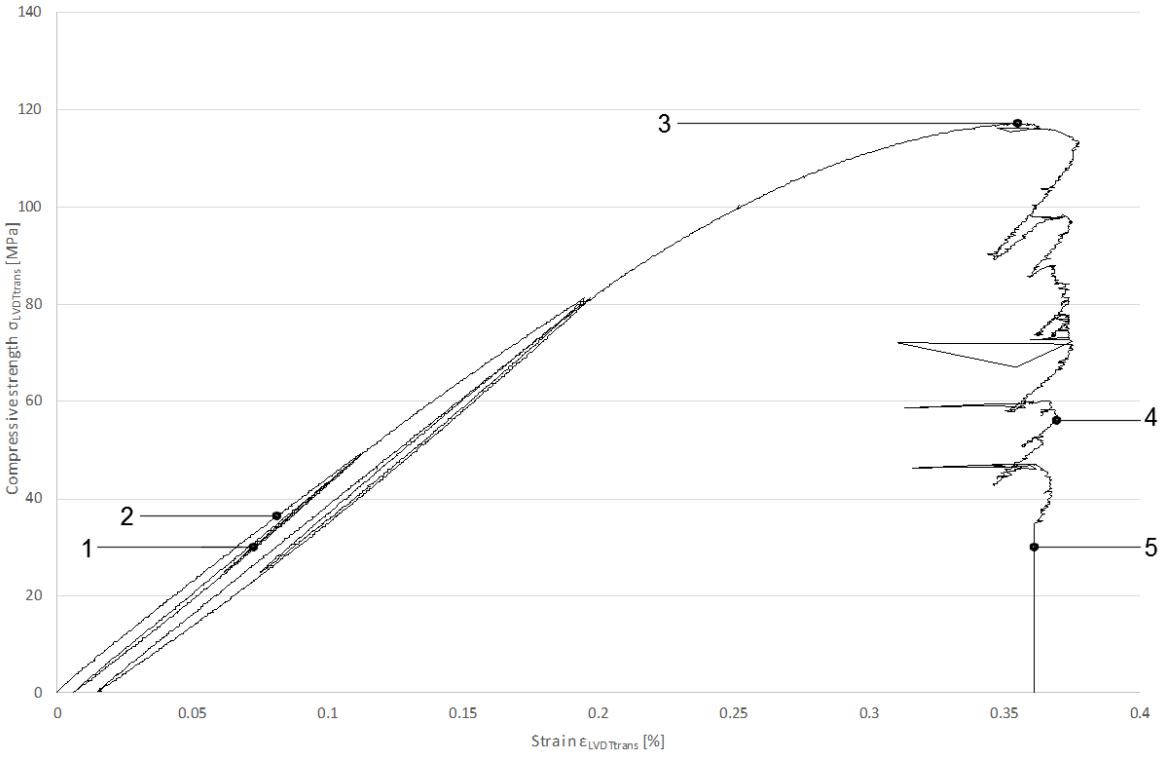

Abbildung 5.1: Schematic of calculation of mechanical properties

1. Young's modulus

   The first unloading loop was used for the determination of the Young's modulus.

2. Deformation modulus

   At the same stress level the Young's modulus was calculated, the deformation modulus was determined on the primary loading curve.

3. UCS and fracture energy

   The uniaxial compressive strength is the maximum stress the specimen could receive. The fracture energy was then calculated as the energy stored at the maximum stress level, meaning the area under the primary loading curve up to the level of uniaxial compressive strength. The specific fracture energy could then be determined by dividing the fracture energy with the UCS and therefore being able to compare stored energies of different rock samples. [Gehring1995]

4. Energy at 50 %

   The energy was again calculated to the point when the stress level reaches 50 % of UCS

again after the peak.

5. Energy at 30 %

   Like in point 4, the energy was calculated at the stress level of 30 % of UCS after the peak. As evident in figure 5.1 the test was sometimes terminated before the limit of 30 % was reached. This had different reasons, for example, some specimens were too brittle so that the instruments could not adjust and the specimen would fail continuously, others stagnated at a stress level and it was not efficient to keep the test going. When this happened, the energy levels may be changed.

6. total Energy

   Calculated energy under the complete stress-strain curve. This is of course always falsified when the test is terminated. This can be seen in the post-failure curves.

5.1.2 Evaluation of rockburst parameters

For the determination of rockburst parameters, another loop had to be executed to obtain the required parameters. This loop, executed at about 70 - 80 % of UCS provided information for W_{ET} and PES. If for whatever reason, the loop could not be executed at the required level, the parameters could still be evaluated, although small errors had to be accepted.

Because the uniaxial compressive strength of all samples from the first series were estimated very conservatively and only one specimen per aggregate was tested, the loops were set significantly lower than required. The parameters could still be evaluated, although small errors had to be accepted.

To check if inflating the curves would render the same results, one specimen of every type in the second series was tested with two loops unloading completely. Unfortunately, the quartz showed unusual behaviour during the first loop which affected the whole stress-strain curve. Therefore, the quartz sample was not taken into account and compared. W_{ET} and PES were calculated twice, using both loops and the results were compared in table 5.1, showing that the differences were insignificant.

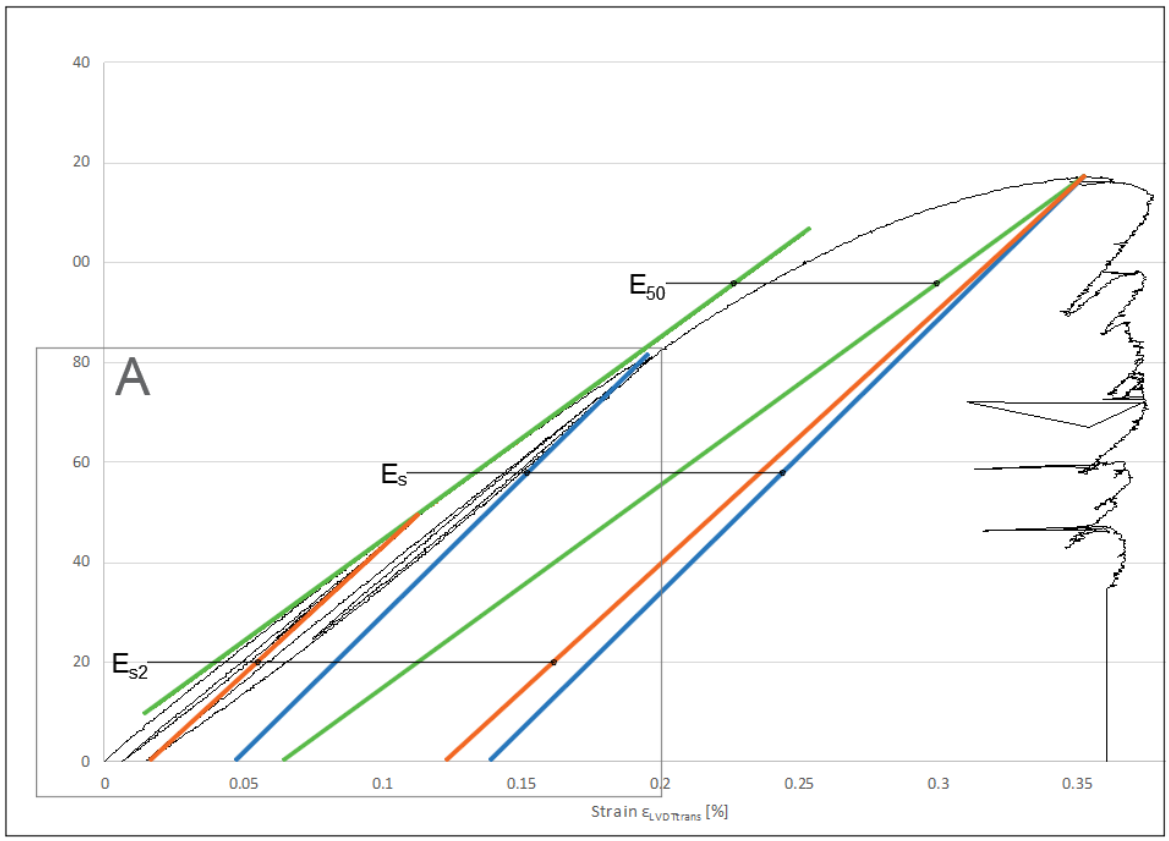

Abbildung 5.2: Schematic of the calculation of moduli required for rockburst parameter

The figure above shows the positioning of the different modules used for the rockburst parameters BIM and PES. The green lines portray the modulus taken at 50 % of the UCS and the horizontal movement of the modulus to the position where the energy/area was calculated at. The same was done with the orange and blue lines, which depict the tangential unloading modules for parameter PES. As can be seen on the shifted lines the E_s (the unloading tangential modulus from the second loop) and the E_{s2} (the control tangential unloading modulus) differ slightly but not so much that it had a big influence on the end results.

Figure 5.3 shows how the area under the smaller curve was inflated to approximate one at 70 %.

Areas not automatically determined by Matlab were calculated with the trapezoid rule, which approximates integration of an area. In the following equations, the single trapezoid areas are defined as A_i.

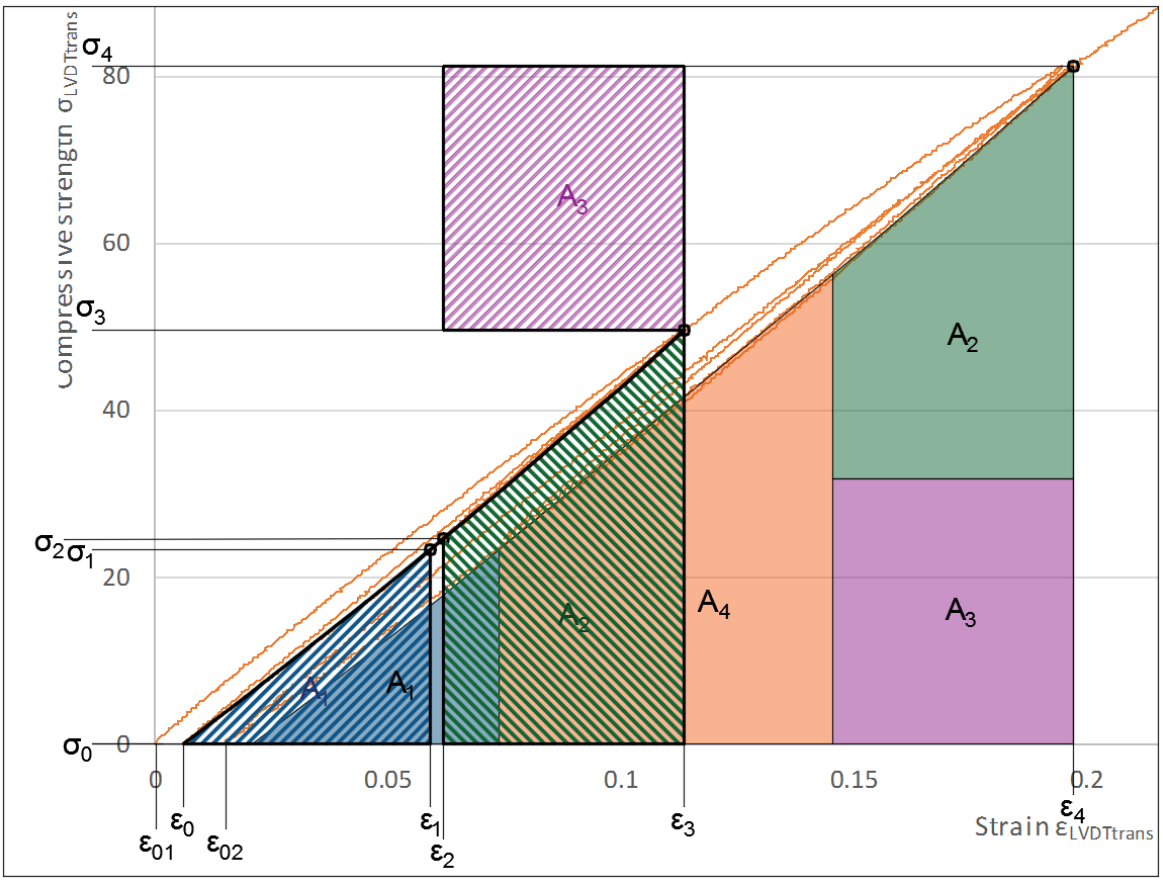

Abbildung 5.3: Schematic of the calculation of W_{ET}

$$\Phi_c = \sum_{i=01}^{4} A_i \tag{5.1}$$

$$\Phi_{sp} = \sum_{i=02}^{4} A_i \tag{5.2}$$

$$\Phi_{st} = \Phi_c - \Phi_{sp} \tag{5.3}$$

Equations 5.1, 5.2 and 5.10 show how the areas for W_{ET} were determined.

$$A_1 = \sum_{i=0}^{1} A_i \tag{5.4}$$

$$A_2 = \sum_{i=2}^{3} A_i \tag{5.5}$$

$$A_3 = (\epsilon_3 - \epsilon 2) * (\sigma 4 - \sigma_3) \tag{5.6}$$

$$m = \frac{\sigma_2 - \sigma_1}{10 * (\epsilon_2 - \epsilon_1)} \tag{5.7}$$

Value m describes the gradient of the centre part of the curve and was used to inflate the area.

$$A_4 = \frac{\sigma_4 - \sigma_3}{m} * \frac{\sigma_1 + \sigma_2 - \sigma_3 + \sigma_4}{2} \tag{5.8}$$

$$\Phi_{sp2} = A_1 + A_2 + A_3 + A_4 \tag{5.9}$$

$$\Phi_{st2} = \Phi_c - \Phi_{sp2} \tag{5.10}$$

Tabelle 5.1

		Talc	Marble	Limestone	UHPC
Φ_c	[MPa]	0.078	0.084	0.237	0.313
Φ_{sp}	[MPa]	0.056	0.070	0.216	0.262
Φ_{st}	[MPa]	0.022	0.014	0.021	0.050
W_{ET}	[-]	2.6	5.1	10.2	5.2
A_1	[MPa]	0.004	0.006	0.016	0.019
A_2	[MPa]	0.010	0.019	0.047	0.055
A_3	[MPa]	0.012	0.017	0.052	0.058
A_4	[MPa]	0.028	0.029	0.102	0.129
Φ_{sp2}	[MPa]	0.043	0.070	0.217	0.261
Φ_{st2}	[MPa]	0.019	0.013	0.020	0.052
W_{ET2}	[-]	2.1	5.2	11.0	5.0
E_s	[GPa]	37.1	56.6	50.0	46.57
PES	[kJ/m^3]	72.2	120.9	391.0	512.0
E_{s2}	[GPa]	34.42	56.2	51.0	45.4
PES_2	[kJ/m^3]	77.8	121.7	383.1	525.4

As can be seen in the table above, index F and index F_2, the index 2 indicating the results derived from the lower loop at about 40 % do not differ a lot and therefore the results derived from the first series were considered applicable for comparison.

5.2 Schmidt-hammer/Rebound-test

First series

Tabelle 5.2: Schmidth-hammer Results

		Talc	Marble	Limestone	Quartz	UHPC
σ_c	[MPa]	55	135	140	190	160
deviation	[MPa]	30	50	60	80	60

Second series

Tabelle 5.3: Schmidth-hammer Results

		Talc	Marble	Limestone	Quartz	UHPC
σ_c	[MPa]	39	105	105	117	110
deviation	[MPa]	30	40	40	50	40

As can be seen in the results the results of the first series matched up quite well with the end results, but because of possible earlier failure, the limits for loops were set very conservatively. The results of the second series generated much lower values, so the actual results of the first series were considered in setting limits.

5.3 Dynamic Young's Modulus

First series

Tabelle 5.4: Dynamic Young's Modulus

		Talc	Marble	Limestone	Quartz	UHPC
Sonic wave velocity q	[m/s]	3576	4730	4800	4776	4556
Edyn radial	[GPa]	25.59	47.13	45.23	48.99	41.18
Sonic wave velocity l	[m/s]	3693	4334	4462	4530	4430
Edyn axial	[GPa]	27.30	39.56	39.09	44.06	43.57

Second series

Tabelle 5.5: Dynamic Young's Modulus

		Talc	Marble	Limestone	Quartz	UHPC
Sonic wave velocity q	[m/s]	3773	4723	4698	4681	4581
Edyn radial	[GPa]	28.18	44.91	45.56	49.25	45.03
Sonic wave velocity l	[m/s]	3935	4489	4489	4547	4396
Edyn axial	[GPa]	30.68	40.60	41.60	46.47	41.48

Both, the radial and axial dynamic Young's modulus were calculated, but in general, the results derived from the axial measurements coincided more with the actual results from

the uniaxial compression tests, deviating about 5 to 10 %, while the ones measured radially deviate up to 17 %.

5.4 Splitting Tension Test

Tabelle 5.6: Splitting Tensile Strength first series

		Talc	Marble	Limestone	Quartz	UHPC
σ_t	[MPa]	5.23	8.43	10.18	11.65	11.76

Tabelle 5.7: Splitting Tensile Strength second series

		Talc	Marble	Limestone	Quartz	UHPC
σ_t	[MPa]	5.35	7.44	5.48	9.44	6.71

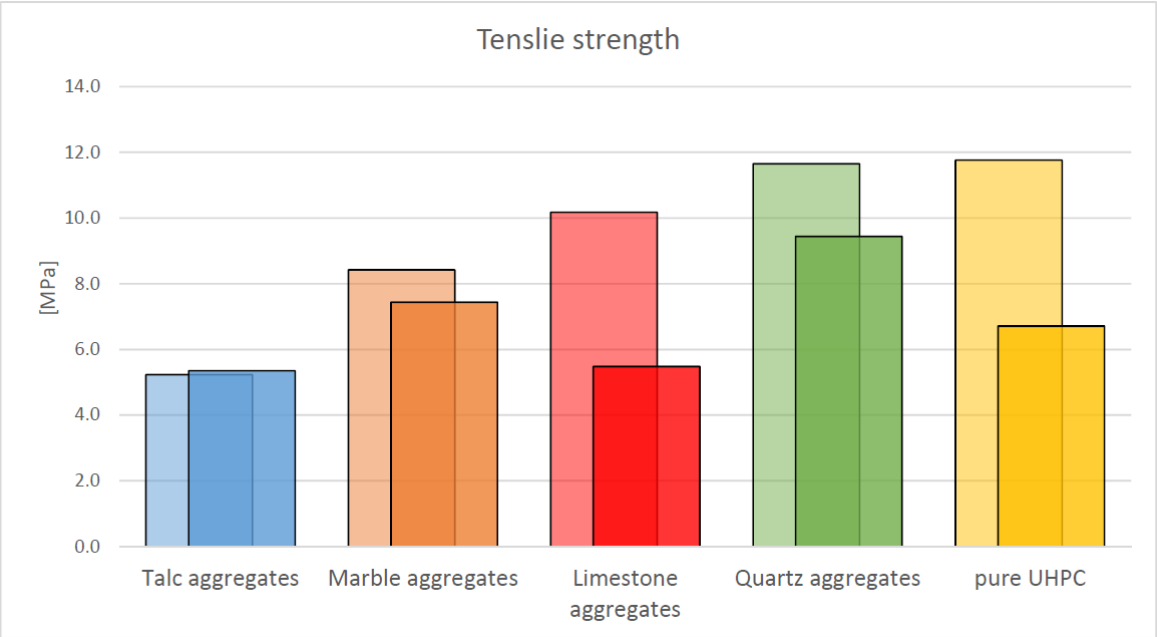

Abbildung 5.4: Comparing tensile strength from the first and second series

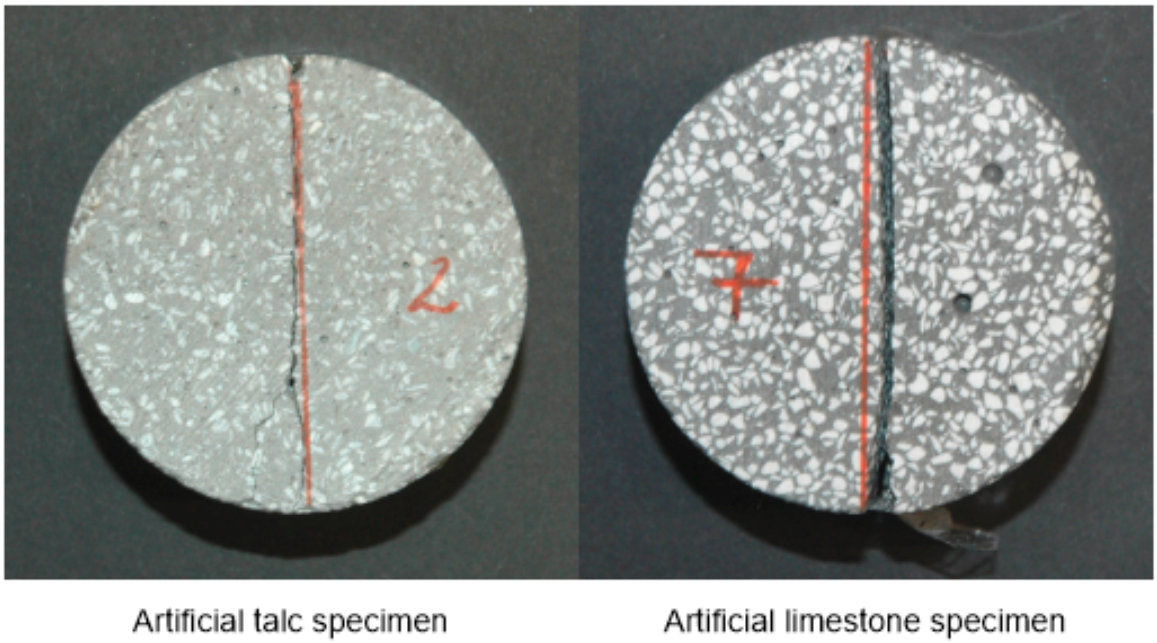

Abbildung 5.5: Fracture behaviour of specimen

Figure 5.4 shows the results from splitting tensile tests from both testing series. Samples with talc aggregates displayed the same tensile strength, despite differences in structure. While the artificial marble samples showed a decrease in tensile strength of about 12 % and quartz samples of 20 %, the tensile strength of the limestone and pure UHPC samples dropped by about 45 %. This was explained by the lower content of microsilica in the matrix. Microsilica is an ultrafine powder with an average paricle diameter of 150 nm. A higher content of microsilica improves the bond between matrix and aggregates, which leads to a higher tensile strength, but increases the viscosity of the concrete. That is why less of it was used in the second series.

5.5 Pore size and amount

Tabelle 5.8: Pores by comparing densities

		Talc	Marble	Limestone	Quartz	UHPC
First series						
bulk density	[kg/dm^3]	2.32	2.41	2.28	2.39	2.33
true density	[kg/dm^3]	2.68	2.57	2.57	2.65	2.67
Pores	[%]	13.4	6.2	11.3	9.8	12.7
Second series						
Bulk density	[kg/dm^3]	2.27	2.44	2.34	2.42	2.37
true density	[kg/dm^3]	2.67	2.67	2.65	2.64	2.68
Pores	[%]	15.0	8.6	11.8	8.5	11.5
Δ Pores	[-]	-1.5	-2.3	-0.5	1.3	1.3

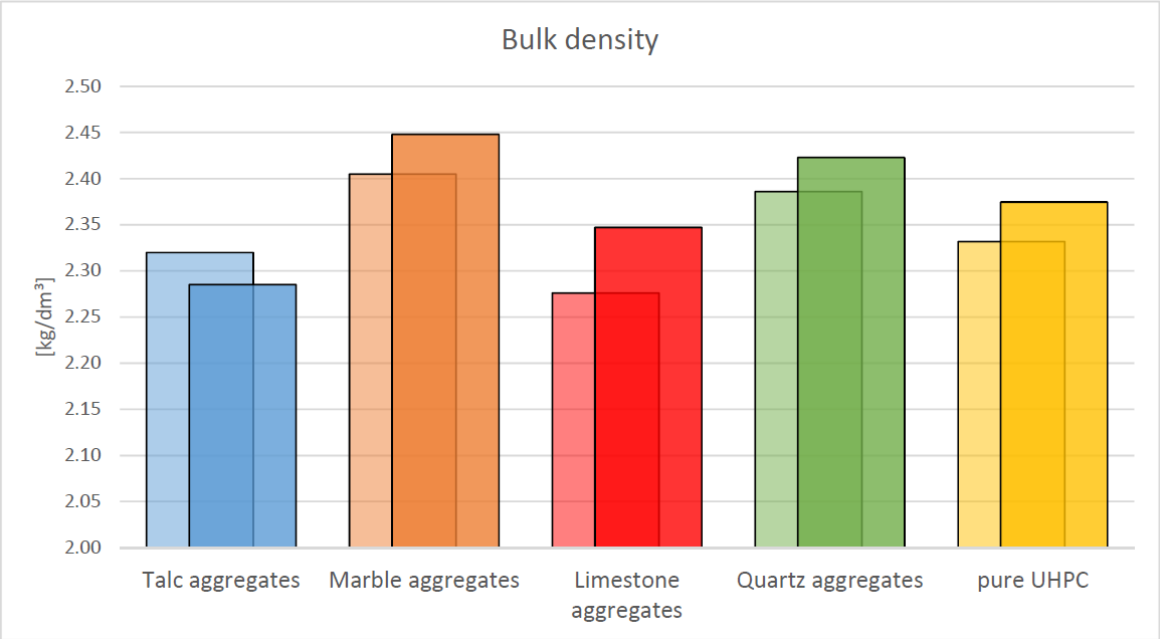

Abbildung 5.6: Comparing bulk density from the first and second series

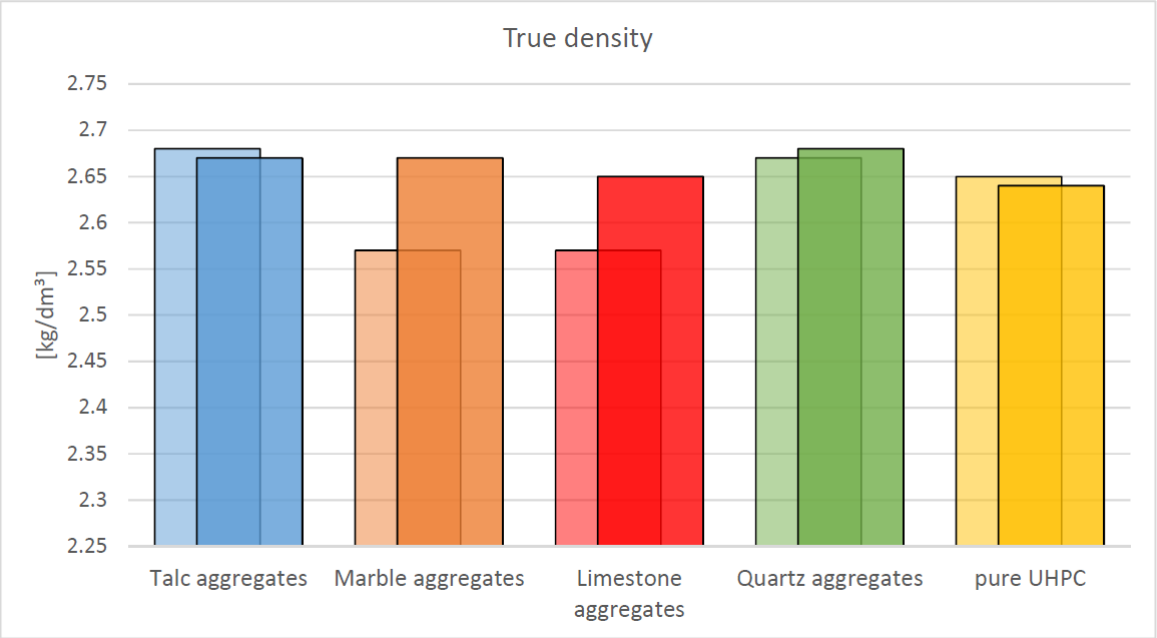

Abbildung 5.7: Comparing young's modulus from the first and second series

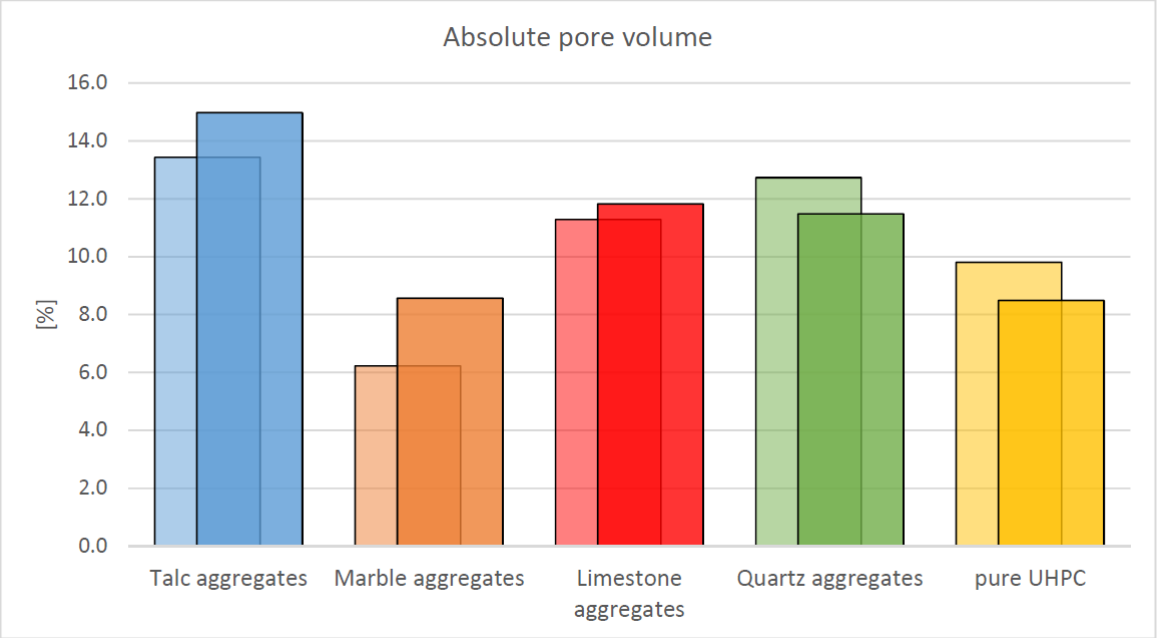

Abbildung 5.8: Comparing absolute pore volume from the first and second series

The initial assumption was, that because the second series was vibrated longer, the pore volume would decrease considerably, especially when the specimens were examined visually. As can be seen in table 5.8 this is not always the case and there is no simple conclusion to be drawn regarding the change in porosity.

- Quartz aggregates and UHPC
  Actually, in this case, the theory panned out except that because of a higher WZ ratio the number of gel pores increased and falsified the results by adding to the pore volume.
- Limestone and Marble aggregates
  The density from the second series is higher than from the first, which concurs with the theory noted above, but the true density of the second series became much smaller than the first one, thus resulting in higher porosity than the first series.
  Because these two aggregates were the only ones used in this project containing calcite, the reason for this anomaly was sought in a chemical reaction taking place during the concreting process. And for why the decrease only happened during the first and not the second series it was theorized that because the second series was mixed with a higher WZ ratio, the calcite could react with the excess water, not used for the hydration process, while in the first series the W/Z ratio was cut to a minimum and almost the whole water was used up for hydration. Therefore, the calcite had to react with other contents of the mixture. An examination could be done about what exactly happened, but this is concrete technology and could have been the topic of another project. (The reason the absolute pore volume has increased might be because of a reduction of plasticiser in the concrete recipe of the second series.) preliminary
- Talc
  (Pore volume of the artificial talc samples increased as well, which, assumably happened because of the decrease of plasitciser as well.) preliminary

5.5.1 Peintner-Gottsbacher Method (kleiner Scherz am Rande - i weiss allerdings nit wie i des nennen soll)

Because the absolute pore volume was not comparable to the compaction pore volume, a different approach was made in defining visible pores starting at about 1 mm.

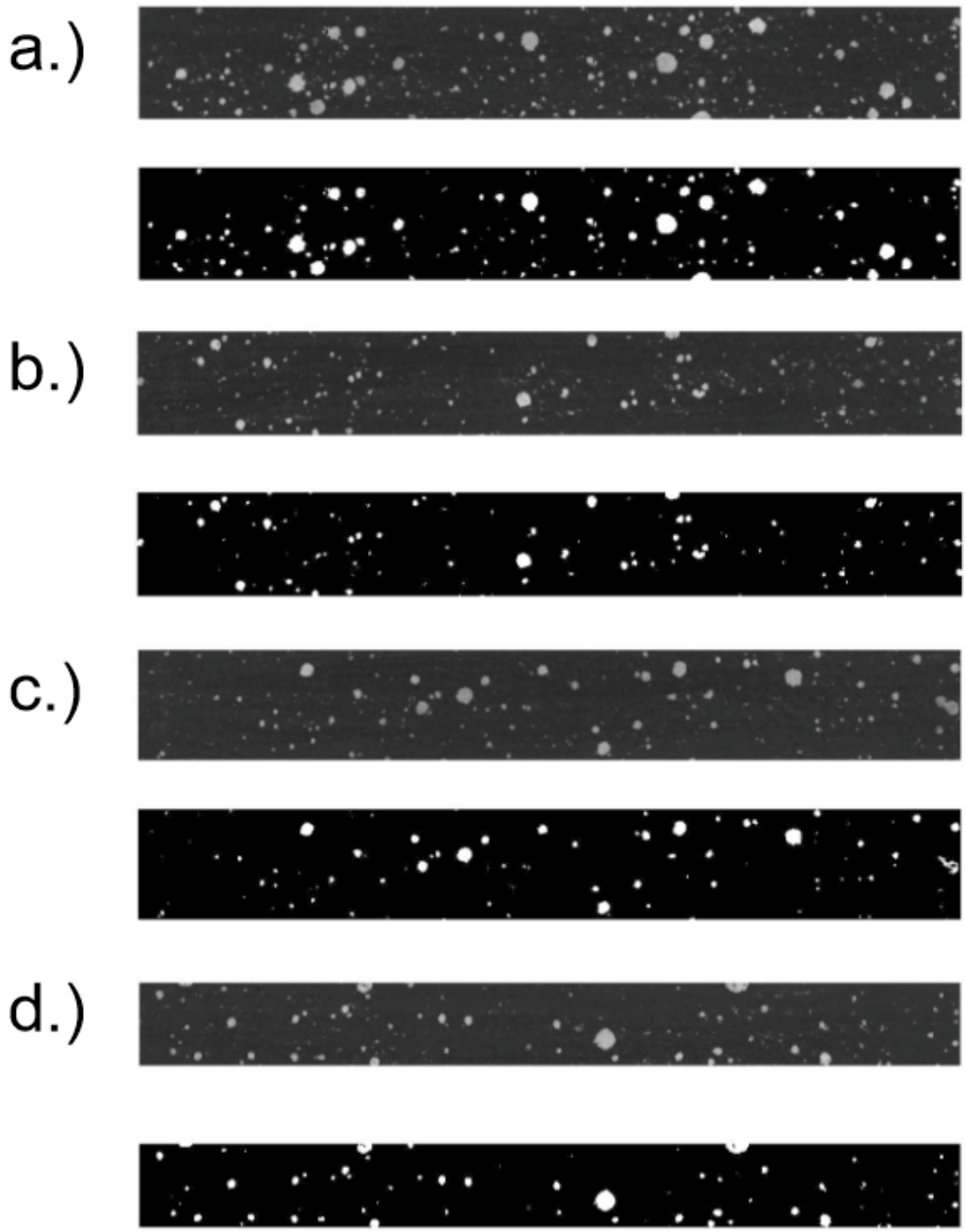

Abbildung 5.9: Comparison of the scanned tapes and the Mat lab figures - artificial quartz sample

Figure 5.9 shows the chalk on adhesive tape scanned in greyscale and the black and white figures analysed by Mat lab. At close view, it can be detected that not all pores from the scan are transferred onto the Mat lab figure. This has to do with the fact that the balance of black and white was not set ideally.

The following tables show the ratio of visible pores from the first and the second series. It shows clearly the difference between first and second series.

Tabelle 5.9: Comparison of pores of artificial quartz samples

	Pores in %	
	First series	Second series
a	4.65	0.16
b	2.29	0.00
c	2.33	0.05
d	2.81	0.19
Average	3.0	0.1

Tabelle 5.10: Comparison of pores of artificial limestone samples

	Pores in %	
	First series	Second series
a	5.13	0.85
b	3.72	0.37
c	6.11	0.24
d	5.12	0.90
Average	5.0	0.6

It was observed that pores with a diameter greater than 1 mm decrease from up to 5 % to well under 0.5 % in volume. In addition it photographs showed, that overall, said pores were more evenly distributed.

5.6 Uniaxial Compression Test

First series

Tabelle 5.11: Uniaxial Compressive Test - Results

		Talc	Marble	Limestone	Quartz	UHPC
σ_c	[MPa]	62.31	110.79	163.23	192.09	199.83
Young's Modulus	[GPa]	27.3	45.91	41.75	52.08	45.04
Deformation Modulus	[GPa]	19.38	39.87	39.17	49.83	42.75
ν	[-]	0.23	0.22	0.23	0.2	0.2
Specific weight	[kN^3]	22.76	23.59	22.33	23.41	22.88
total Energy	[kJ/m^3]	135.73	234.8	282.69	232.59	290.03
Energy 100%	[kJ/m^3]	137.79	233.20	382.10	434.47	594.25
Energy 50%	[kJ/m^3]	142.73	238.76	308.62	317.72	403.62
Energy 30%	[kJ/m^3]	137.20	233.45	281.87	278.61	338.35
w_B	[-]E^{-3}	2.21	2.10	2.34	2.26	2.97

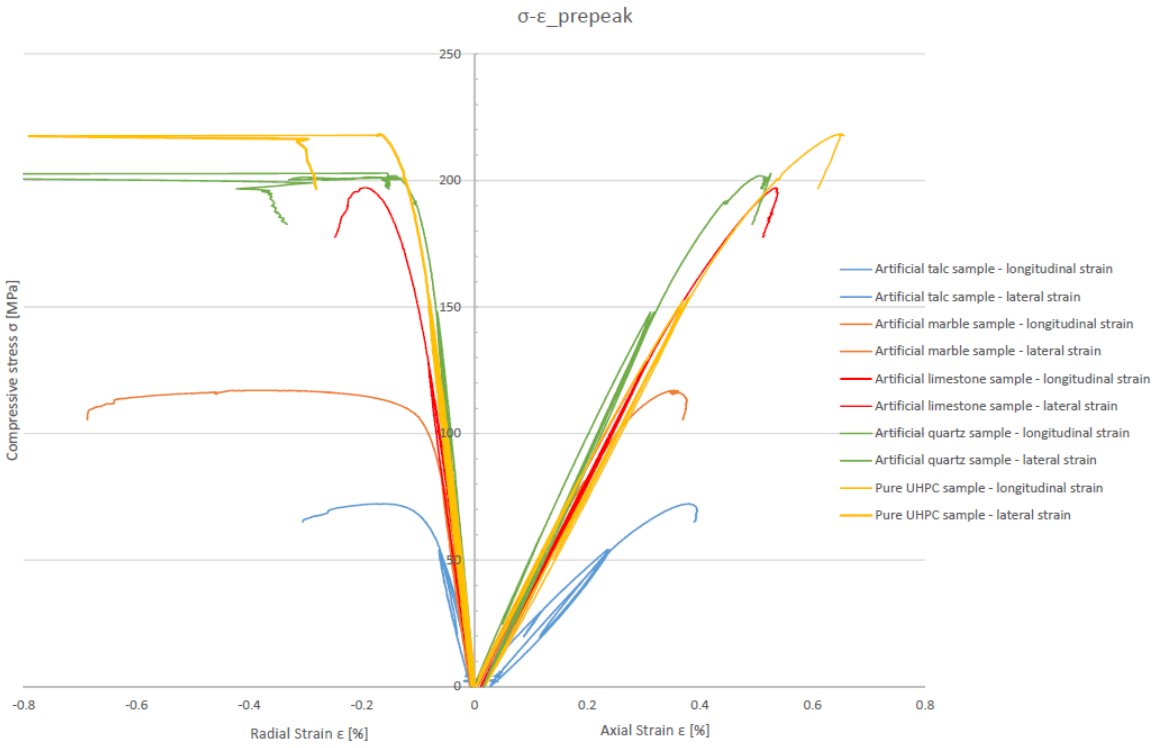

Abbildung 5.10: Results of the Uniaxial compression test of the second series

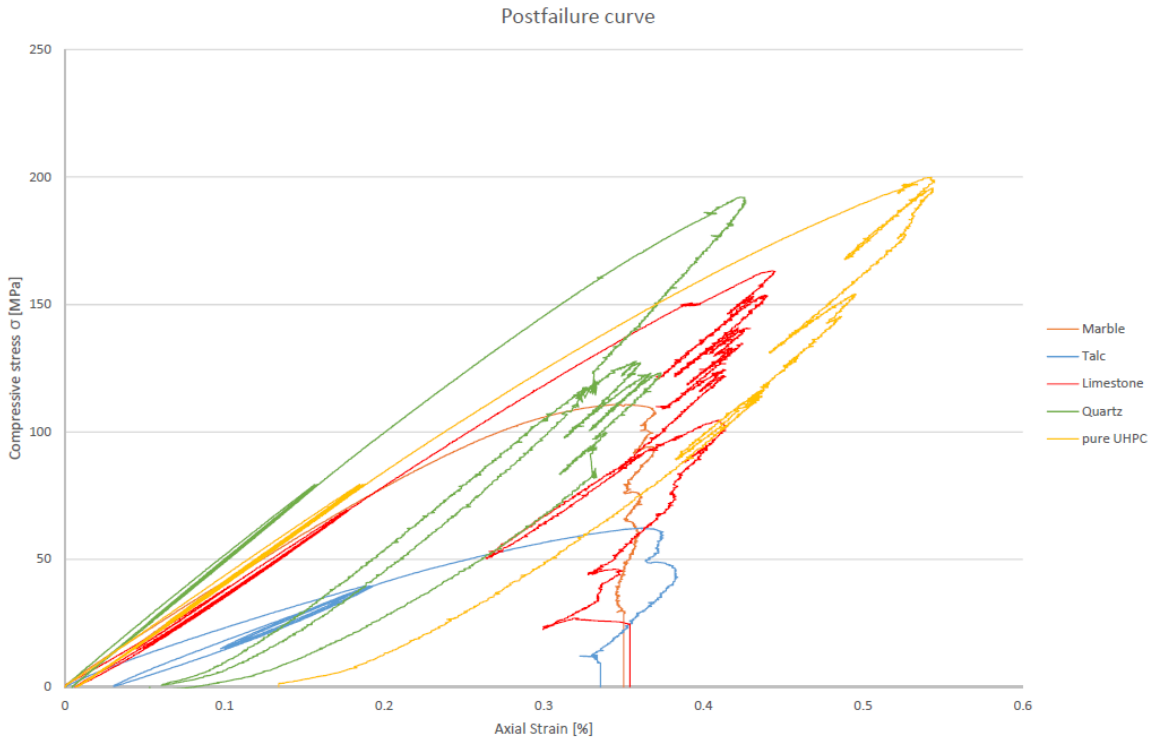

Abbildung 5.11: Results of the Uniaxial compression test with post-failure area of the first series

Second series

Tabelle 5.12: Uniaxial Compressive Test - Results

		Talc	Marble	Limestone	Quartz	UHPC
σ_c	[MPa]	72.02	117.20	195.23	202.30	213.96
Young's Modulus	[GPa]	31.08	48.75	45.96	51.44	45.03
Deformation Modulus	[GPa]	23.09	42.13	42.94	49.38	43.21
ν	[-]	0.23	0.26	0.22	0.17	0.2
Specific weight	[kN^3]	22.42	24.01	23.03	23.77	23.30
total Energy	[kJ/m^3]	162.0	269.2	469.3	494.5	635.4
Energy 100%	[kJ/m^3]	172.5	262.3	594.6	638.1	840.4
Energy 50%	[kJ/m^3]	168.6	271.8	475.7	612.5	662.9
Energy 30%	[kJ/m^3]	170.6	270.4	469.3	561.4	652.7
w_B	[-]E^{-3}	2.40	2.24	3.05	3.15	3.93

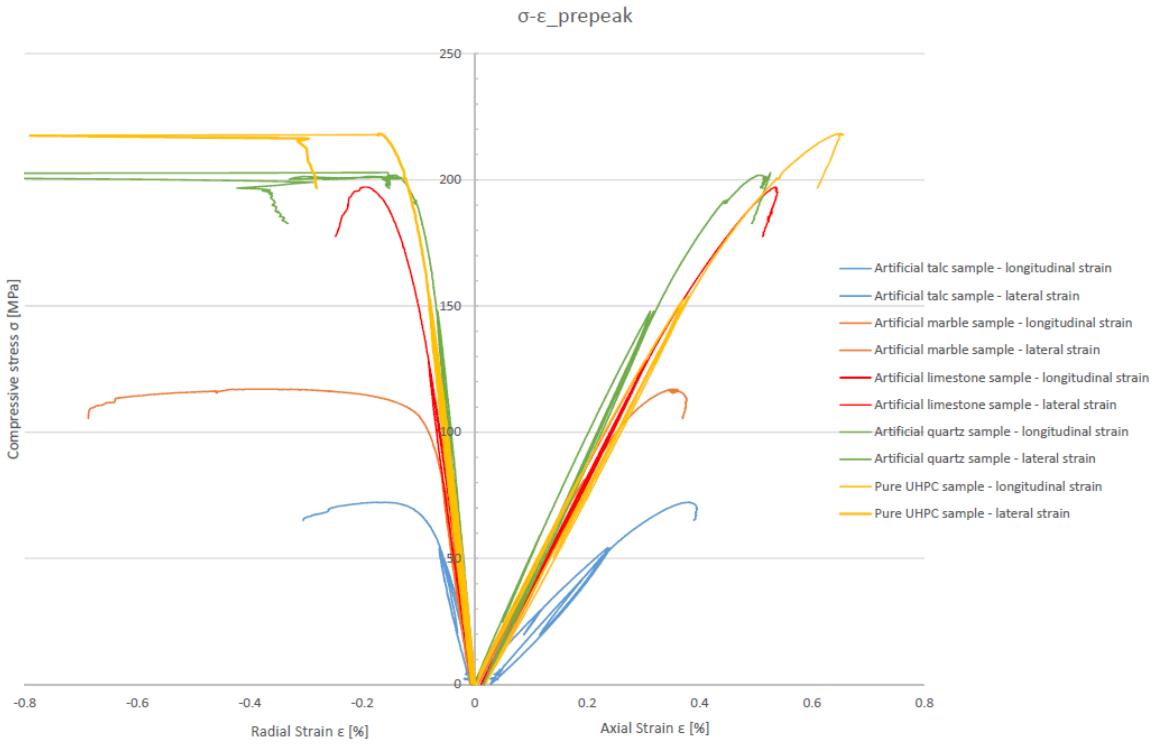

Abbildung 5.12: Results of the Uniaxial compression test of the second series

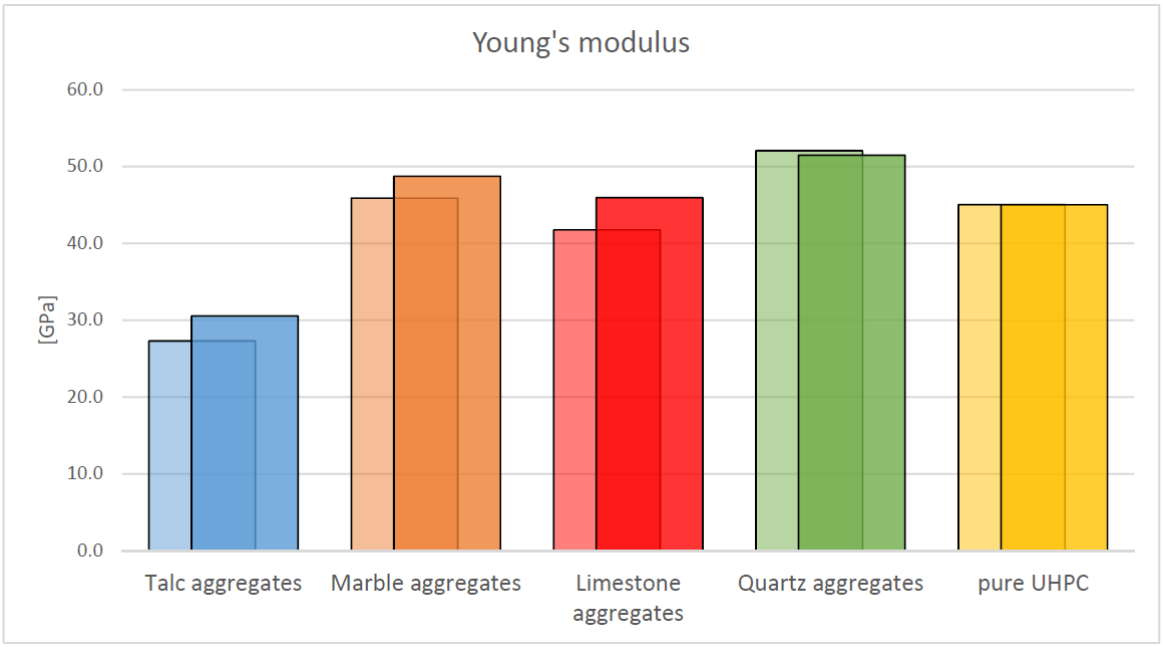

Abbildung 5.13: Comparing young's modulus from the first and second series

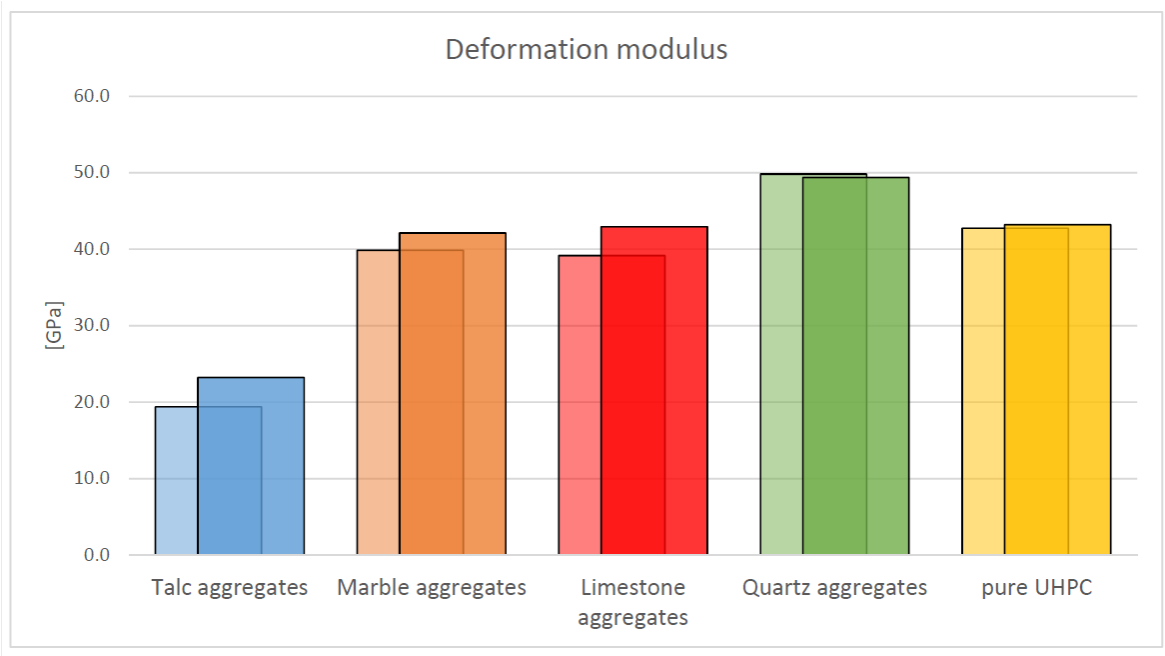

Abbildung 5.14: Comparing deformation modulus from the first and second series

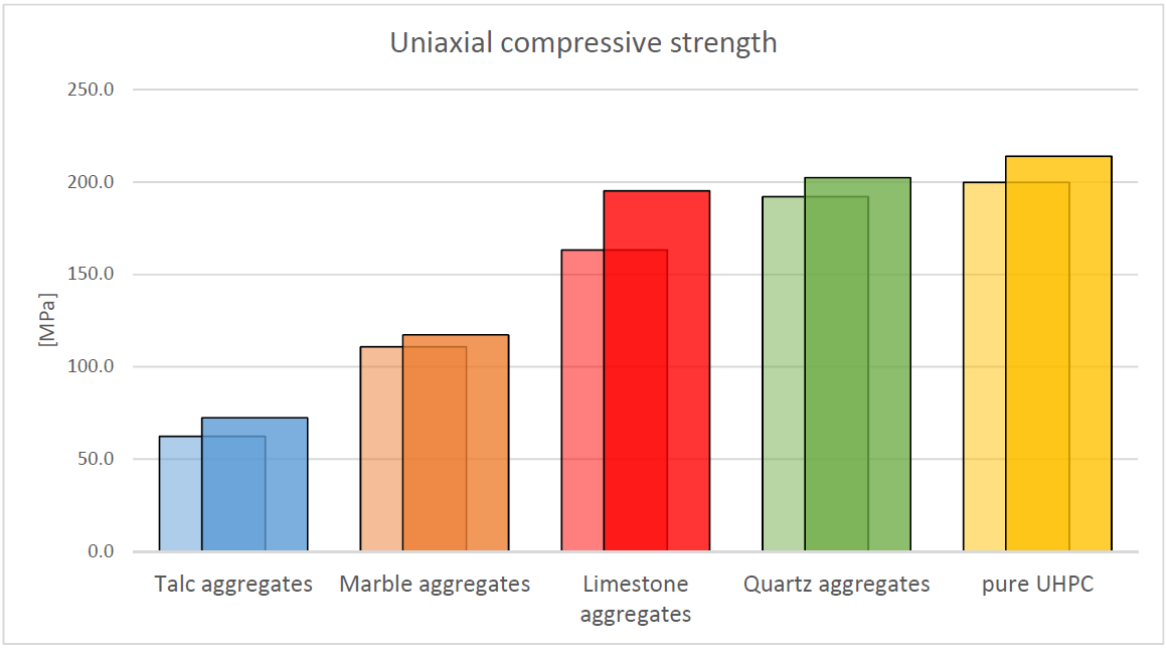

Abbildung 5.15: Comparing young's modulus from the first and second series

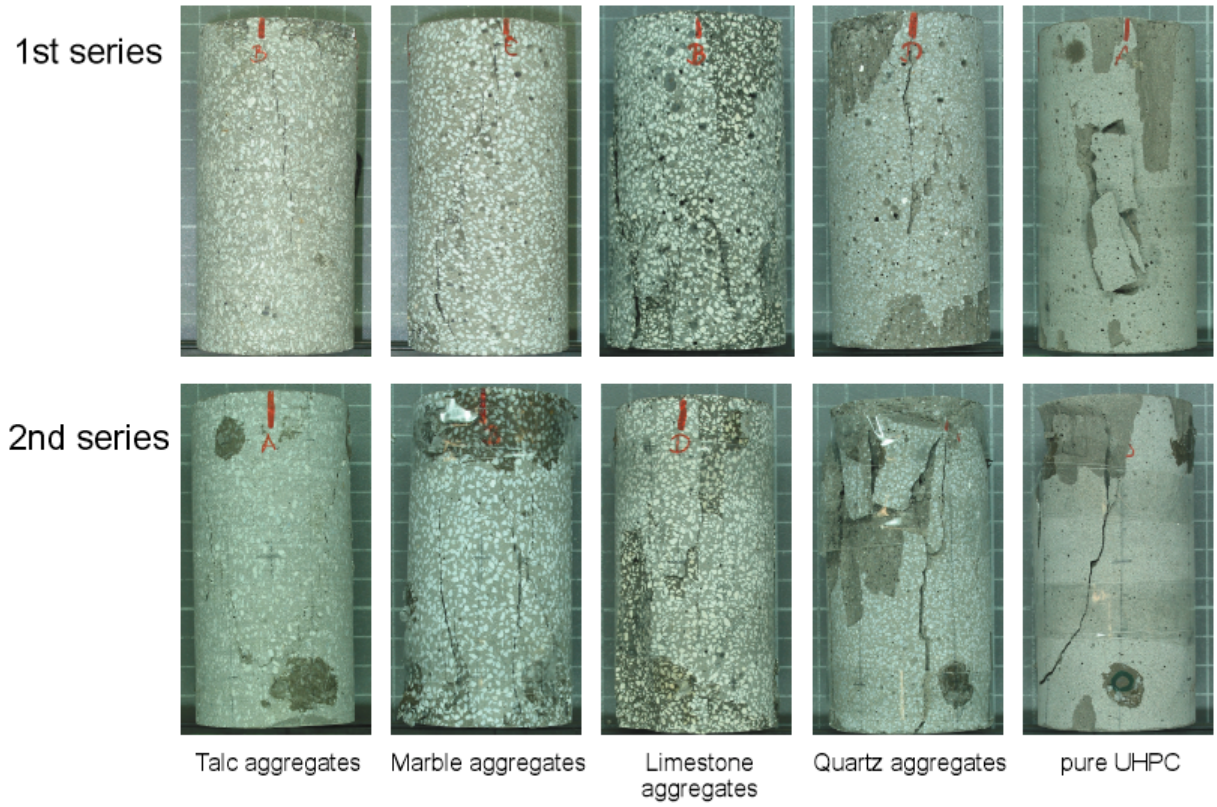

Abbildung 5.16: Fracture behavior

Evident in the Stress-strain curves in the next section is that all samples were defined as class II rocks i.e. no further axial compression took place after peak stress and constant circumferential expansion. Figure 5.17 shows that none of the specimens experienced an increase in energy after peak stress. As is shown in figure 5.16, the fracture behavior did not differ between first and second series. It was observed that samples with talc and marble aggregates developed only vertical cracks, whereas the artificial limestone, quartz and pure UHPC samples also developed shell-like spalling, releasing a lot of energy. The sample containing limestone aggregates also developed deeper cracks than other samples.

After closer evaluation artificial quartz and pure UHPC specimens were defined as particularly brittle and the artificial limestone samples as very brittle pre-peak but more ductile in post-failure behaviour.

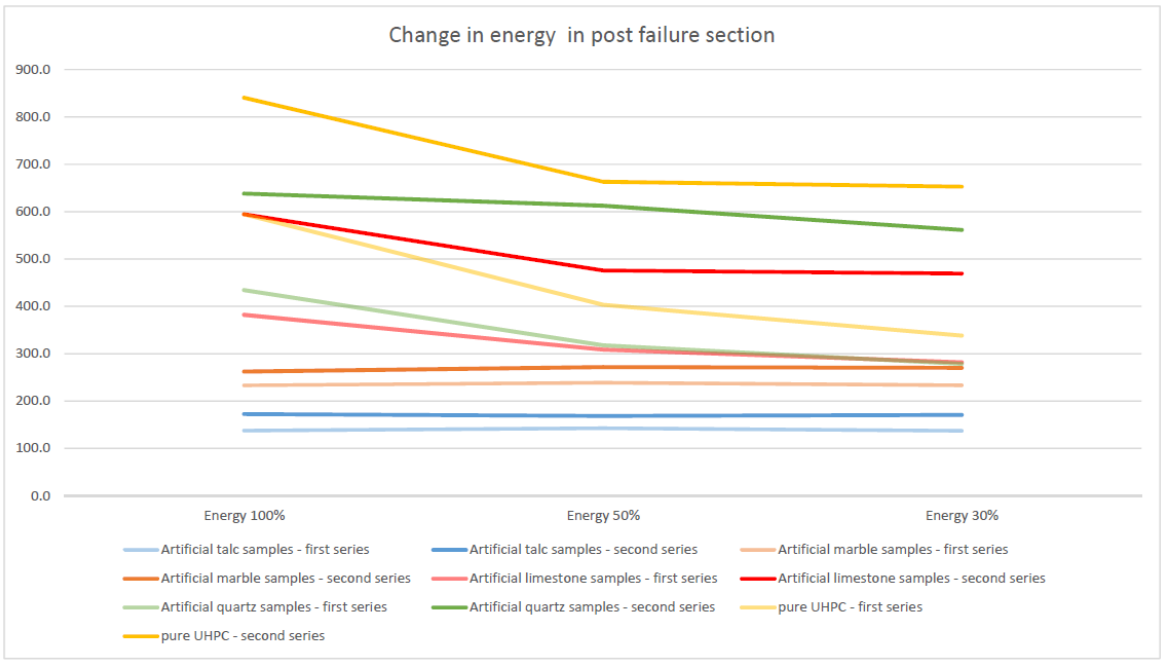

Abbildung 5.17: Orientation of talk grains within the sample

5.6.1 Comparing first and second series

Artificial talc samples

Both the Young's modulus and the compressive strength increased considerably from the first to the second series, due to a reduced pore size and a more uniform distribution of the pores in general. Also, a part played the arrangement of the grains, which due to the short vibration time were directionally oriented, as can be seen in figure 5.19. These oriented grains create a shear surface, which contributes also to an earlier failure.

Because the vibration time was increased in the second series, the talc grains could direct themselves arbitrarily and do not point in a specific direction anymore. See figure (spztalk).

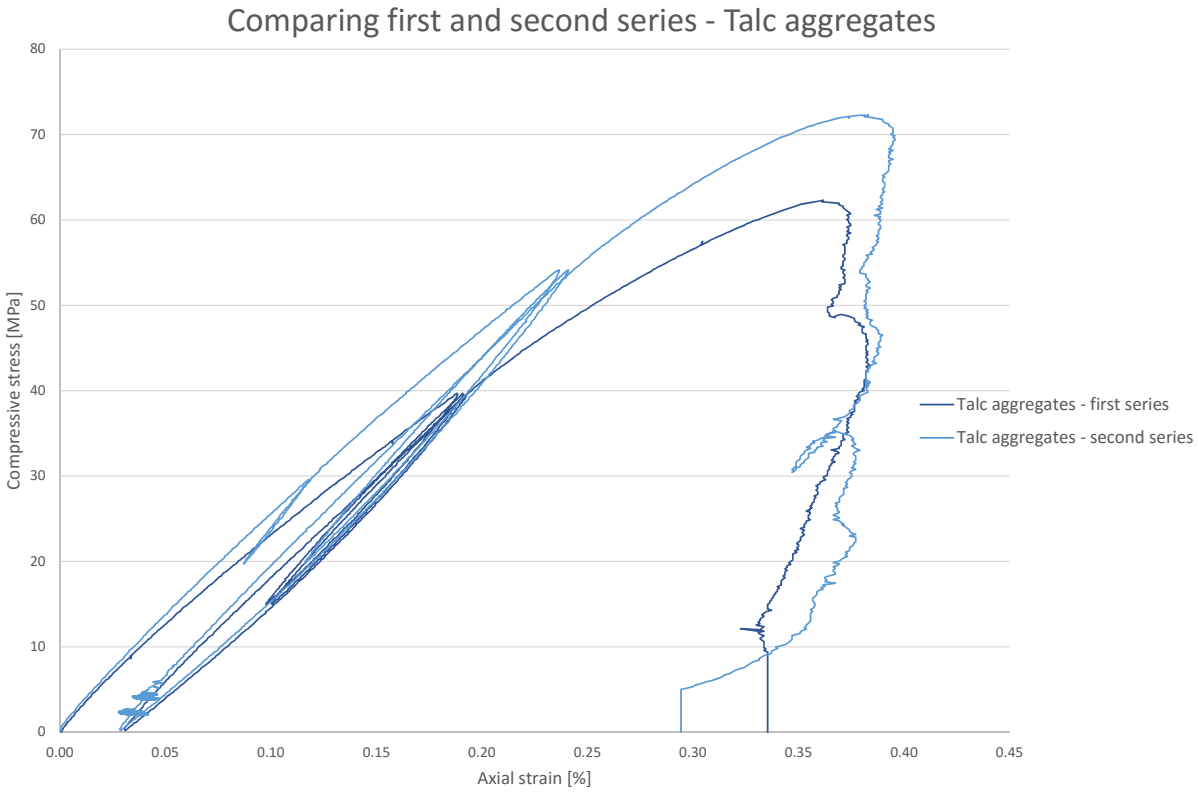

Abbildung 5.18: Comparing first and second series - Talc aggregates

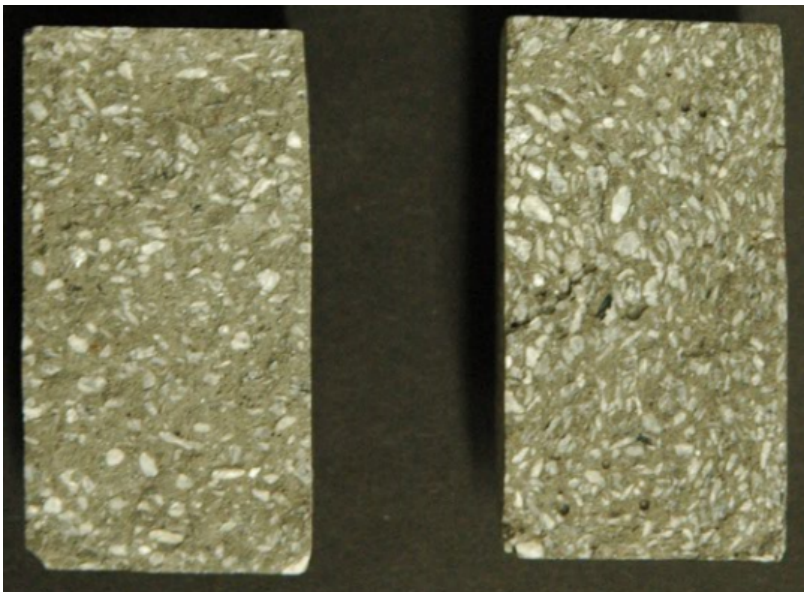

Abbildung 5.19: Orientation of talk grains within the sample

It was assumed, that because the vibration time was extended the pore volume would decrease, but instead the volume has increased which is can only be explained by the fact that the amount of plasticiser was reduced in the second series and therefore smaller pores could not be deaerated.

Artificial marble sample

The difference in Young's modulus and compressive strength can be explained by a different arrangement of the pores and a different pore size, also the chemical reaction that took place in the first but not the second series probably had an effect. Because of a longer vibration the big pores got reduced and pores formed due to the dissolution of calcite did not occur in the second series, but because of a higher water content more gel pores formed. Those alone cannot explain the increase of pore volume in the specimens, so the reduction of plasticisers is probable to also play a part in the pore volume. The post failure behaviour on both the first and the second series are pretty much the same, i.e. at the border between Class I and Class II rock.

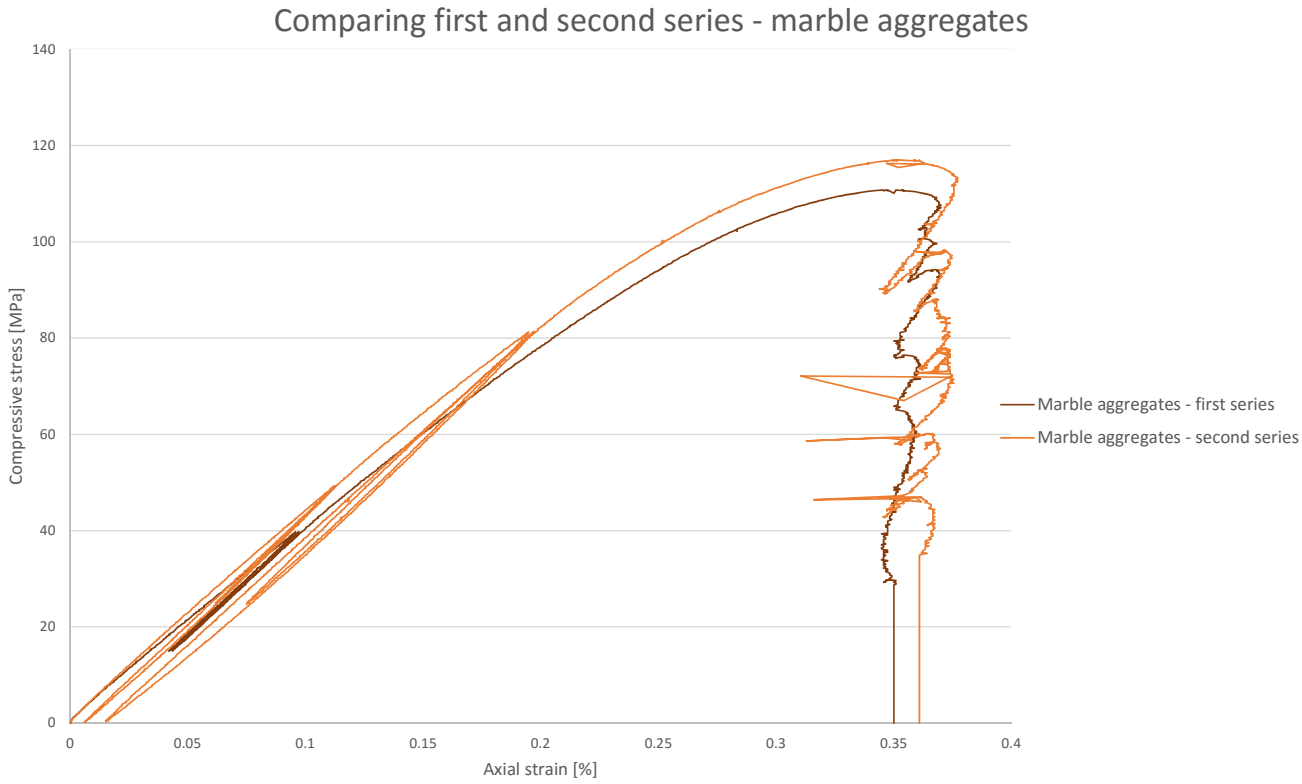

Abbildung 5.20: Comparing first and second series - Talc aggregates

Artificial limestone sample

The Young's modulus of the first and second series is fairly similar to themselves as well as the UHPC and with that also the artificial quartz samples discussed in the next chapter.

The UCS of the artificial limestone samples increases from the first to the second series about 20 % in comparison the pure UHPC sample increases only 7 %. Because of the big decrease in pore size, a higher UCS can develop. The all in all pore volume stays about the same because less plasticiser was used, counteracting the pore loss during extended vibration. Also, the chemical reaction has to be taken into account.

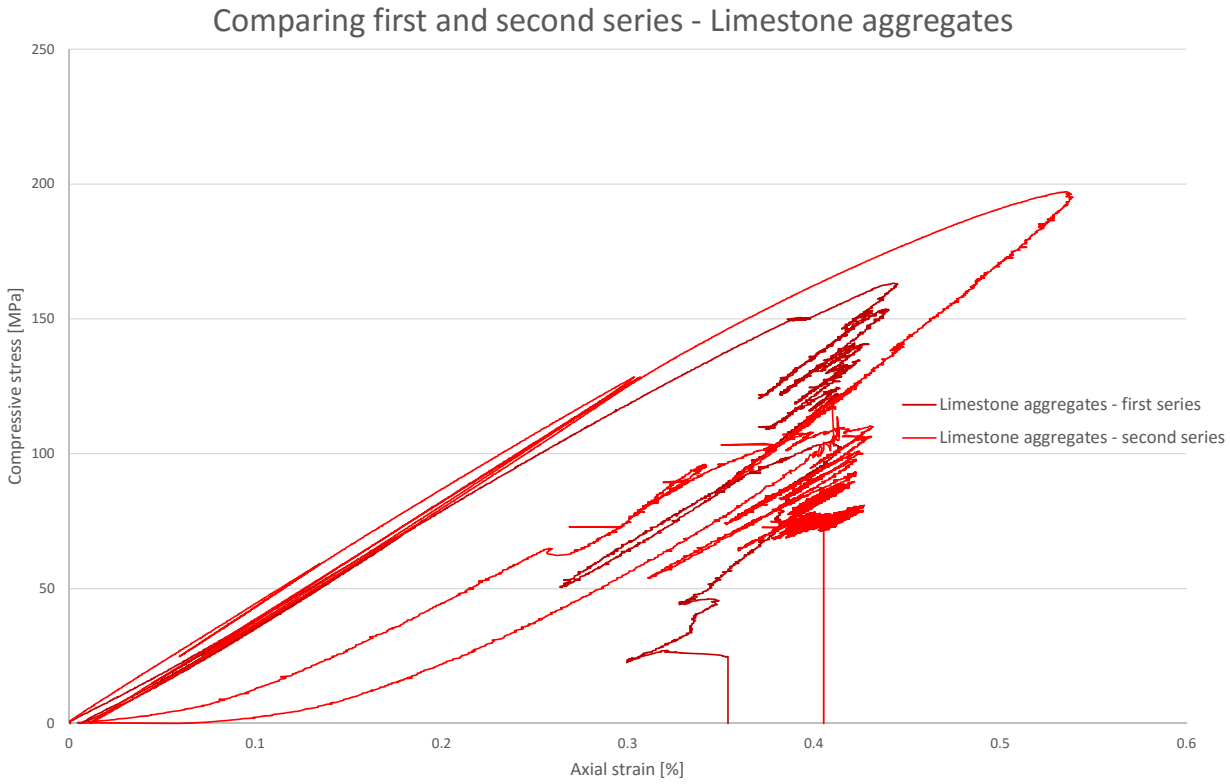

Abbildung 5.21: Comparing first and second series - Talc aggregates

Artificial quartz sample

The difference between the first and the second series is very small due to the fact that a very high homogeneity occurs, due to the quartz being used in the UHPC matrix as well. The Young's modulus shows hardly any change and the UCS increases only very little which can be explained by the reduced pore volume and pore size as well as a better pore distribution.

Abbildung 5.22: Comparing first and second series - Talc aggregates

Pure UHPC

Same as in the artificial quartz sample, the Young's modulus of the pure UHPC sample showed no differences. The UCS increased due to the increased homogeneity due to better pore distribution.

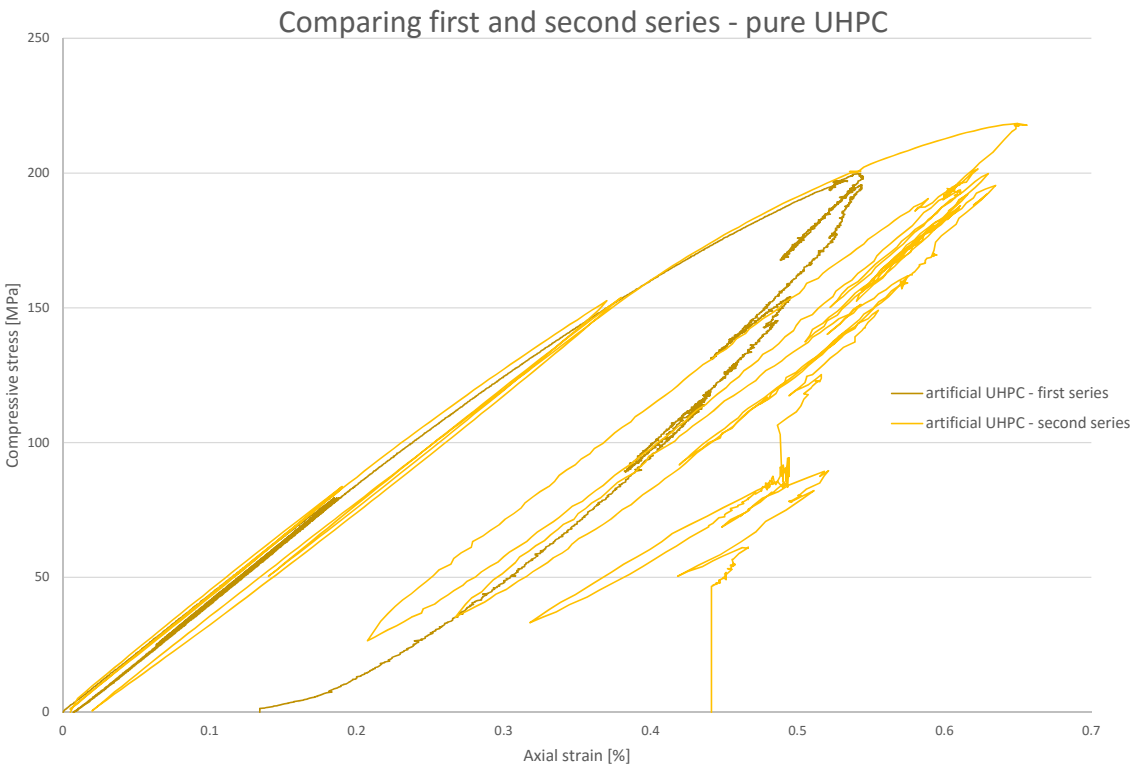

Abbildung 5.23: Comparing first and second series - Talc aggregates

5.7 Comparison of the artificial samples with the matrix

UHPC with talc aggregates vs. pure UHPC

The Young's modulus of the Talc is approximately the same as the Young's modulus of the UHPC with talc aggregates, while the Young's modulus of the pure UHPC is significantly higher. This indicates that the stiffness is mainly influenced by the soft grains of the talc. Because of the size and heterogenic distribution of the pores and the difference in stiffness earlier cracks could form at stress concentrations and an earlier and less brittle failure in comparisons to the pure matrix could take place. Because of less stored energy, a rockburst would also be less violent.

The compressive strength of the artificial talc sample is much smaller than the UCS of the pure UHPC. This is also due to the heterogeneity within the sample.

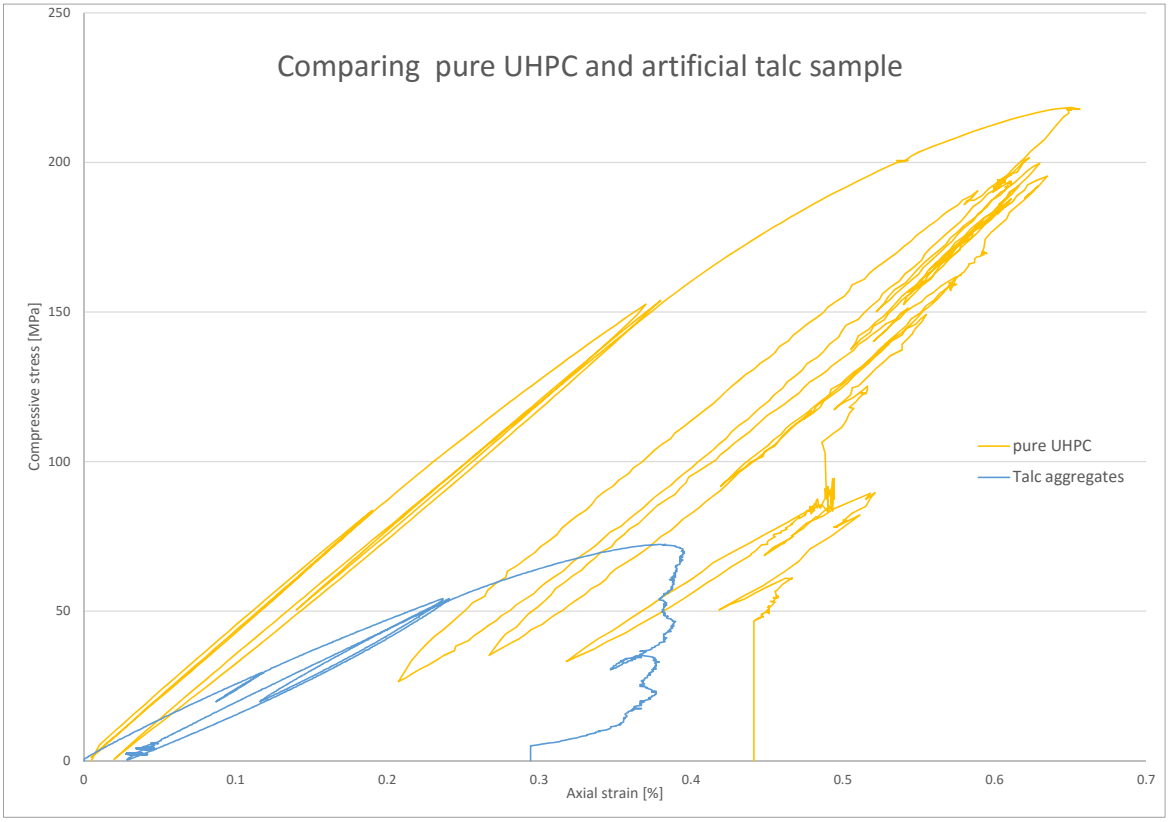

Abbildung 5.24

UHPC with marble aggregates vs. pure UHPC

Because the Young's modulus of the artificial marble sample is similar to the Young's modulus of the pure UHPC, as opposed to the much higher Young's modulus of the marble rock sample, it is assumed that the stiffness is mainly carried by the rock matrix and not the marble grains because of a missing continuous grain skeleton. And as already stated in the chapter above the difference in stiffness, and the arrangement and size of pores lead to a heterogeneous stress pattern which causes cracks to form early and the sample to fail.

Also due to heterogeneity the compressive strength of the artificial marble sample is smaller than the pure UHPC one but bigger than the one from the pure marble rock sample.

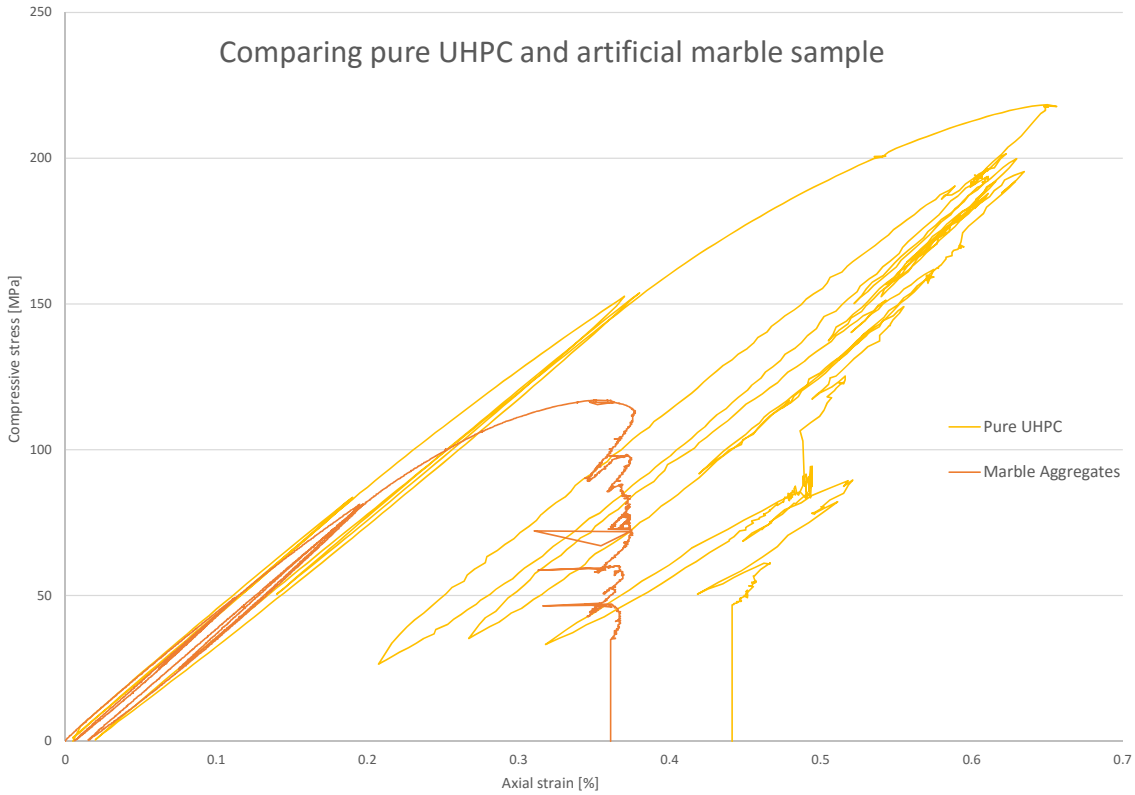

Abbildung 5.25

UHPC with limestone aggregates vs. pure UHPC

The Young's modulus of the original limestone rock sample, the pure UHPC and the artificial limestone sample portray nearly the same Young's modulus. Therefore it goes to show that neither dominate the stiffness.

The UCS from the UHPC, on the other hand, shows significant differences in the compressive strength of the UHPC with limestone aggregates. The limestone rock has, although a lower UCS, a higher one in comparison to the others, especially the quartz see (figure). The heterogeneity is caused by the admixed grains and especially the size and the arrangement of the pores, for the artificial limestone sample has by far the biggest pores.

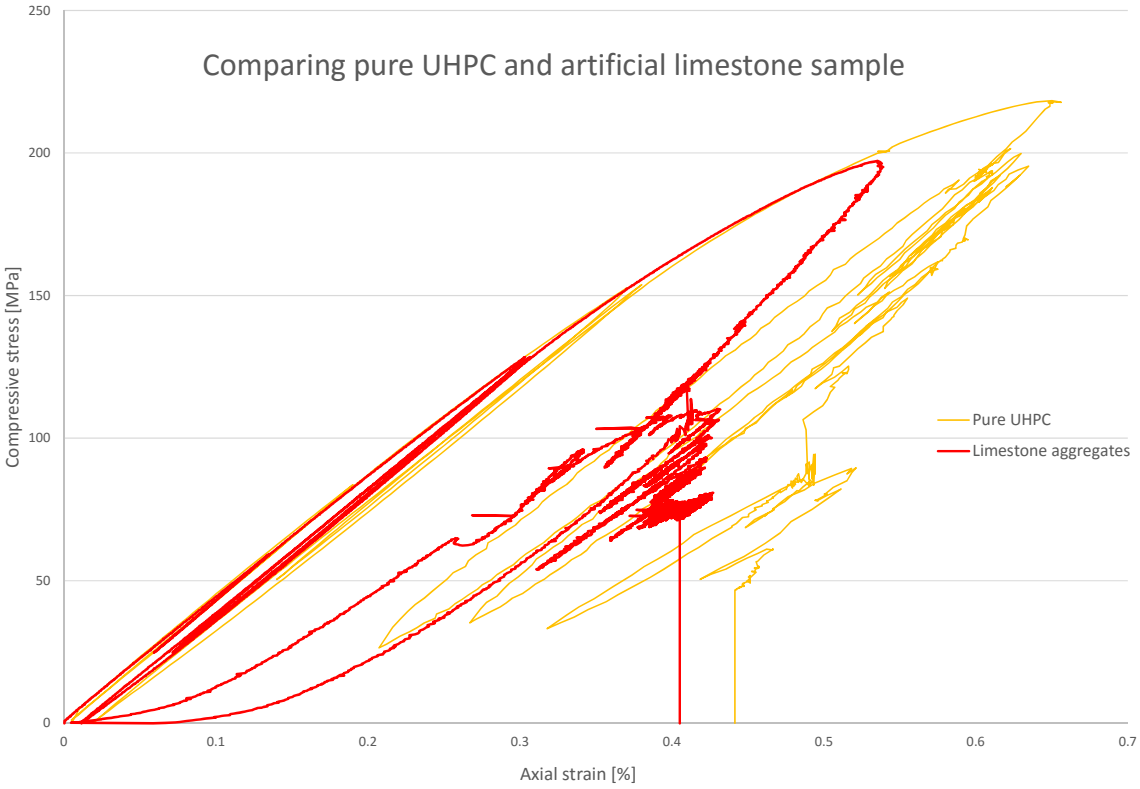

Abbildung 5.26

UHPC with quartz aggregates vs. pure UHPC

The Young's modulus of the sample with the quartz aggregates is only slightly higher. Again both, matrix and aggregates are responsible for the stiffness, with the slightly higher initial Young's modulus of the quartz grains having a bigger impact on the artificial quartz sample than on the pure UHPC specimen. The pure UHPC sample also portrays less pore volume and so this increases the homogeneity and with that the compressive strength.

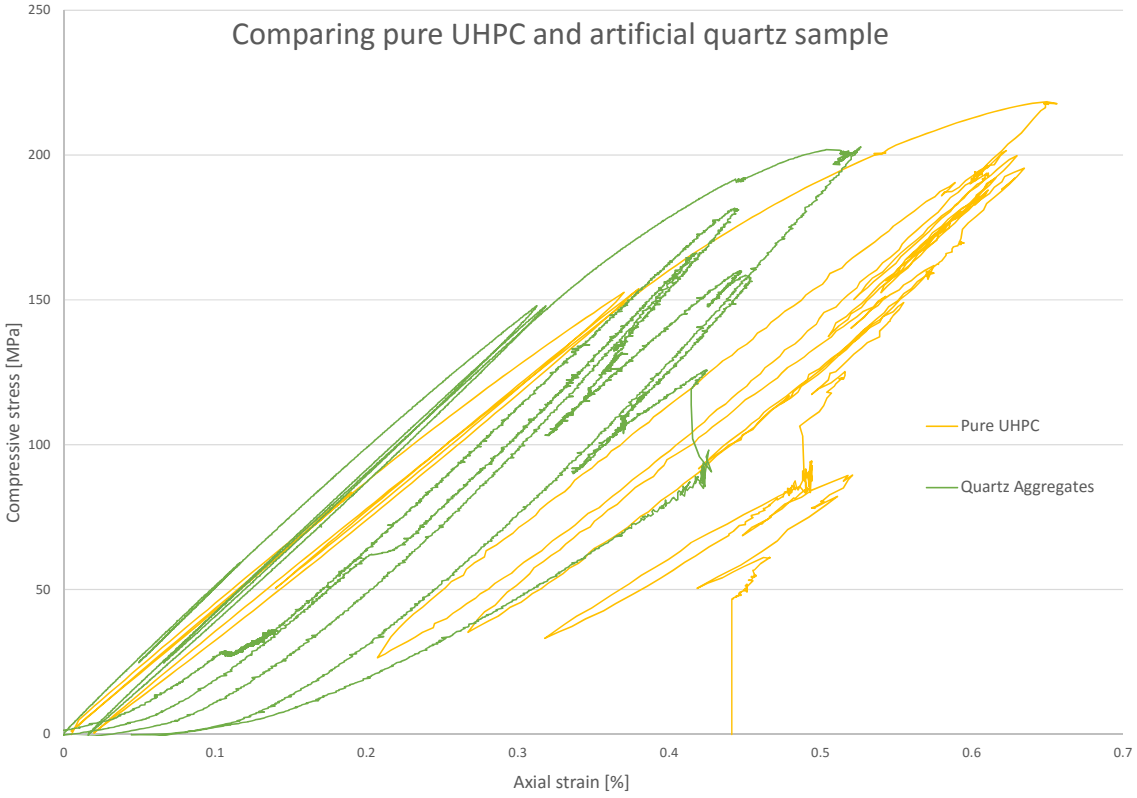

Abbildung 5.27

6 Interpretation

If not specified in the graphs, the lighter colour in the background portrays the results from the first series, while the more prominent values in the front show the results from the second series.

6.1 Comparing rockburst parameters

Talc

Tabelle 6.1: Rock Burst Parameters Talc First Series

Parameter			category	Individual results
B	11.9	[-]	violent rockburst	
PES	55	[kJ/m^3]	the rockburst hazard is low	
W_{ET}	1.4	[-]	no shock	
H_{cr}	322	[m]	-	
BIM	1.6	[-]	the rockburst hazard is low	

Tabelle 6.2: Rock Burst Parameters Talc Second Series

Parameter			category	Individual results		
B	13.5	[-]	violent rockburst	13.4	13.7	13.5
PES	75	[kJ/m^3]	the rockburst hazard is low	73	72	78
W_{ET}	3.0	[-]	weak to medium shock	3.2	2.6	3.2
H_{cr}	380	[m]	[-]	376	389	374
BIM	1.4	[-]	the rockburst hazard is moderate	1.3	1.5	1.4

When the results are observed, only W_{ET} and BIM show significant differences due to the fact that the primary loading curve of the second series is much steeper, resulting in an increase

of the deformation modulus of about 20 %, and also subsequently increase in the modulus determined at 50 % (E_{50}). In addition, the plastic deformation at peak starts earlier in the first series. The difference in PES is due only to the increase in UCS. For comparison see 5.18

Marble

Tabelle 6.3: Rock Burst Parameters Marble First Series

Parameter			category	Individual results
B	13.2	[-]	violent rockburst	
PES	127	[kJ/m^3]	the rockburst hazard is moderate	
W_{ET}	4.2	[-]	weak to medium shock	
H_{cr}	549	[m]	-	
BIM	1.4	[-]	the rockburst hazard is moderate	

Tabelle 6.4: Rock Burst Parameters Marble Second Series

Parameter			category	Individual results		
B	15.7	[-]	strong rockburst	15.7	15.7	15.7
PES	121	[kJ/m^3]	the rockburst hazard is moderate	122	119	121
W_{ET}	5.1	[-]	strong to violent shock	4.9	5.1	5.1
H_{cr}	583	[m]	[-]	580	582	587
BIM	1.6	[-]	the rockburst hazard is low	1.8	1.6	1.5

The difference in W_{ET} is again explained by a steeper primary loading curve. On the other hand, BIM indices are higher, meaning less prone to rockburst in the second series. This is because, when stress-strain diagrams are compared with each other (see figure 5.20), opposed to talc samples, the second series developed more plastic deformation in the last 25 % of the loading. Because this only shows in the latter stages WET is not influenced by this fact.

Limestone

Tabelle 6.5: Rock Burst Parameters Limestone First Series

Parameter			category	Individual results
B	16.0	[-]	strong rockburst	
PES	296	[kJ/m^3]	the rockburst hazard is very high	
W_{ET}	7.2	[-]	strong to violent shock	
H_{cr}	861	[m]	-	
BIM	1.18	[-]	the rockburst hazard is high	

Tabelle 6.6: Rock Burst Parameters Limestone Second Series

Parameter			category	Individual results		
B	35.6	[-]	weak rockburst	34.8	36.1	36.0
PES	381	[kJ/m^3]	the rockburst hazard is very high	350	391	401
W_{ET}	10.6	[-]	strong to violent shock	10.5	10.2	11.0
H_{cr}	990	[m]	[-]	958	1015	998
BIM	1.21	[-]	the rockburst hazard is moderate	1.08	1.29	1.26

Limestone experienced by far the biggest increase in uniaxial compressive strength while simultaneously also a reduction of the tensile strength occurred. This leads to a drastic change in the brittleness index. As shown in the tables 6.5 and 6.6 the brittle behaviour according to B drops from strong rockburst to weak rockburst, which looking at the postfailure curve (5.21) is not very likely. In addition, the increase in PES is concurrent with the higher UCS. The same as in the marble samples, the increase in plastic deformation towards peak strength elevates the BIM, which results in a lower category in regards to rockburst. This is a good example, that the categories are to be viewed with care and the actual results have to be assessed.

Quartz

Tabelle 6.7: Rock Burst Parameters Quartz First Series

Parameter			category	Individual results
B	16.5	[-]	violent rockburst	
PES	339	[kJ/m^3]	the rockburst hazard is very high	
W_{ET}	8.6	[-]	strong to violent shock	
H_{cr}	949	[m]	-	
BIM	1.15	[-]	the rockburst hazard is high	

Tabelle 6.8: Rock Burst Parameters Quartz Second Series

Parameter			category	Individual results		
B	21.4	[-]	strong rockburst	21.4	21.5	21.4
PES	373	[kJ/m^3]	the rockburst hazard is very high	396	372	352
W_{ET}	9.4	[-]	strong to violent shock	(5.9)	9.2	9.6
H_{cr}	970	[m]	[-]	974	971	965
BIM	1.35	[-]	the rockburst hazard is moderate	1.4	1.4	1.3

Due to the lowered tensile strength, is the brittleness index higher than in the first series and changes from violent to strong rockburst. Again, the plastic deformations happening when nearing peak stress show a difference in BIM 5.22.
Because of a faulty display in the primary loading W_{ET} of the first Quartz sample was not considered. This, however, had no effect on other parameters.

Pure UHPC

Tabelle 6.9: Rock Burst Parameters UHPC First Series

Parameter			category	Individual results
B	17.0	[-]	strong rockburst	
PES	416	[kJ/m^3]	the rockburst hazard is very high	
W_{ET}	8.3	[-]	strong to violent shock	
H_{cr}	1010	[m]	-	
BIM	1.23	[-]	the rockburst hazard is moderate	

Tabelle 6.10: Rock Burst Parameters UHPC Second Series

Parameter			category	Individual results		
B	31.9	[-]	weak rockburst	32.5	32.1	31.1
PES	461	[kJ/m^3]	the rockburst hazard is very high	512	443	427
W_{ET}	9.6	[-]	strong to violent shock	10.5	9.2	9.2
H_{cr}	1060	[m]	[-]	1082	1066	1032
BIM	1.34	[-]	the rockburst hazard is moderate	1.4	1.4	1.3

As with the limestone samples, the tensile strength of the pure UHPC also dropped about 45 % from the first to the second series, thus influencing the brittleness index immensely. As in the above, plastic deformation occurs prepeak and decreases the rockburst hazard regarding BIM 5.23.

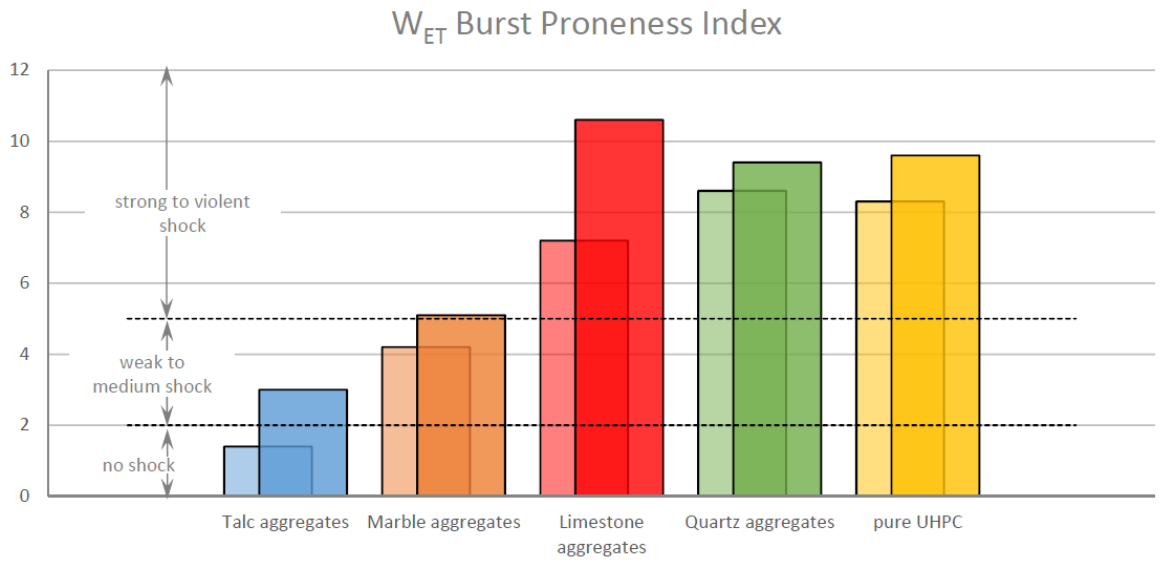

Abbildung 6.1: Evaluation of W_{ET}

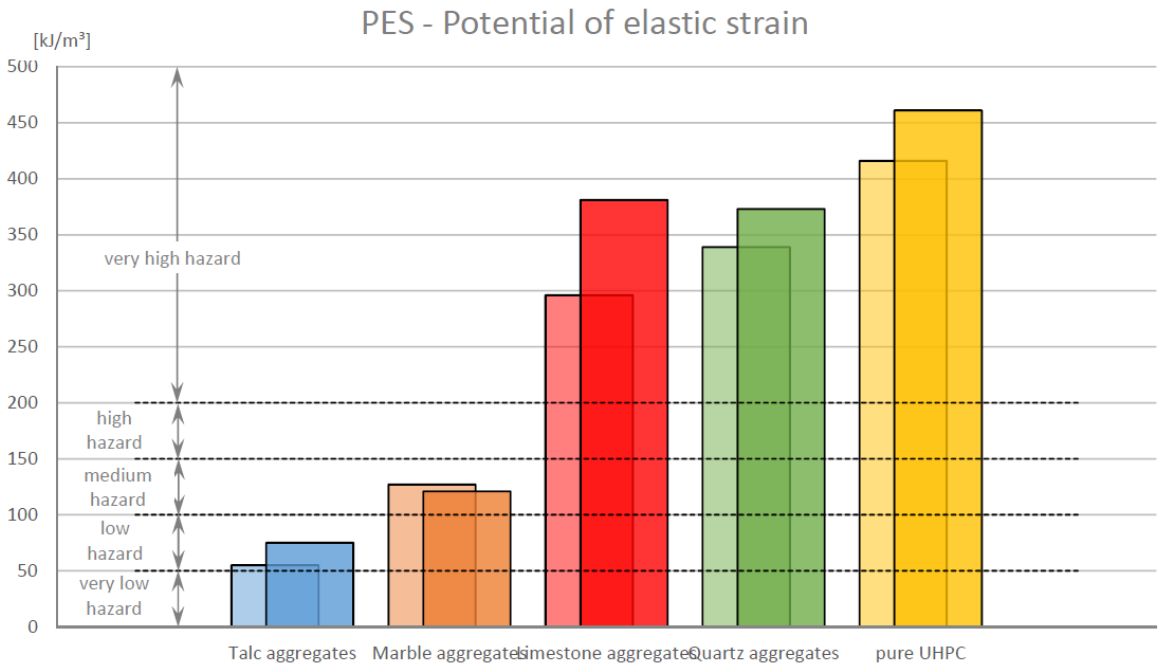

Abbildung 6.2: Evaluation of PES

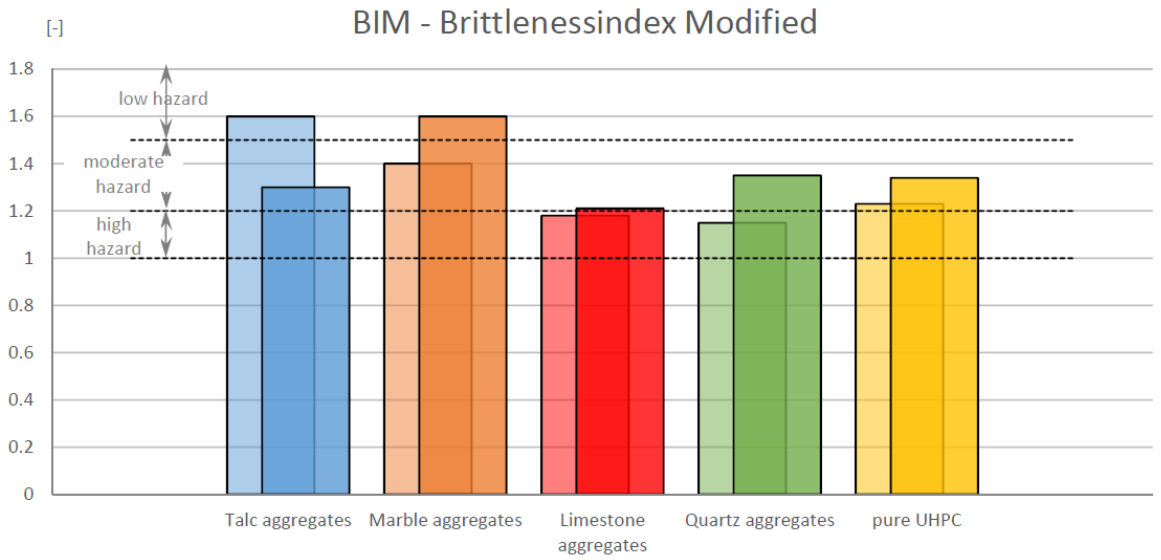

Abbildung 6.3: Evaluation of Brittlenessindex Modified

When comparing the results of rockburst parameters of different materials with each other, it can be observed that the PES, BIM and W_{ET} fit together quite well, while the brittleness index portrayed somewhat of an outlier, not really fitting with the other parameters, as well as the initial expectation after observing the specimens and the results from the conducted tests. The energy based parameters show for the artificial talc samples overall weak to moderate rockburst, for the marble moderate rockburst hazard and for limestone, quartz and pure

UHPC a high rockburst hazard. This fits quite well with the assumption that the more homogeneous a material is, the more prone to rockburst it is.

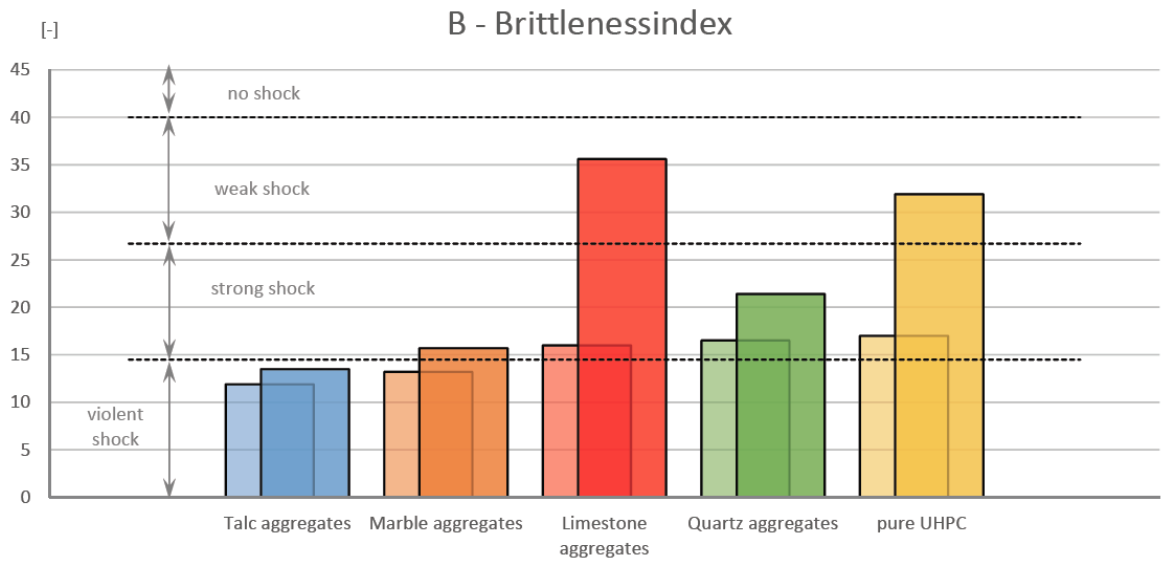

Abbildung 6.4: Evaluation of the Brittleness Index

Regarding the brittleness index, it might be the case that because the „rock“ actually is made of concrete and the tensile strength of UHPC is actually (as tested in the concrete laboratory) only about 3 - 5 % of the UCS, while a rule of thumb for actual rock is 10 %. In this instance, it might just be the case that for UHPC this parameter's categories have to be adjusted.

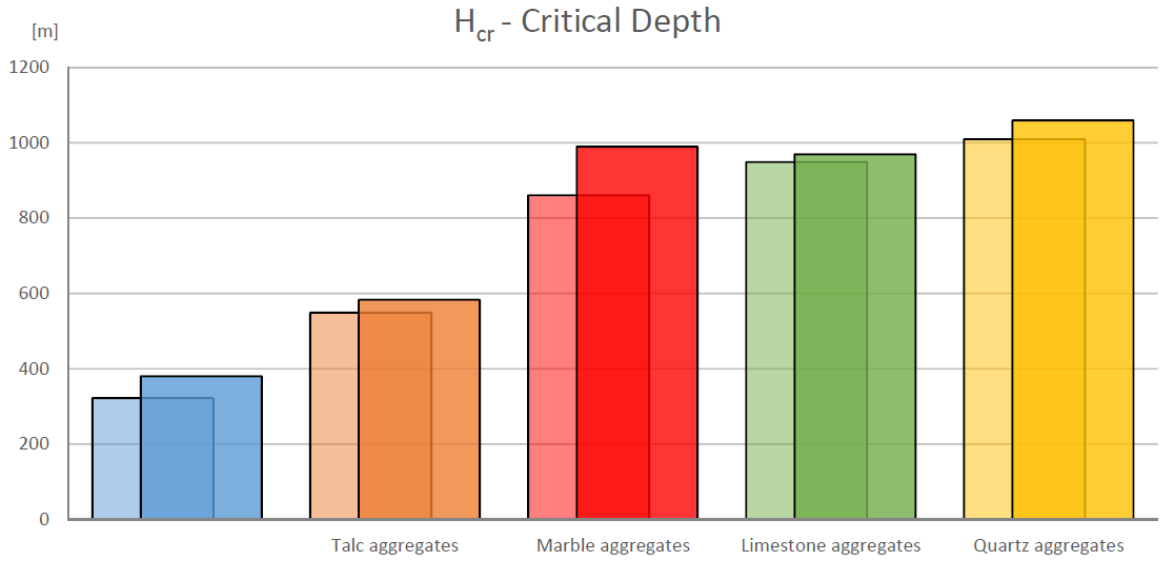

Abbildung 6.5: Evaluation of H_{cr}

Regarding the energy based parameters, it makes sense to evaluate all three, for they take

different characteristics into account. The PES, for example, is the only one considering the uniaxial compressive strength, and not just in a proportion. The W_{ET} is mainly influenced by the primary loading curve and the unloading curve, which is highly dependable on the Young's modulus and the properties of BIM is affected most by again the primary loading curve, especially the last 20 % before peak, when more or less plastic deformation occurs.

6.2 Consclusion

Due to the results derived from the tested samples it was evident that increasing stiffness heterogenity i.e. matrix, aggregates and unevenly distributed pores, result in a lower uniaxial compressive strength. The stiffness is mainly driven by the softer material without a continuous grain skeleton. Also when comparing the first and the second series, although this was not the initial purpos Although it was not the initial purpose of the project to compare first and second series, it is worth noting that distribution and size of pores play a bigger role than the total void ratio.

Regarding the rockburst criteria chosen in this project, the boundaries that are associated with them, have to be treated with care, for some of them seem rather arbitrarily set.

6.3 Outlook

The research project will continue by further analysis of the artificial samples by CT scan and Object Based Image Analysis (OBIA) and the acoustic emission tests will be analysed and compared with the evaluated results. These methods should give a better understanding about the cracking process. Also similar tests will be performed on actual rock samples.

Literaturverzeichnis

Aubertin, M.; Gill, D. (1988). Une méthodologie d'évaluation du potentiel de coups de terrain dans les mines d'abitibi. *Colloque sur le Contrôl de terrain (AMMQ).*

Aubertin, M.; Gill, D. S. R. (1994). On the use of brittleness index modified (bim) to estimate the post-peak behaviour on rocks. *Proceedings of the 1st North American Rock Mechanics Symposium.*

Hou, F. (1989). Criterion and prevention measurements measure for rockburst in circle tunnel. (in chinese. *Rock mechanics application in the engineering.*

Kaiser, P.K.; Cai, M. Keynote lecture: Rockburst damage mechanisms and support design principles, 1–22.

Kwa´sniewski, M.; Szutkowski, I. W. J.-A. (1994). Study of ability of coal from seam 510 for storing elastic energy in the aspect of assessment of hazard in porabka-klimontow colliery. *Sci. Rept. Silesian Technical University, Poland.*

Li, Tianbin; Xiao, X. S. Y. (2006). Comprehensive integrated methods of rockburst prediction in underground engineering. *IAEG 2006 Paper number 594*, 1–10.

Neyman, B.; Szecówka, Z. Z. W. (1972). Wirksame verfahren zur bekämpfung von gebirgsschlägen im steinkohlenbergbau der volksrepublik polen (paper in german). *V. Internationaler Kongress für Gebirgsdruckforschung*, 1–9.

Qiao, C.S., T. Z. (2007). Study of the possibility of rockburst in dong-gua-shan copper mine. *Chinese J. Rock Mech. Eng.*, *17*, 917–921.

Tang, B. (2000). Rockburst control using destress blasting. Thesis, McGill University, Montreal Canada.

Thuro, K. (1996). Bohrbarkeit beim konventionellen sprengvortrieb (in german). *MÜNCHNER GEOLOGISCHE HEFTE Reihe B: Angewandte Geologie*, *B1.*

Wang, J.-A. & Park, H. (2001). Comprehensive prediction of rockburst based on analysis of strain energy in rocks. *Tunneling and Underground Space Technology*, *16*, 49–57.

Anhang A

TU Graz
Graz University of Technology

INSTITUT FÜR BODENMECHANIK UND GRUNDBAU
GEOTECHNISCHES LABOR

RECHBAUERSTRASE 12, 8010 GRAZ, AUSTRIA
Tel: +43(0)316/873-6237 Fax: +43(0)316/873-6238

AUFTRAGGEBER:	BEZEICHNUNG: UHPC with Quartz Aggregates	LABORNUMMER:
	BODENART:	PROJEKTNUMMER:: 268
PROJEKT: first series	BEARBEITER: Peintner	DATUM:

KORNDICHTE ÖNORM B 4413:2010

1	Pyknometer-Nr.				103	116	127
2	Tara	g	m_0	T	44.2438	43.4893	43.9602
3	Trockenmasse Probe + Tara	g	m_1	L	64.1023	62.9898	63.4448
4	Trockenmasse Probe	g	m_2	3-2	19.8585	19.5005	19.4846
5	Masse Pyknometer + Wasser + Probe (unter Auftrieb) bei t °C	g	m_3	L	155.4559	155.2367	156.5298
6	Versuchstemperatur Probe + Wasser	°C	t	L	23.95	23.8	23.9
7	Temperaturkorrektur von 20° zu t °C	g	Δm	T	-0.089	-0.086	-0.089
8	Masse Pyknometer + Wasser bei 20 °C	g	m_4	T	143.15843	143.16057	144.48094
9	Masse Pyknometer +Wasser bei t °C	g	m_5	7+8	143.06943	143.07457	144.39194
10	Dichte Wasser bei t °C	g/cm³	ρ_w	T	0.9974	0.9974	0.9974
11	Bodenvolumen	cm³	V_K	$\frac{(9+4-5)}{10}$	7.492	7.358	7.366
12	Korndichte	Mg/m³	ρ_s	$\frac{4}{11}$	2.651	2.650	2.645
13	Mittelwert aus allen Versuchen	Mg/m³	ρs,i.M.		2.65		

ANMERKUNG:

INSTITUT FÜR BODENMECHANIK UND GRUNDBAU
GEOTECHNISCHES LABOR

RECHBAUERSTRASE 12, 8010 GRAZ, AUSTRIA
Tel: +43(0)316/873-6237 Fax: +43(0)316/873-6238

AUFTRAGGEBER:	BEZEICHNUNG: UHPC with Talc Aggregates	LABORNUMMER:
	BODENART:	PROJEKTNUMMER:: 268
PROJEKT: First series	BEARBEITER: Peintner	DATUM:

KORNDICHTE ÖNORM B 4413:2010

1	Pyknometer-Nr.				36	128	110
2	Tara	g	m_0	T	47.8557	44.5602	44.0219
3	Trockenmasse Probe + Tara	g	m_1	L	67.6581	64.372	63.671
4	Trockenmasse Probe	g	m_2	3-2	19.8024	19.8118	19.6491
5	Masse Pyknometer + Wasser + Probe (unter Auftrieb) bei t °C	g	m_3	L	160.5131	155.2859	155.1462
6	Versuchstemperatur Probe + Wasser	°C	t	L	23.6	23.7	23.5
7	Temperaturkorrektur von 20° zu t °C	g	Δm	T	-0.081	-0.084	-0.079
8	Masse Pyknometer + Wasser bei 20 °C	g	m_4	T	148.14985	142.92682	142.87056
9	Masse Pyknometer +Wasser bei t °C	g	m_5	7+8	148.06885	142.84282	142.79156
10	Dichte Wasser bei t °C	g/cm³	ρ_w	T	0.9974	0.9974	0.9975
11	Bodenvolumen	cm³	V_K	$\frac{(9+4-5)}{10}$	7.377	7.388	7.313
12	Korndichte	Mg/m³	ρ_s	$\frac{4}{11}$	2.684	2.682	2.687
13	Mittelwert aus allen Versuchen	Mg/m³	ρs,i.M.		2.68		

ANMERKUNG:

TU Graz
Graz University of Technology

INSTITUT FÜR BODENMECHANIK UND GRUNDBAU
GEOTECHNISCHES LABOR

RECHBAUERSTRASE 12, 8010 GRAZ, AUSTRIA
Tel: +43(0)316/873-6237 Fax: +43(0)316/873-6238

AUFTRAGGEBER:	BEZEICHNUNG: UHPC with Marble Aggregates	LABORNUMMER:
	BODENART:	PROJEKTNUMMER:: 268
PROJEKT: First series	BEARBEITER: Peintner	DATUM:

KORNDICHTE ÖNORM B 4413:2010

1	Pyknometer-Nr.				116	36	110
2	Tara	g	m_0	T	43.4892	47.8574	44.026
3	Trockenmasse Probe + Tara	g	m_1	L	53.897	57.8334	54.2152
4	Trockenmasse Probe	g	m_2	3-2	10.4078	9.976	10.1892
5	Masse Pyknometer + Wasser + Probe (unter Auftrieb) bei t °C	g	m_3	L	149.5038	154.2145	150.1004
6	Versuchstemperatur Probe + Wasser	°C	t	L	21.5	22.1	21.8
7	Temperaturkorrektur von 20° zu t °C	g	Δm	T	-0.032	-0.046	-0.039
8	Masse Pyknometer + Wasser bei 20 °C	g	m_4	T	143.16346	148.15155	143.87495
9	Masse Pyknometer +Wasser bei t °C	g	m_5	7+8	143.13146	148.10555	143.83595
10	Dichte Wasser bei t °C	g/cm³	ρ_w	T	0.9979	0.9978	0.9978
11	Bodenvolumen	cm³	V_K	$\frac{(9+4-5)}{10}$	4.044	3.876	3.933
12	Korndichte	Mg/m³	ρ_s	$\frac{4}{11}$	2.574	2.574	2.591
13	Mittelwert aus allen Versuchen	Mg/m³	ρs,i.M.		2.57		

ANMERKUNG:

TU Graz
Graz University of Technology

INSTITUT FÜR BODENMECHANIK UND GRUNDBAU
GEOTECHNISCHES LABOR

RECHBAUERSTRASE 12, 8010 GRAZ, AUSTRIA
Tel: +43(0)316/873-6237 Fax: +43(0)316/873-6238

AUFTRAGGEBER:	BEZEICHNUNG: UHPC without Aggregates	LABORNUMMER:
	BODENART:	PROJEKTNUMMER::
PROJEKT: First series	BEARBEITER: Peintner	DATUM:

KORNDICHTE ÖNORM B 4413:2010

1	Pyknometer-Nr.				107	108	109
2	Tara	g	m_0	T	43.9105	44.6019	43.9933
3	Trockenmasse Probe + Tara	g	m_1	L	63.4679	64.2374	63.7192
4	Trockenmasse Probe	g	m_2	3-2	19.5574	19.6355	19.7259
5	Masse Pyknometer + Wasser + Probe (unter Auftrieb) bei t °C	g	m_3	L	156.3204	155.5762	155.9037
6	Versuchstemperatur Probe + Wasser	°C	t	L	21	21.05	20.65
7	Temperaturkorrektur von 20° zu t °C	g	Δm	T	-0.021	-0.021	-0.013
8	Masse Pyknometer + Wasser bei 20 °C	g	m_4	T	144.08686	143.28695	143.55477
9	Masse Pyknometer +Wasser bei t °C	g	m_5	7+8	144.06586	143.26595	143.54177
10	Dichte Wasser bei t °C	g/cm³	ρ_w	T	0.9980	0.9980	0.9981
11	Bodenvolumen	cm³	V_K	$\frac{(9+4-5)}{10}$	7.317	7.340	7.378
12	Korndichte	Mg/m³	ρ_s	$\frac{4}{11}$	2.673	2.675	2.674
13	Mittelwert aus allen Versuchen	Mg/m³	ρs,i.M.		2.67		

ANMERKUNG:

INSTITUT FÜR BODENMECHANIK UND GRUNDBAU
GEOTECHNISCHES LABOR

RECHBAUERSTRASE 12, 8010 GRAZ, AUSTRIA
Tel: +43(0)316/873-6237 Fax: +43(0)316/873-6238

AUFTRAGGEBER:	BEZEICHNUNG: UHPC with Limestone Aggregates	LABORNUMMER:
	BODENART:	PROJEKTNUMMER::
PROJEKT: First series	BEARBEITER: Peintner	DATUM:

KORNDICHTE ÖNORM B 4413:2010

1	Pyknometer-Nr.				107	108	116
2	Tara	g	m_0	T	43.9128	44.603	43.4905
3	Trockenmasse Probe + Tara	g	m_1	L	65.6279	68.991	65.7295
4	Trockenmasse Probe	g	m_2	3-2	21.7151	24.388	22.239
5	Masse Pyknometer + Wasser + Probe (unter Auftrieb) bei t °C	g	m_3	L	157.3143	158.1939	156.759
6	Versuchstemperatur Probe + Wasser	°C	t	L	22.4	22.1	21.95
7	Temperaturkorrektur von 20° zu t °C	g	Δm	T	-0.053	-0.046	-0.041
8	Masse Pyknometer + Wasser bei 20 °C	g	m_4	T	144.08916	143.28805	143.16177
9	Masse Pyknometer +Wasser bei t °C	g	m_5	7+8	144.03616	143.24205	143.12077
10	Dichte Wasser bei t °C	g/cm³	ρ_w	T	0.9977	0.9978	0.9978
11	Bodenvolumen	cm³	V_K	$\frac{(9+4-5)}{10}$	8.456	9.457	8.620
12	Korndichte	Mg/m³	ρ_s	$\frac{4}{11}$	2.568	2.579	2.580
13	Mittelwert aus allen Versuchen	Mg/m³	ρs,i.M.		2.58		

ANMERKUNG:

TU Graz
Graz University of Technology

INSTITUT FÜR BODENMECHANIK UND GRUNDBAU
GEOTECHNISCHES LABOR

RECHBAUERSTRASE 12, 8010 GRAZ, AUSTRIA
Tel: +43(0)316/873-6237 Fax: +43(0)316/873-6238

AUFTRAGGEBER:	BEZEICHNUNG: UHPC with Limestone Aggregates (2)	LABORNUMMER:
	BODENART:	PROJEKTNUMMER::
PROJEKT: First series	BEARBEITER: Peintner	DATUM:

KORNDICHTE ÖNORM B 4413:2010

1	Pyknometer-Nr.				107	36	25
2	Tara	g	m_0	T	43.9113	47.8584	44.2492
3	Trockenmasse Probe + Tara	g	m_1	L	63.7736	67.8092	63.9812
4	Trockenmasse Probe	g	m_2	3-2	19.8623	19.9508	19.732
5	Masse Pyknometer + Wasser + Probe (unter Auftrieb) bei t °C	g	m_3	L	156.1696	160.2919	156.1901
6	Versuchstemperatur Probe + Wasser	°C	t	L	22.6	22.3	22.4
7	Temperaturkorrektur von 20° zu t °C	g	Δm	T	-0.057	-0.05	-0.053
8	Masse Pyknometer + Wasser bei 20 °C	g	m_4	T	144.08766	148.15255	144.19398
9	Masse Pyknometer +Wasser bei t °C	g	m_5	7+8	144.03066	148.10255	144.14098
10	Dichte Wasser bei t °C	g/cm³	ρ_w	T	0.9977	0.9977	0.9977
11	Bodenvolumen	cm³	V_K	$\frac{(9+4-5)}{10}$	7.741	7.779	7.700
12	Korndichte	Mg/m³	ρ_s	$\frac{4}{11}$	2.566	2.565	2.562
13	Mittelwert aus allen Versuchen	Mg/m³	ρs,i.M.		2.56		

ANMERKUNG:

INSTITUT FÜR BODENMECHANIK UND GRUNDBAU
GEOTECHNISCHES LABOR

RECHBAUERSTRASE 12, 8010 GRAZ, AUSTRIA
Tel: +43(0)316/873-6237 Fax: +43(0)316/873-6238

AUFTRAGGEBER:	BEZEICHNUNG:	LABORNUMMER:
	UHPC with Limestone Aggregates	
	BODENART:	PROJEKTNUMMER::
PROJEKT:		268
	BEARBEITER:	DATUM:
Masterarbeit	PEC	30.03.2017

KORNDICHTE ÖNORM B 4413:2010

1	Pyknometer-Nr.				110	107	116
2	Tara	g	m_0	T	44.022	43.9108	43.4923
3	Trockenmasse Probe + Tara	g	m_1	L	63.8153	63.4948	63.2738
4	Trockenmasse Probe	g	m_2	3-2	19.7933	19.584	19.7815
5	Masse Pyknometer + Wasser + Probe (unter Auftrieb) bei t °C	g	m_3	L	156.1515	156.2331	155.429
6	Versuchstemperatur Probe + Wasser	°C	t	L	22.8	22.8	22.75
7	Temperaturkorrektur von 20° zu t °C	g	Δm	T	-0.062	-0.062	-0.06
8	Masse Pyknometer + Wasser bei 20 °C	g	m_4	T	143.87095	144.08716	143.16357
9	Masse Pyknometer +Wasser bei t °C	g	m_5	7+8	143.80895	144.02516	143.10357
10	Dichte Wasser bei t °C	g/cm³	ρ_w	T	0.9976	0.9976	0.9976
11	Bodenvolumen	cm³	V_K	$\frac{(9+4-5)}{10}$	7.469	7.394	7.474
12	Korndichte	Mg/m³	ρ_s	$\frac{4}{11}$	2.650	2.649	2.647
13	Mittelwert aus allen Versuchen	Mg/m³	ρs,i.M.		2.65		

ANMERKUNG:

INSTITUT FÜR BODENMECHANIK UND GRUNDBAU
GEOTECHNISCHES LABOR

RECHBAUERSTRASE 12, 8010 GRAZ, AUSTRIA
Tel: +43(0)316/873-6237 Fax: +43(0)316/873-6238

AUFTRAGGEBER:	BEZEICHNUNG: UHPC without Aggregates	LABORNUMMER:
	BODENART:	PROJEKTNUMMER:: 268
PROJEKT: Masterarbeit	BEARBEITER: PEC	DATUM: 30.03.2017

KORNDICHTE ÖNORM B 4413:2010

1	Pyknometer-Nr.				128	102	25
2	Tara	g	m_0	T	44.5672	44.6668	44.2494
3	Trockenmasse Probe + Tara	g	m_1	L	64.428	64.4437	64.1479
4	Trockenmasse Probe	g	m_2	3-2	19.8608	19.7769	19.8985
5	Masse Pyknometer + Wasser + Probe (unter Auftrieb) bei t °C	g	m_3	L	155.2961	155.9122	156.5937
6	Versuchstemperatur Probe + Wasser	°C	t	L	23.35	24.1	23.85
7	Temperaturkorrektur von 20° zu t °C	g	Δm	T	-0.074	-0.093	-0.086
8	Masse Pyknometer + Wasser bei 20 °C	g	m_4	T	142.93382	143.5994	144.19418
9	Masse Pyknometer +Wasser bei t °C	g	m_5	7+8	142.85982	143.5064	144.10818
10	Dichte Wasser bei t °C	g/cm³	ρ_w	T	0.9975	0.9973	0.9974
11	Bodenvolumen	cm³	V_K	$\frac{(9+4-5)}{10}$	7.443	7.391	7.432
12	Korndichte	Mg/m³	ρ_s	$\frac{4}{11}$	2.668	2.676	2.677
13	Mittelwert aus allen Versuchen	Mg/m³	ρs,i.M.		2.68		

ANMERKUNG:128 ist übergekocht - recht viel ausgetreten. 102 auch ausgetreten aber VIEL weniger.

TU Graz
Graz University of Technology

INSTITUT FÜR BODENMECHANIK UND GRUNDBAU
GEOTECHNISCHES LABOR

RECHBAUERSTRASE 12, 8010 GRAZ, AUSTRIA
Tel: +43(0)316/873-6237 Fax: +43(0)316/873-6238

AUFTRAGGEBER:	BEZEICHNUNG:	LABORNUMMER:
	UHPC with Marble Aggregates	
	BODENART:	PROJEKTNUMMER::
PROJEKT:		268
	BEARBEITER:	DATUM:
Masterarbeit	PEC	23.03.2016

KORNDICHTE ÖNORM B 4413:2010

1	Pyknometer-Nr.				12	110	102
2	Tara	g	m_0	T	48.8564	44.0233	44.669
3	Trockenmasse Probe + Tara	g	m_1	L	68.7509	64.0589	65.0002
4	Trockenmasse Probe	g	m_2	3-2	19.8945	20.0356	20.3312
5	Masse Pyknometer + Wasser + Probe (unter Auftrieb) bei t °C	g	m_3	L	161.6473	156.3671	156.2752
6	Versuchstemperatur Probe + Wasser	°C	t	L	23	23.35	23.25
7	Temperaturkorrektur von 20° zu t °C	g	Δm	T	-0.0670	-0.074	-0.072
8	Masse Pyknometer + Wasser bei 20 °C	g	m_4	T	149.24338	143.87225	143.6016
9	Masse Pyknometer +Wasser bei t °C	g	m_5	7+8	149.17638	143.79825	143.5296
10	Dichte Wasser bei t °C	g/cm³	ρ_w	T	0.9976	0.9975	0.9975
11	Bodenvolumen	cm³	V_K	$\frac{(9+4-5)}{10}$	7.442	7.485	7.604
12	Korndichte	Mg/m³	ρ_s	$\frac{4}{11}$	2.673	2.677	2.674
13	Mittelwert aus allen Versuchen	Mg/m³	ρs,i.M.		2.67		

ANMERKUNG:

TU Graz
Graz University of Technology

INSTITUT FÜR BODENMECHANIK UND GRUNDBAU
GEOTECHNISCHES LABOR

RECHBAUERSTRASE 12, 8010 GRAZ, AUSTRIA
Tel: +43(0)316/873-6237 Fax: +43(0)316/873-6238

AUFTRAGGEBER:	BEZEICHNUNG:	LABORNUMMER:
	UHPC with Talc Aggregates	
	BODENART:	PROJEKTNUMMER::
PROJEKT:		268
	BEARBEITER:	DATUM:
Masterarbeit	PEC	29.03.2017

KORNDICHTE ÖNORM B 4413:2010

1	Pyknometer-Nr.				25	107	102
2	Tara	g	m_0	T	44.255	43.918	44.673
3	Trockenmasse Probe + Tara	g	m_1	L	64.0118	63.5235	64.5837
4	Trockenmasse Probe	g	m_2	3-2	19.7568	19.6055	19.9107
5	Masse Pyknometer + Wasser + Probe (unter Auftrieb) bei t °C	g	m_3	L	156.5114	156.3082	156.0108
6	Versuchstemperatur Probe + Wasser	°C	t	L	23.3	23	22.7
7	Temperaturkorrektur von 20° zu t °C	g	Δm	T	-0.074	-0.067	-0.06
8	Masse Pyknometer + Wasser bei 20 °C	g	m_4	T	144.19978	144.09436	143.6056
9	Masse Pyknometer +Wasser bei t °C	g	m_5	7+8	144.12578	144.02736	143.5456
10	Dichte Wasser bei t °C	g/cm³	ρ_w	T	0.9975	0.9976	0.9976
11	Bodenvolumen	cm³	V_K	$\frac{(9+4-5)}{10}$	7.390	7.342	7.463
12	Korndichte	Mg/m³	ρ_s	$\frac{4}{11}$	2.674	2.670	2.668
13	Mittelwert aus allen Versuchen	Mg/m³	ρs,i.M.		2.67		

ANMERKUNG:

INSTITUT FÜR BODENMECHANIK UND GRUNDBAU
GEOTECHNISCHES LABOR

RECHBAUERSTRASE 12, 8010 GRAZ, AUSTRIA
Tel: +43(0)316/873-6237 Fax: +43(0)316/873-6238

AUFTRAGGEBER:	BEZEICHNUNG: UHPC with Quartz Aggregates	LABORNUMMER:
	BODENART:	PROJEKTNUMMER:: 268
PROJEKT: Masterarbeit	BEARBEITER: PEC	DATUM: 28.03.2017

KORNDICHTE ÖNORM B 4413:2010

1	Pyknometer-Nr.				116	128	115
2	Tara	g	m_0	T	43.4889	44.5604	45.0608
3	Trockenmasse Probe + Tara	g	m_1	L	63.1539	65.3455	64.7791
4	Trockenmasse Probe	g	m_2	3-2	19.665	20.7851	19.7183
5	Masse Pyknometer + Wasser + Probe (unter Auftrieb) bei t °C	g	m_3	L	155.3742	155.8178	157.1201
6	Versuchstemperatur Probe + Wasser	°C	t	L	21.45	21.6	21.3
7	Temperaturkorrektur von 20° zu t °C	g	Δm	T	-0.03	-0.035	-0.028
8	Masse Pyknometer + Wasser bei 20 °C	g	m_4	T	143.16017	142.92702	144.87182
9	Masse Pyknometer +Wasser bei t °C	g	m_5	7+8	143.13017	142.89202	144.84382
10	Dichte Wasser bei t °C	g/cm³	ρ_w	T	0.9979	0.9979	0.9980
11	Bodenvolumen	cm³	V_K	$\frac{(9+4-5)}{10}$	7.436	7.876	7.457
12	Korndichte	Mg/m³	ρ_s	$\frac{4}{11}$	2.644	2.639	2.644
13	Mittelwert aus allen Versuchen	Mg/m³	ρs,i.M.		2.64		

ANMERKUNG:

Anhang B

Gruppe **G**eotechnik **G**raz
TU-Graz
Labor für Felsmechanik und Tunnelbau

Rechbauerstraße 12, A-8010 Graz
Tel: ++43-316/873-8114
Fax: ++43-316/873-8618
e-mail: tunnel@tugraz.at

Projekt: Versuche Angelika Überwimmer *GZ:* 95268

Auftraggeber: Institut für Felsmechanik

Labornr.:	268.18	*Bezeichnung:*
Länge [mm]:	101,8	
Durchmesser [mm]:	50,6	
Gewicht [g]:	492,1	
Dichte [kg/dm³]:	2,405	

Versuchsanordnung: Einaxialer Druckversuch

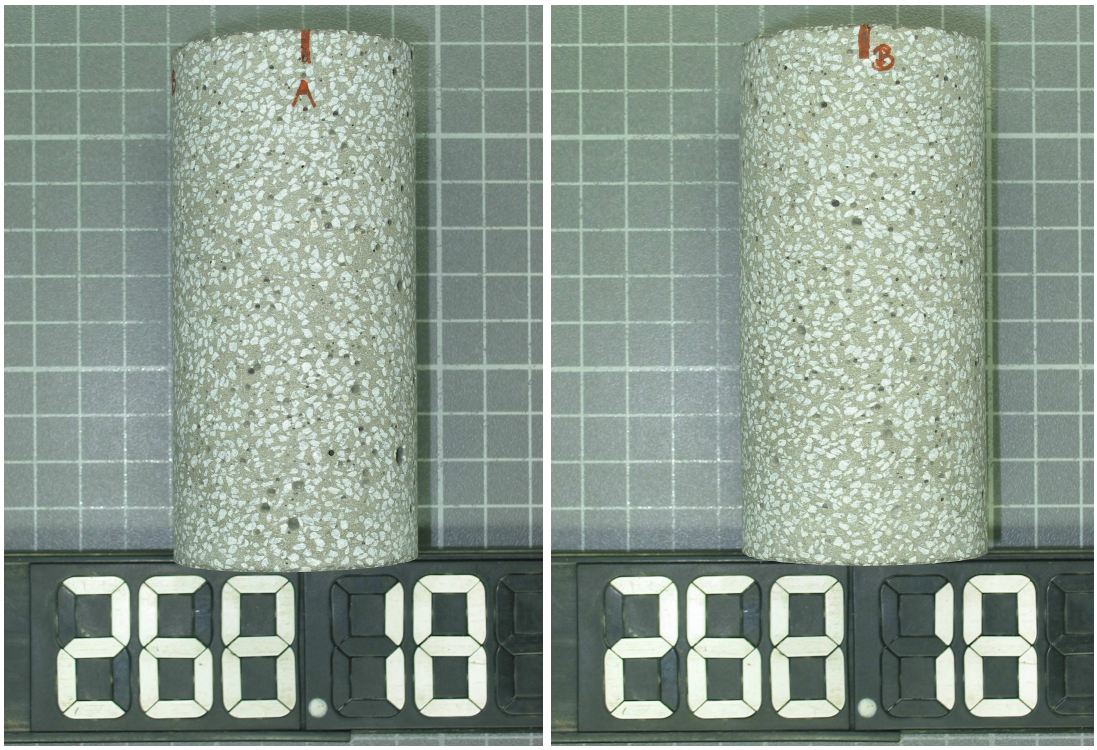

Abbildungen: Probe vor Versuch in Richtung A bzw. B

Gruppe **G**eotechnik **G**raz
TU-Graz
Labor für Felsmechanik und Tunnelbau

Rechbauerstraße 12, A-8010 Graz
Tel: ++43-316/873-8114
Fax: ++43-316/873-8618
e-mail: tunnel@tugraz.at

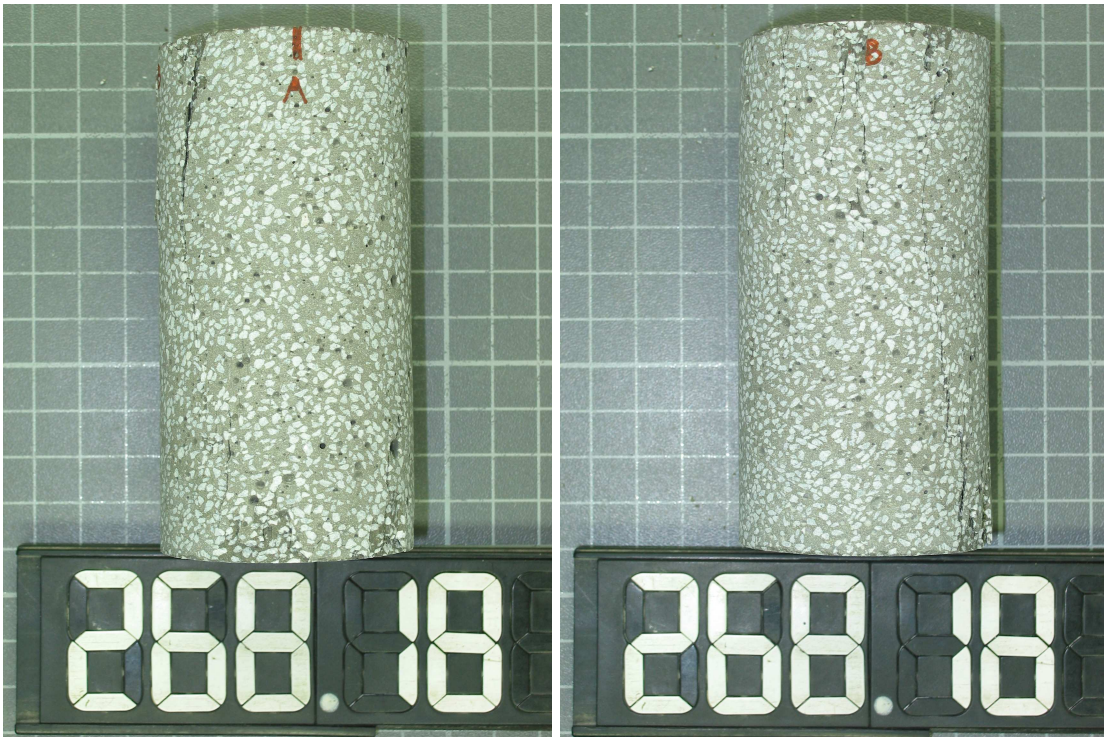

Abbildungen: Probe nach Versuch in Richtung A bzw. B

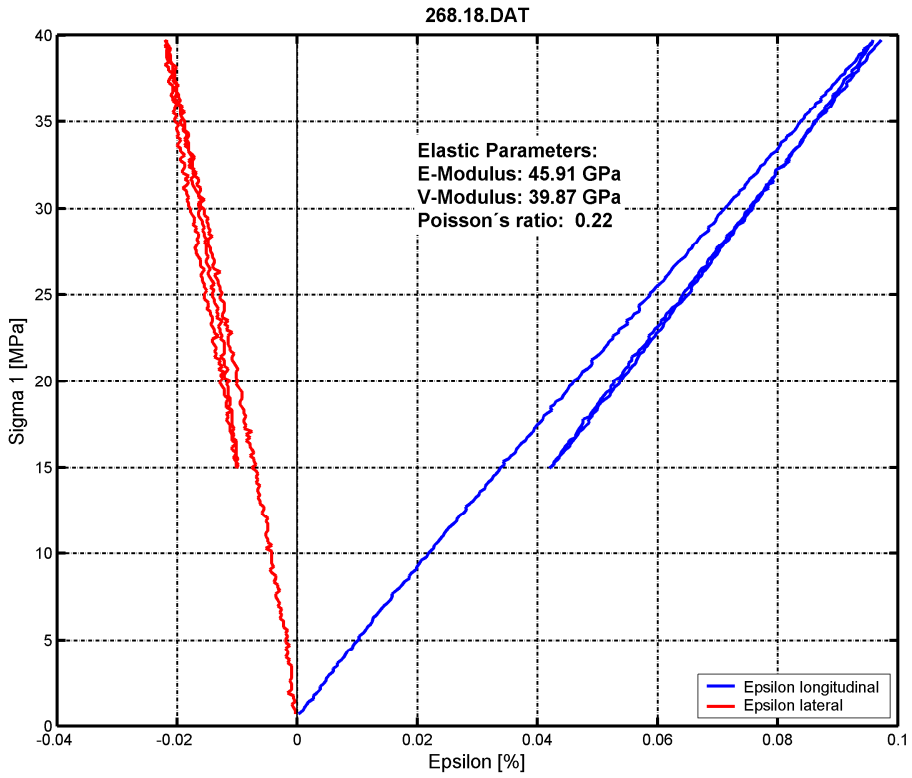

Gruppe Geotechnik Graz
TU-Graz
Labor für Felsmechanik und Tunnelbau

Rechbauerstraße 12, A-8010 Graz
Tel: ++43-316/873-8114
Fax: ++43-316/873-8618
e-mail: tunnel@tugraz.at

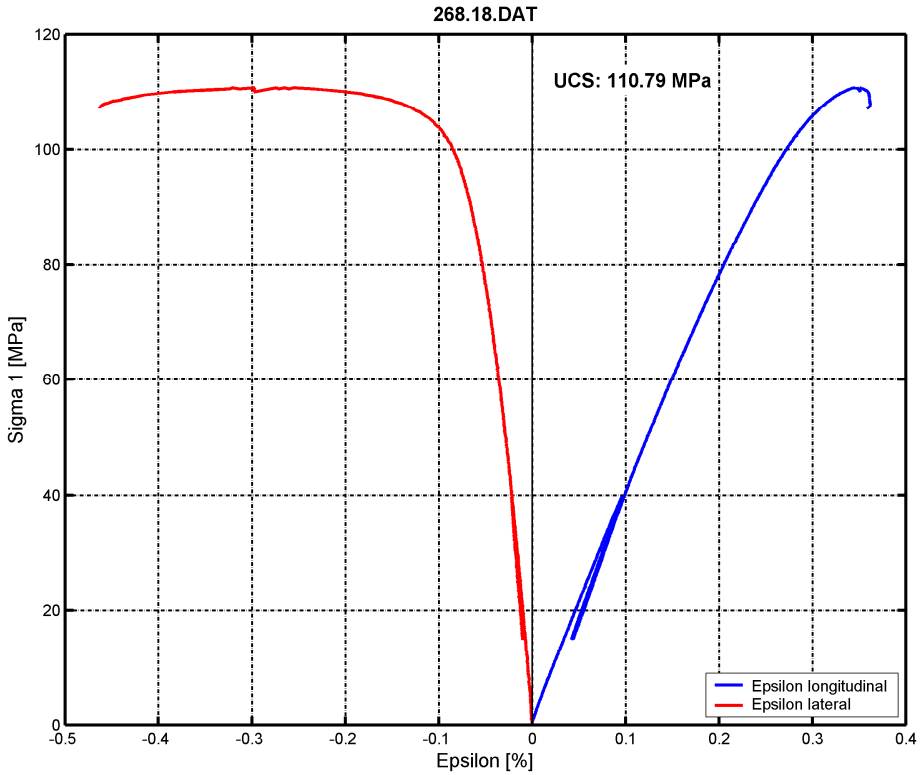

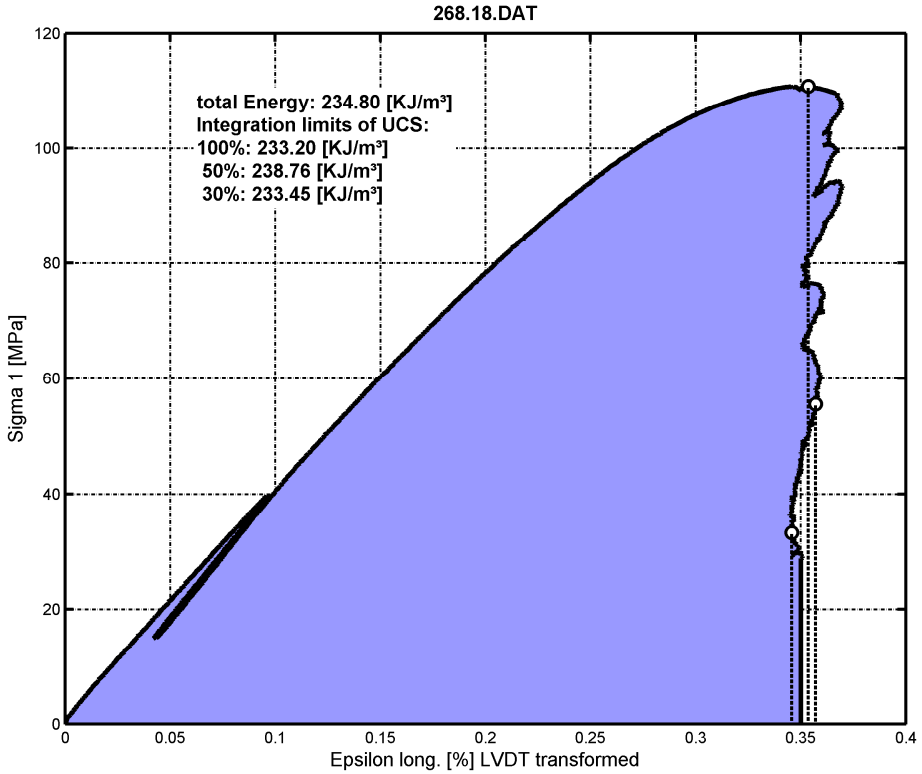

Gruppe **G**eotechnik **G**raz
TU-Graz
Labor für Felsmechanik und Tunnelbau

Rechbauerstraße 12, A-8010 Graz
Tel: ++43-316/873-8114
Fax: ++43-316/873-8618
e-mail: tunnel@tugraz.at

Projekt: Versuche Angelika Überwimmer *GZ:* 95268

Auftraggeber: Institut für Felsmechanik

Labornr.:	268.19	*Bezeichnung:*
Länge [mm]:	101,9	
Durchmesser [mm]:	50,6	
Gewicht [g]:	476,0	
Dichte [kg/dm³]:	2,322	

Versuchsanordnung: Einaxialer Druckversuch

Abbildungen: Probe vor Versuch in Richtung A bzw. B

Gruppe **G**eotechnik **G**raz
TU-Graz
Labor für Felsmechanik und Tunnelbau

Rechbauerstraße 12, A-8010 Graz
Tel: ++43-316/873-8114
Fax: ++43-316/873-8618
e-mail: tunnel@tugraz.at

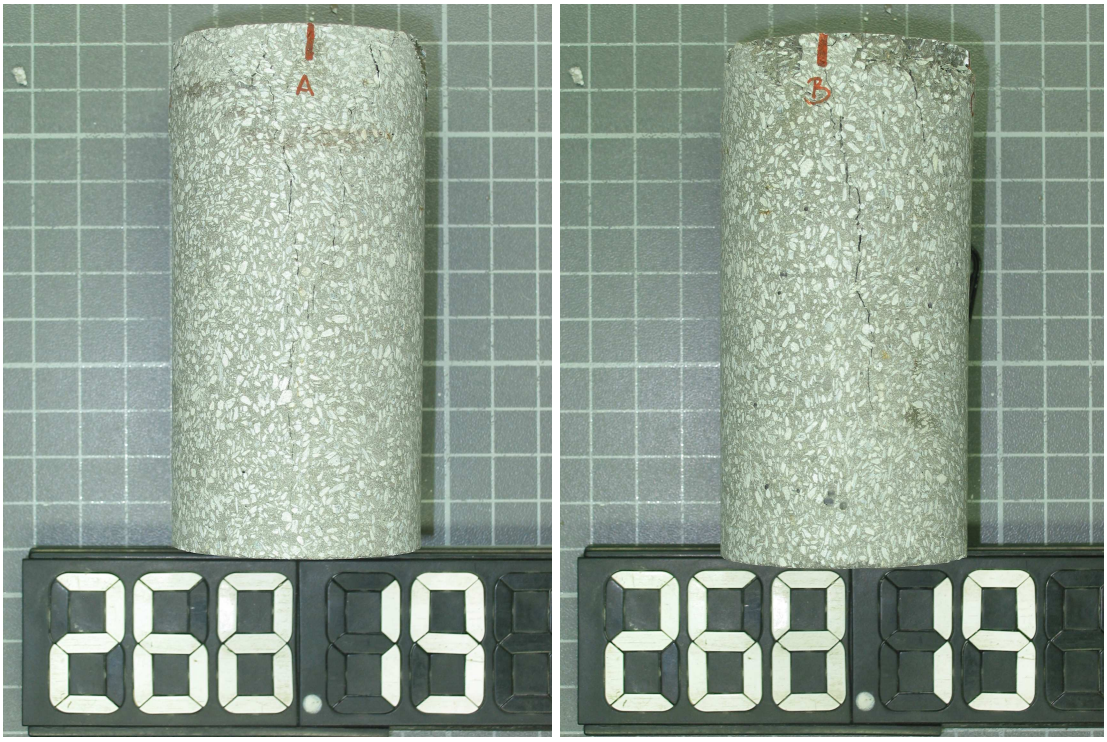

Abbildungen: Probe nach Versuch in Richtung A bzw. B

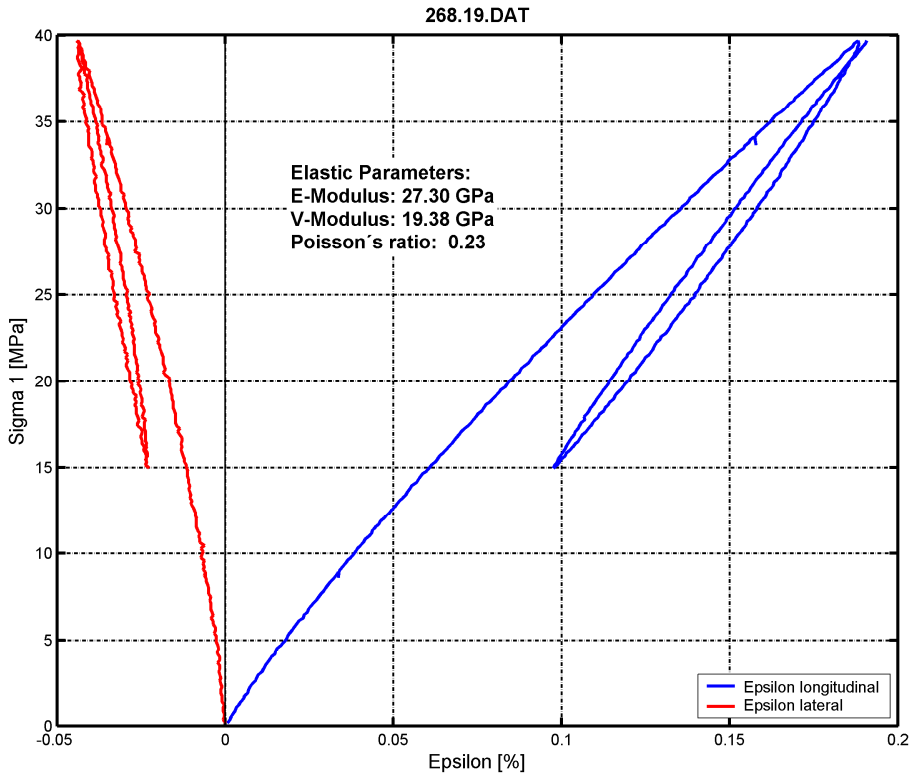

Gruppe **G**eotechnik **G**raz
TU-Graz
Labor für Felsmechanik und Tunnelbau

Rechbauerstraße 12, A-8010 Graz
Tel: ++43-316/873-8114
Fax: ++43-316/873-8618
e-mail: tunnel@tugraz.at

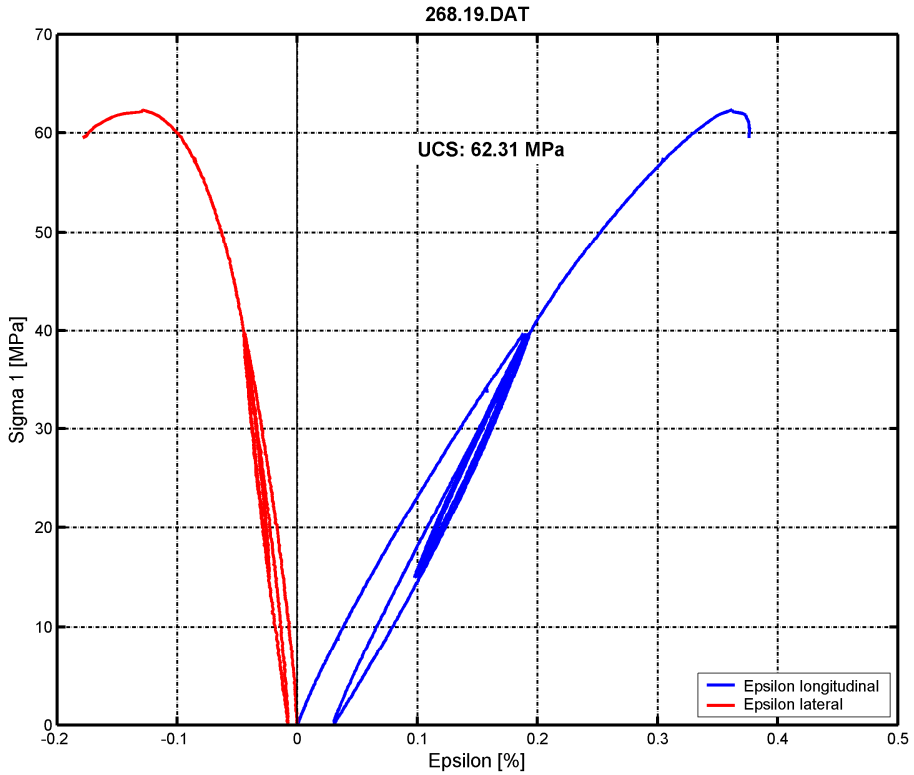

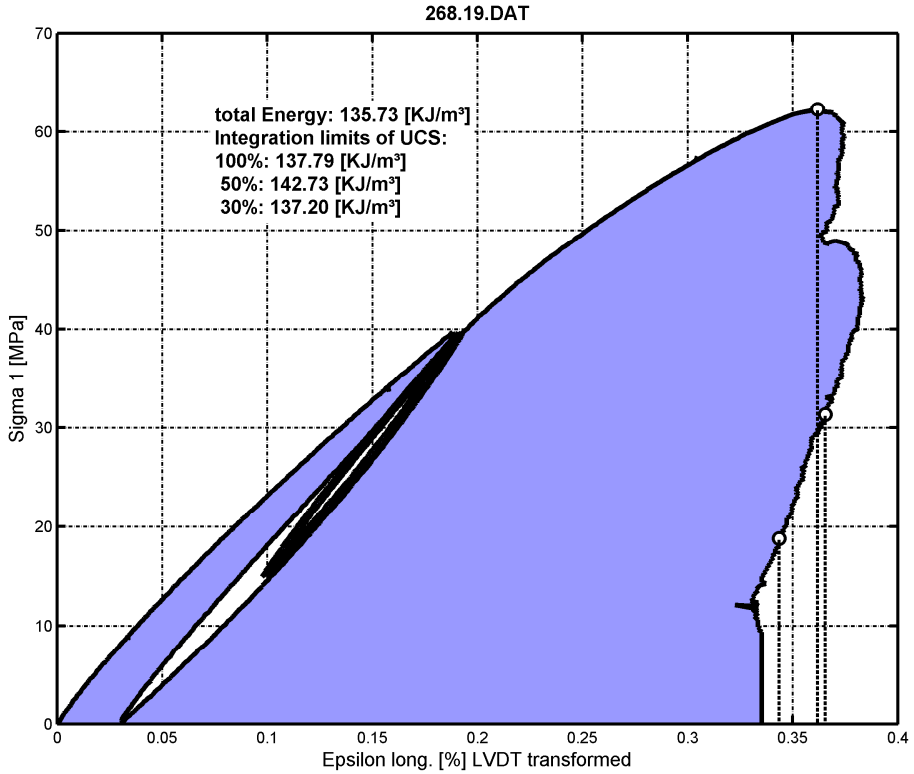

Gruppe **G**eotechnik **G**raz
TU-Graz
Labor für Felsmechanik und Tunnelbau

Rechbauerstraße 12, A-8010 Graz
Tel: ++43-316/873-8114
Fax: ++43-316/873-8618
e-mail: tunnel@tugraz.at

Projekt: Versuche Angelika Überwimmer *GZ:* 95268

Auftraggeber: Institut für Felsmechanik

Labornr.:	268.20	*Bezeichnung:*
Länge [mm]:	94,6	
Durchmesser [mm]:	50,6	
Gewicht [g]:	432,8	
Dichte [kg/dm³]:	2,276	

Versuchsanordnung: Einaxialer Druckversuch

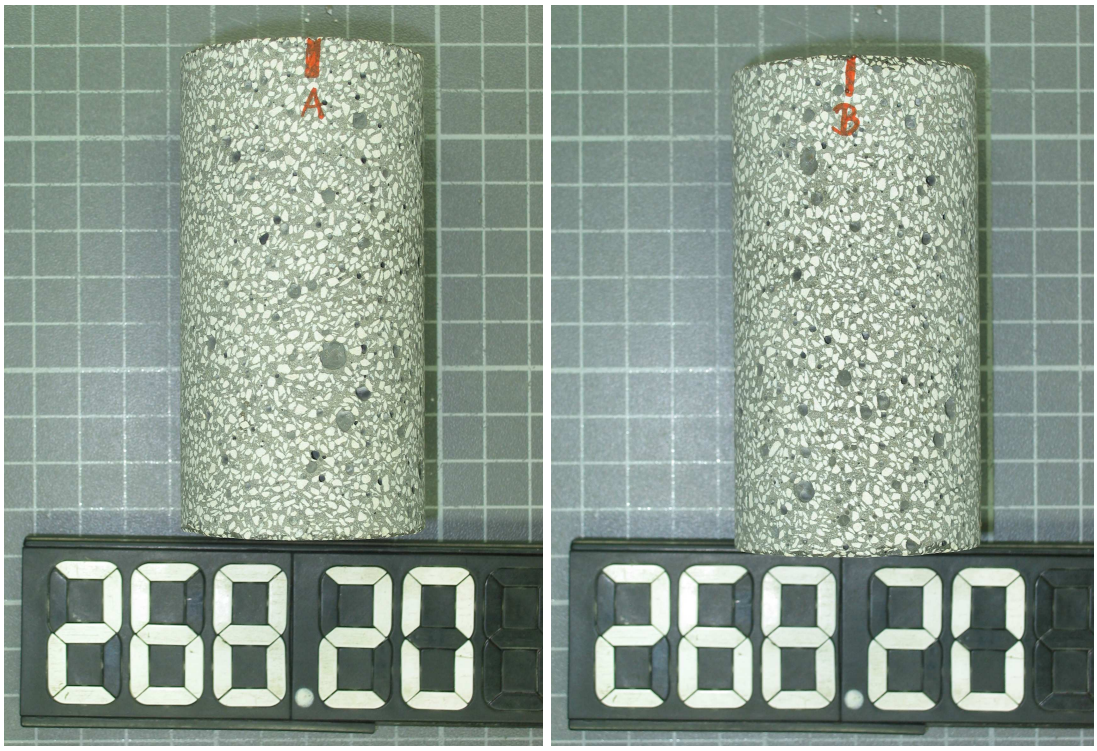

Abbildungen: Probe vor Versuch in Richtung A bzw. B

Gruppe **G**eotechnik **G**raz
TU-Graz
Labor für Felsmechanik und Tunnelbau

Rechbauerstraße 12, A-8010 Graz
Tel: ++43-316/873-8114
Fax: ++43-316/873-8618
e-mail: tunnel@tugraz.at

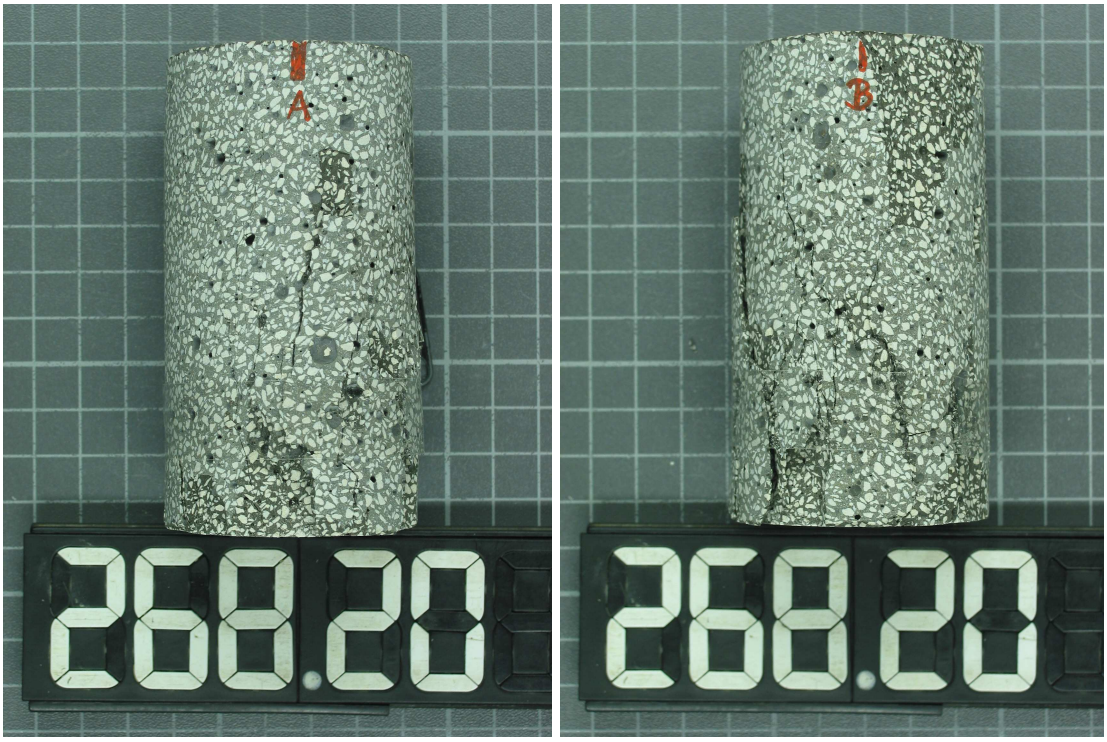

Abbildungen: Probe nach Versuch in Richtung A bzw. B

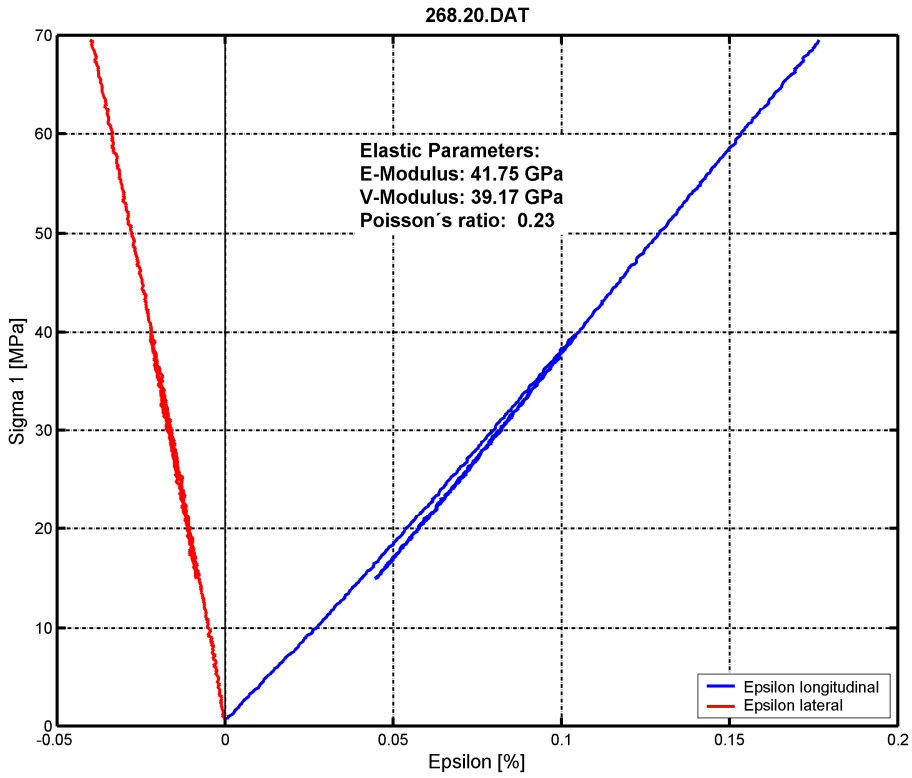

Gruppe **G**eotechnik **G**raz
TU-Graz
Labor für Felsmechanik und Tunnelbau

Rechbauerstraße 12, A-8010 Graz
Tel: ++43-316/873-8114
Fax: ++43-316/873-8618
e-mail: tunnel@tugraz.at

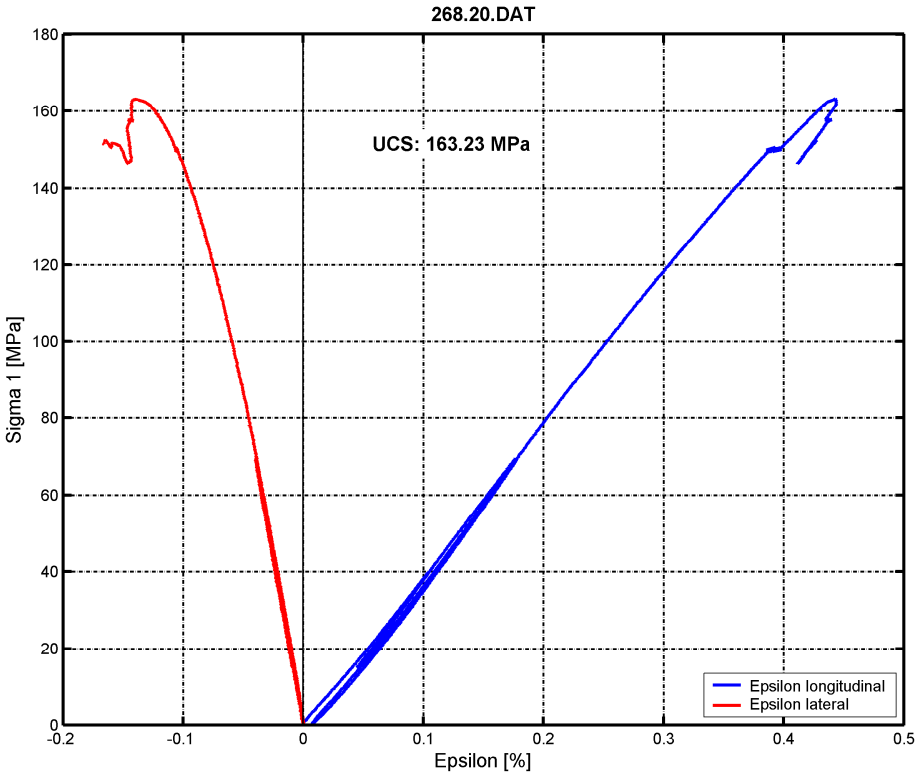

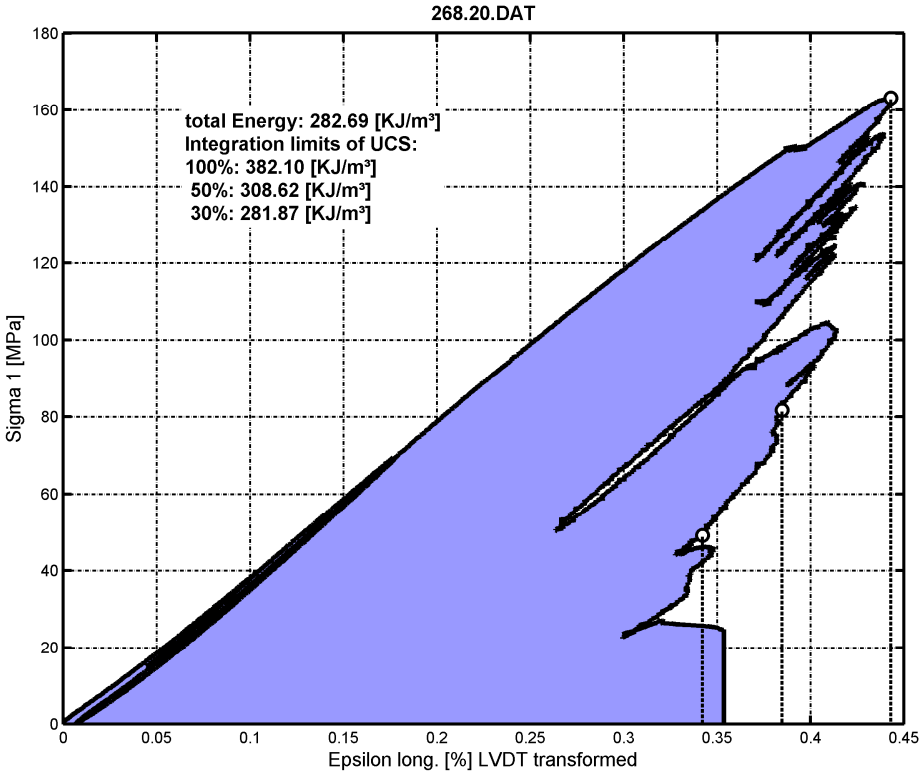

Gruppe **G**eotechnik **G**raz
TU-Graz
Labor für Felsmechanik und Tunnelbau

Rechbauerstraße 12, A-8010 Graz
Tel: ++43-316/873-8114
Fax: ++43-316/873-8618
e-mail: tunnel@tugraz.at

Projekt: Versuche Angelika Überwimmer *GZ:* 95268

Auftraggeber: Institut für Felsmechanik

Labornr.:	268.21	*Bezeichnung:*
Länge [mm]:	101,9	
Durchmesser [mm]:	50,6	
Gewicht [g]:	489,3	
Dichte [kg/dm³]:	2,386	

Versuchsanordnung: Einaxialer Druckversuch

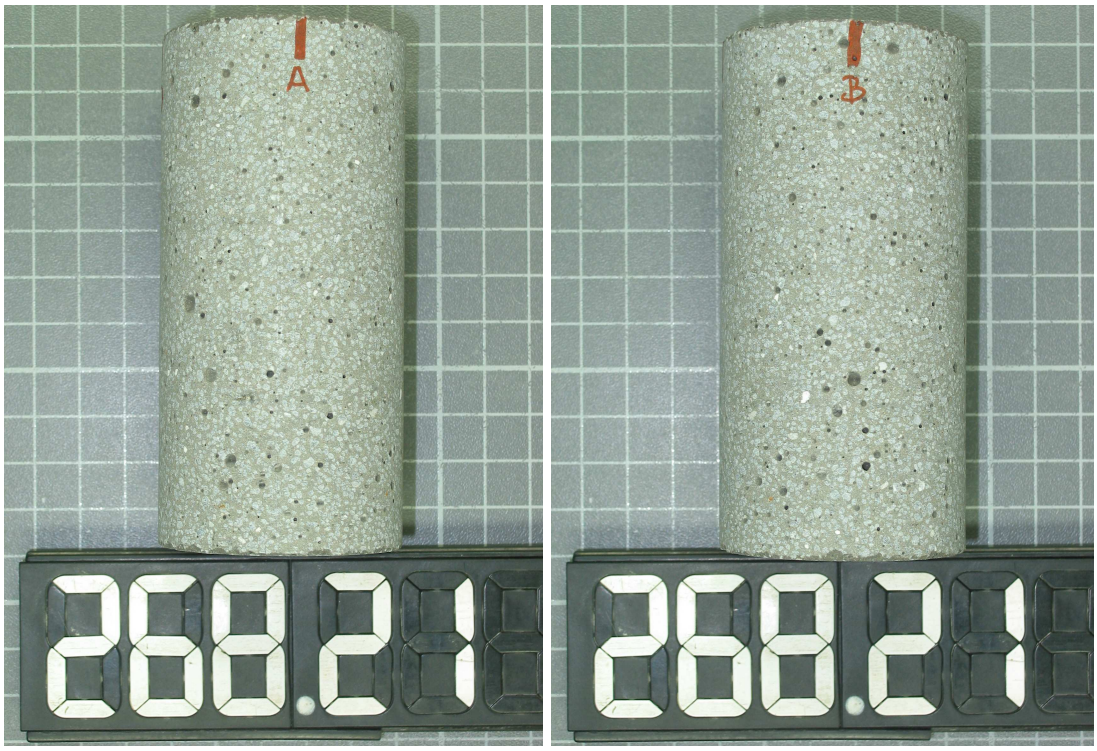

Abbildungen: Probe vor Versuch in Richtung A bzw. B

Gruppe **G**eotechnik **G**raz
TU-Graz
Labor für Felsmechanik und Tunnelbau

Rechbauerstraße 12, A-8010 Graz
Tel: ++43-316/873-8114
Fax: ++43-316/873-8618
e-mail: tunnel@tugraz.at

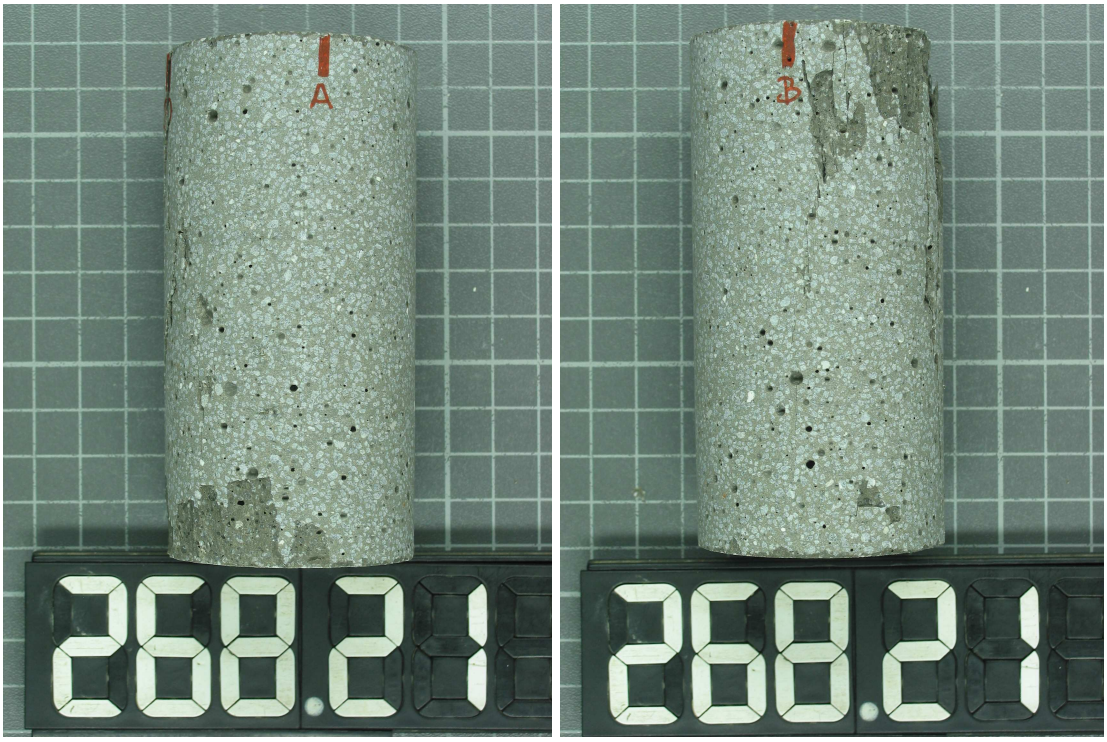

Abbildungen: Probe nach Versuch in Richtung A bzw. B

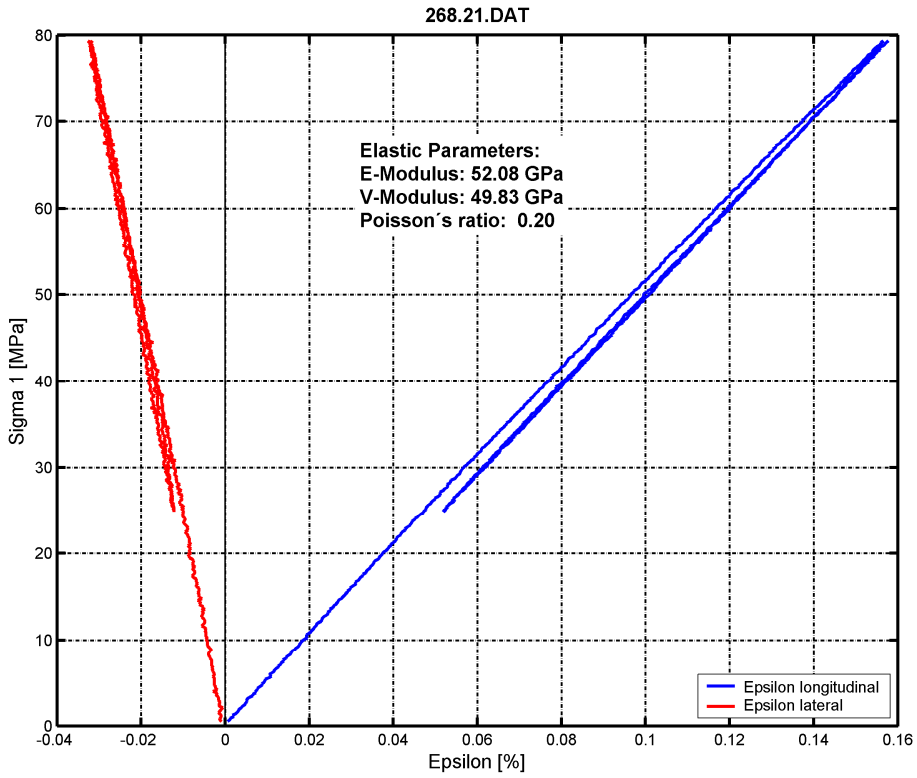

Gruppe **G**eotechnik **G**raz
TU-Graz
Labor für Felsmechanik und Tunnelbau

Rechbauerstraße 12, A-8010 Graz
Tel: ++43-316/873-8114
Fax: ++43-316/873-8618
e-mail: tunnel@tugraz.at

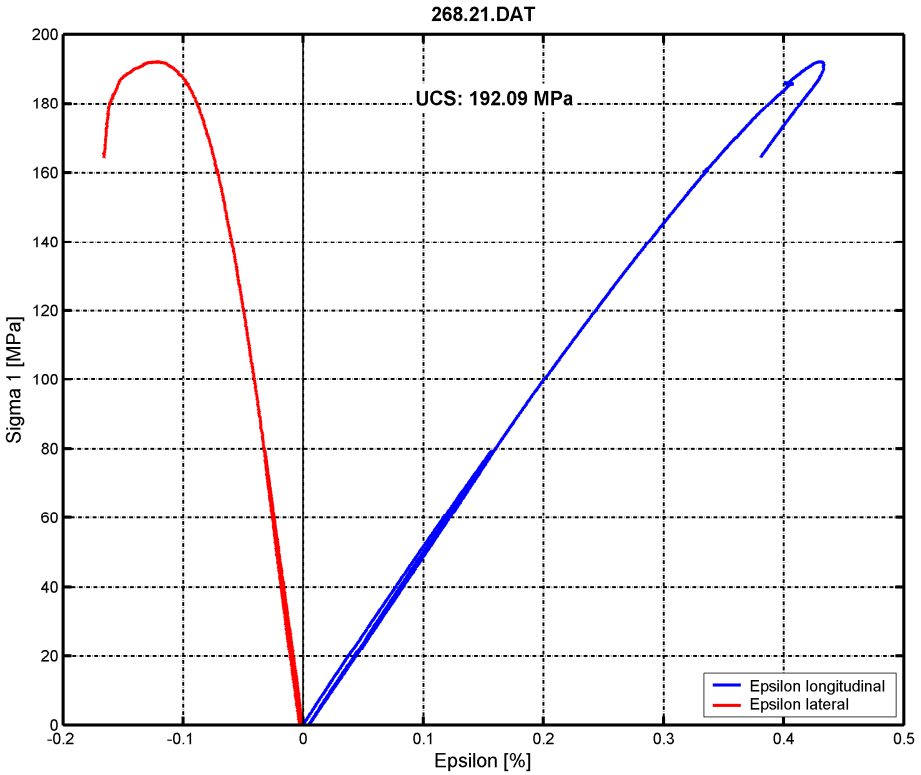

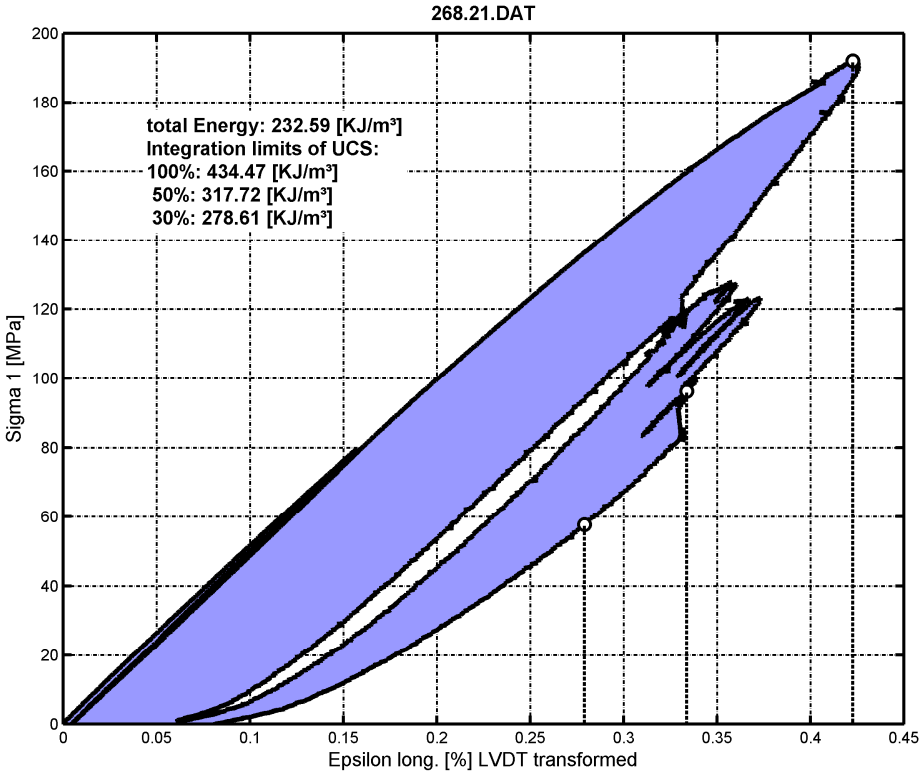

Gruppe **G**eotechnik **G**raz
TU-Graz
Labor für Felsmechanik und Tunnelbau

Rechbauerstraße 12, A-8010 Graz
Tel: ++43-316/873-8114
Fax: ++43-316/873-8618
e-mail: tunnel@tugraz.at

Projekt: Versuche Angelika Überwimmer *GZ:* 95268

Auftraggeber: Institut für Felsmechanik

Labornr.:	268.22	*Bezeichnung:*
Länge [mm]:	101,4	
Durchmesser [mm]:	50,6	
Gewicht [g]:	476,1	
Dichte [kg/dm³]:	2,332	

Versuchsanordnung: Einaxialer Druckversuch

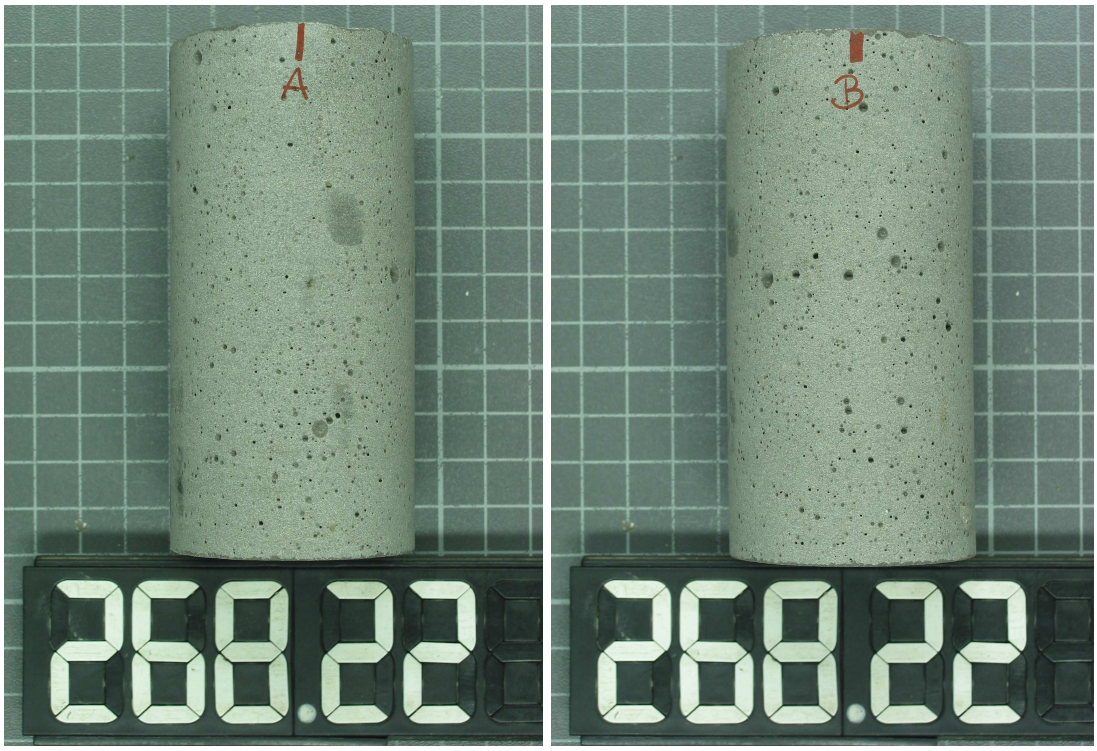

Abbildungen: Probe vor Versuch in Richtung A bzw. B

Gruppe **G**eotechnik **G**raz
TU-Graz
Labor für Felsmechanik und Tunnelbau

Rechbauerstraße 12, A-8010 Graz
Tel: ++43-316/873-8114
Fax: ++43-316/873-8618
e-mail: tunnel@tugraz.at

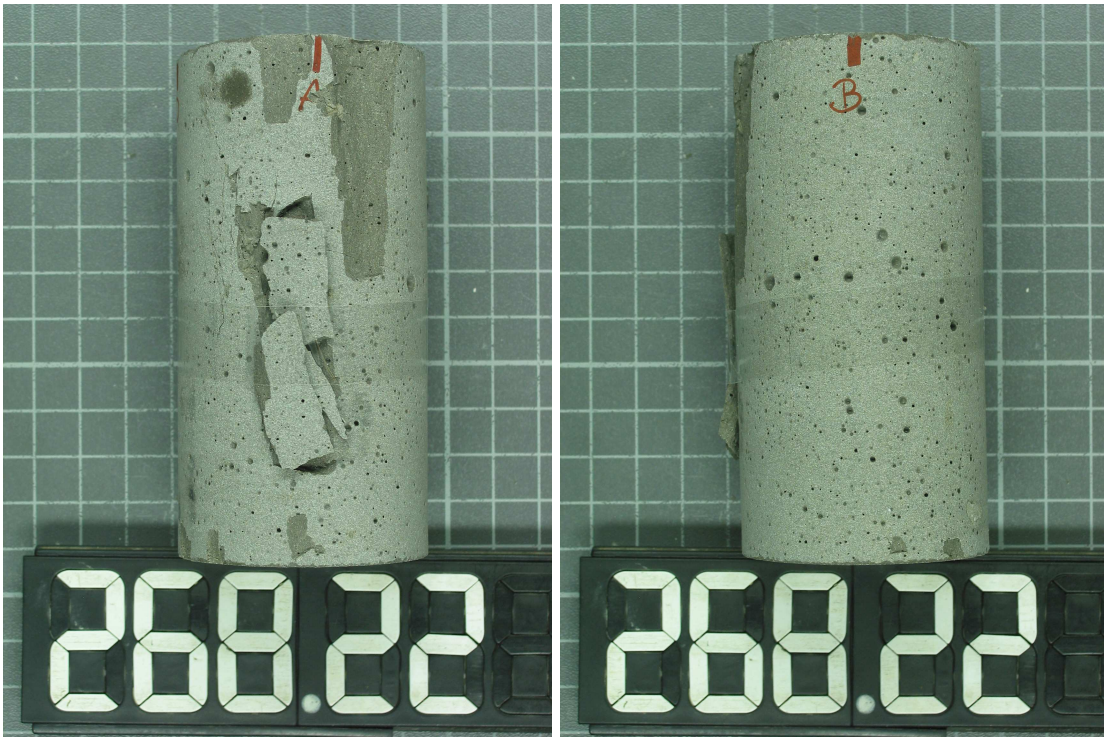

Abbildungen: Probe nach Versuch in Richtung A bzw. B

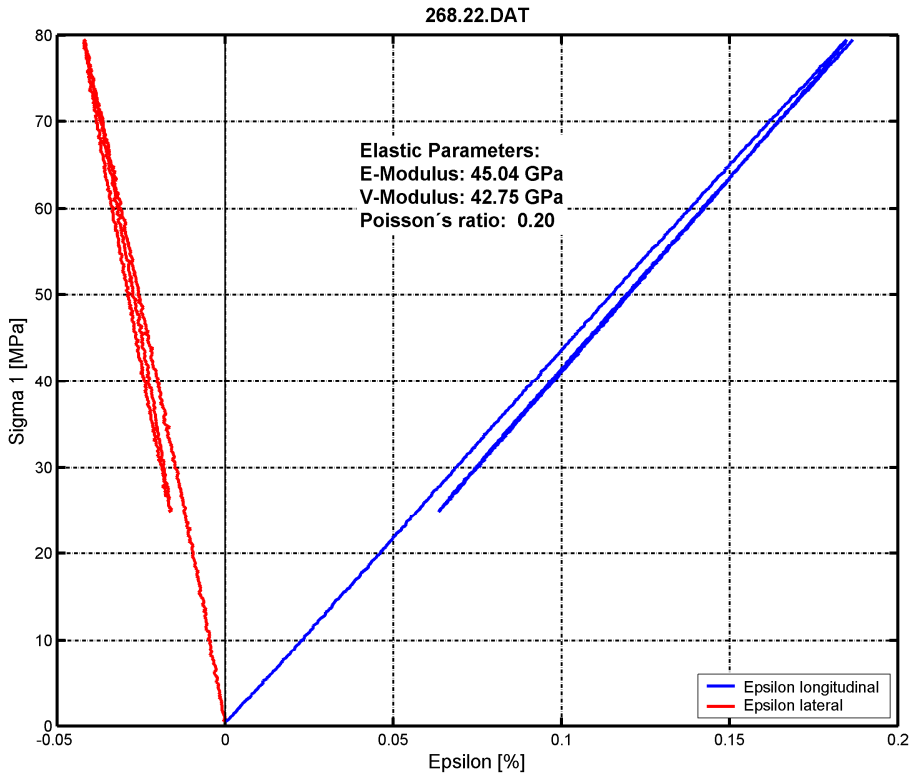

Gruppe Geotechnik Graz
TU-Graz
Labor für Felsmechanik und Tunnelbau

Rechbauerstraße 12, A-8010 Graz
Tel: ++43-316/873-8114
Fax: ++43-316/873-8618
e-mail: tunnel@tugraz.at

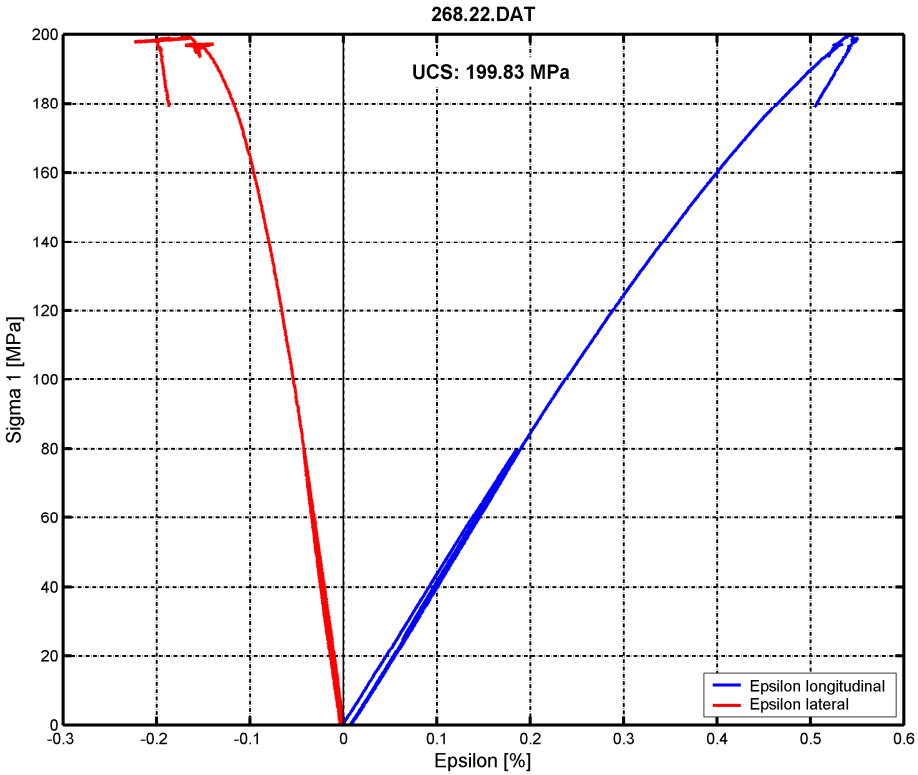

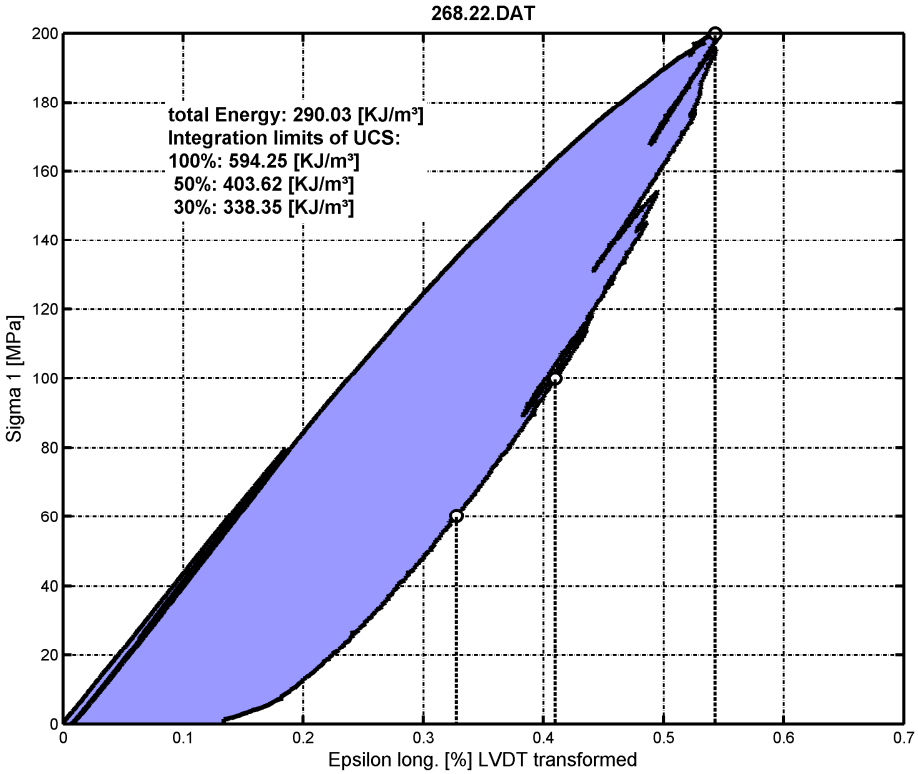

Gruppe **G**eotechnik **G**raz
TU-Graz
Labor für Felsmechanik und Tunnelbau

Rechbauerstraße 12, A-8010 Graz
Tel: ++43-316/873-8114
Fax: ++43-316/873-8618
e-mail: tunnel@tugraz.at

Projekt: Versuche Angelika Überwimmer *GZ:* 95268

Auftraggeber: Institut für Felsmechanik

Labornr.:	268.23	*Dichte [kg/dm³]:*	2,45
Länge [mm]:	101,83	*Lithologie :*	
Durchmesser [mm]:	50,77		
Gewicht [g]:	505,1		

Versuchsanordnung: Einaxialer Druckversuch

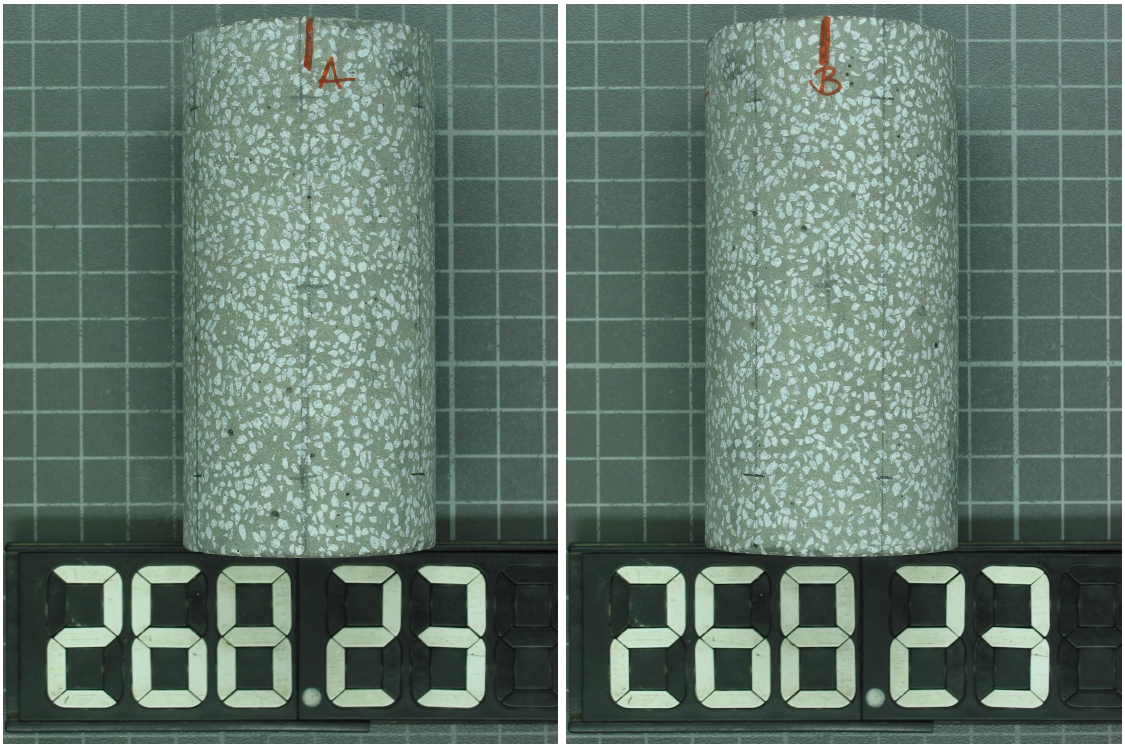

Abbildungen: Probe vor Versuch in Richtung A bzw. B

Gruppe **G**eotechnik **G**raz
TU-Graz
Labor für Felsmechanik und Tunnelbau

Rechbauerstraße 12, A-8010 Graz
Tel: ++43-316/873-8114
Fax: ++43-316/873-8618
e-mail: tunnel@tugraz.at

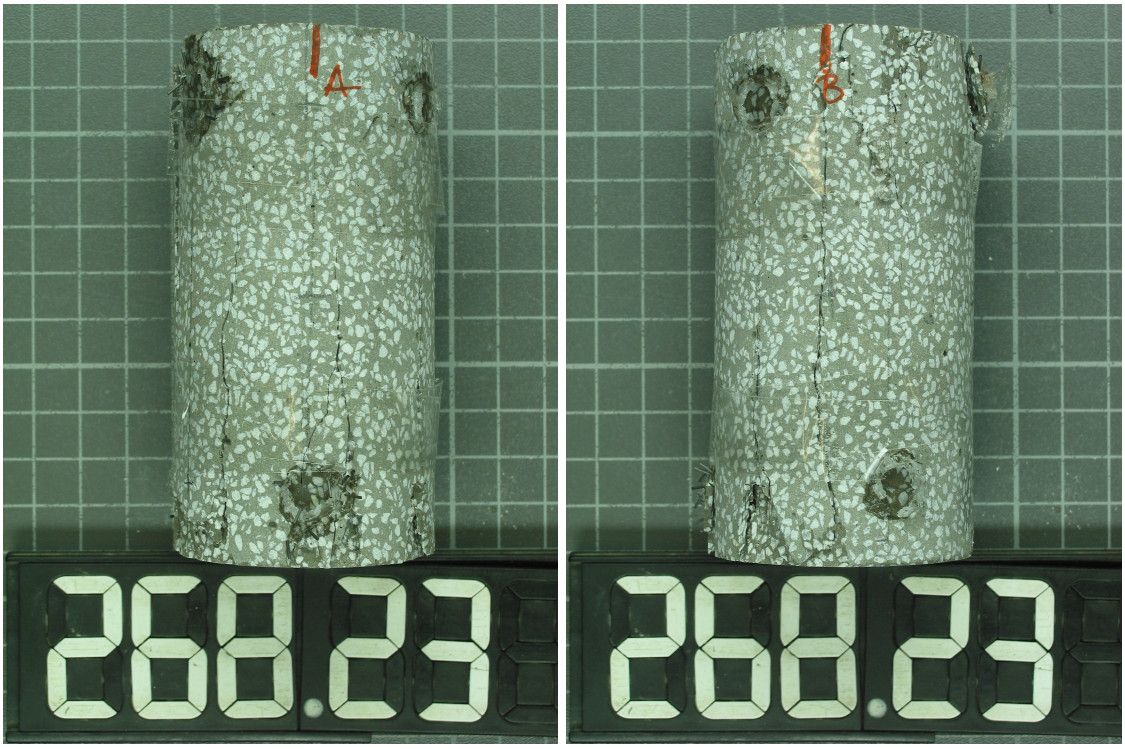

Abbildungen: Probe nach Versuch in Richtung A bzw. B

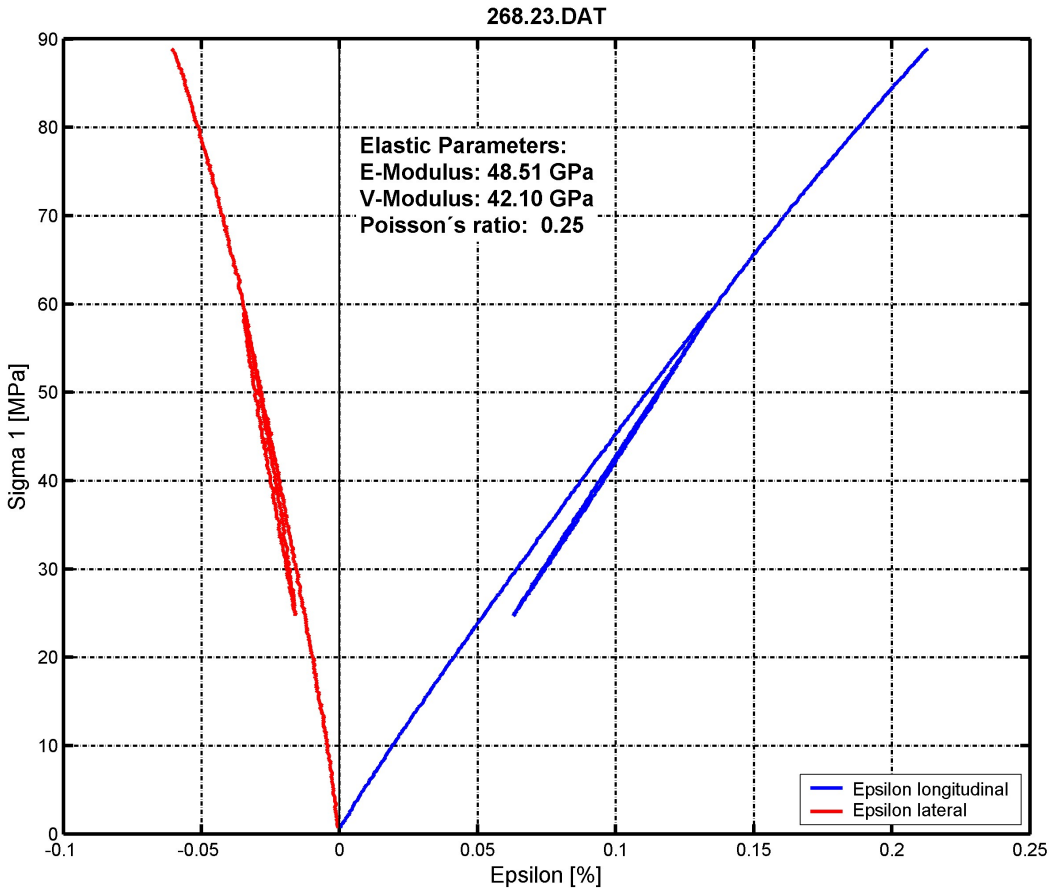

Gruppe **G**eotechnik **G**raz
TU-Graz
Labor für Felsmechanik und Tunnelbau

Rechbauerstraße 12, A-8010 Graz
Tel: ++43-316/873-8114
Fax: ++43-316/873-8618
e-mail: tunnel@tugraz.at

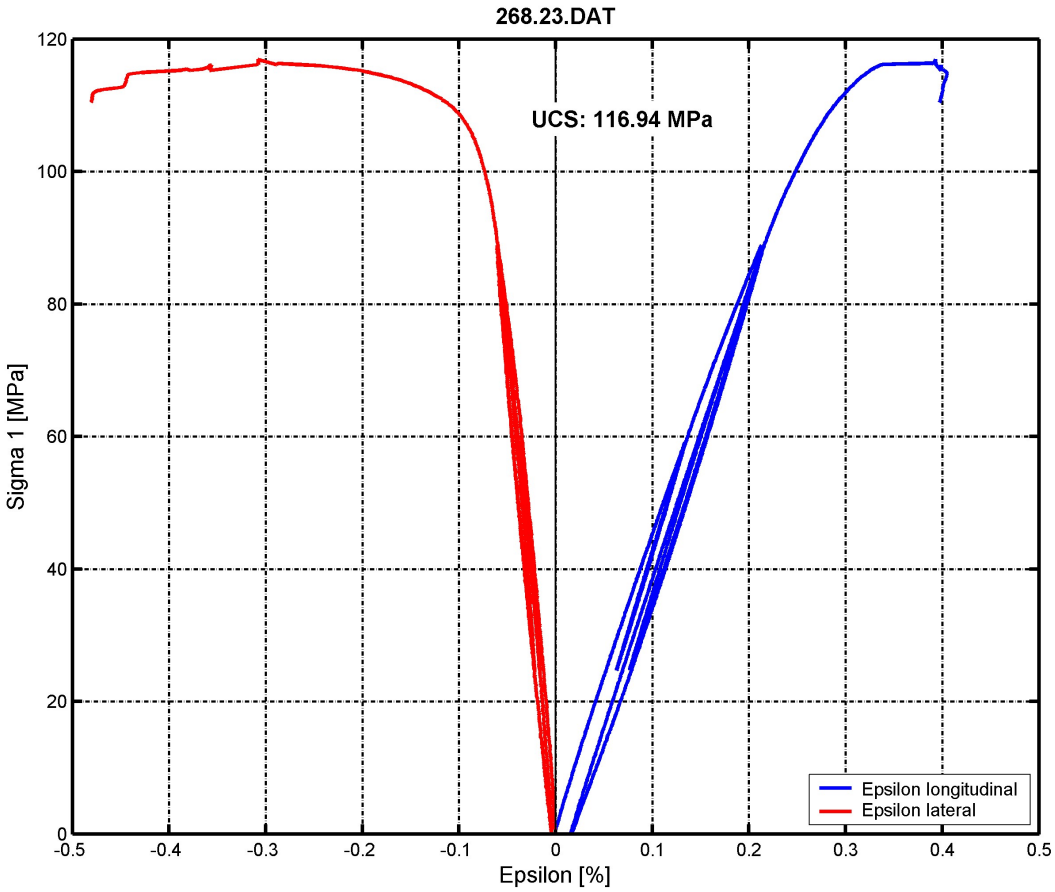

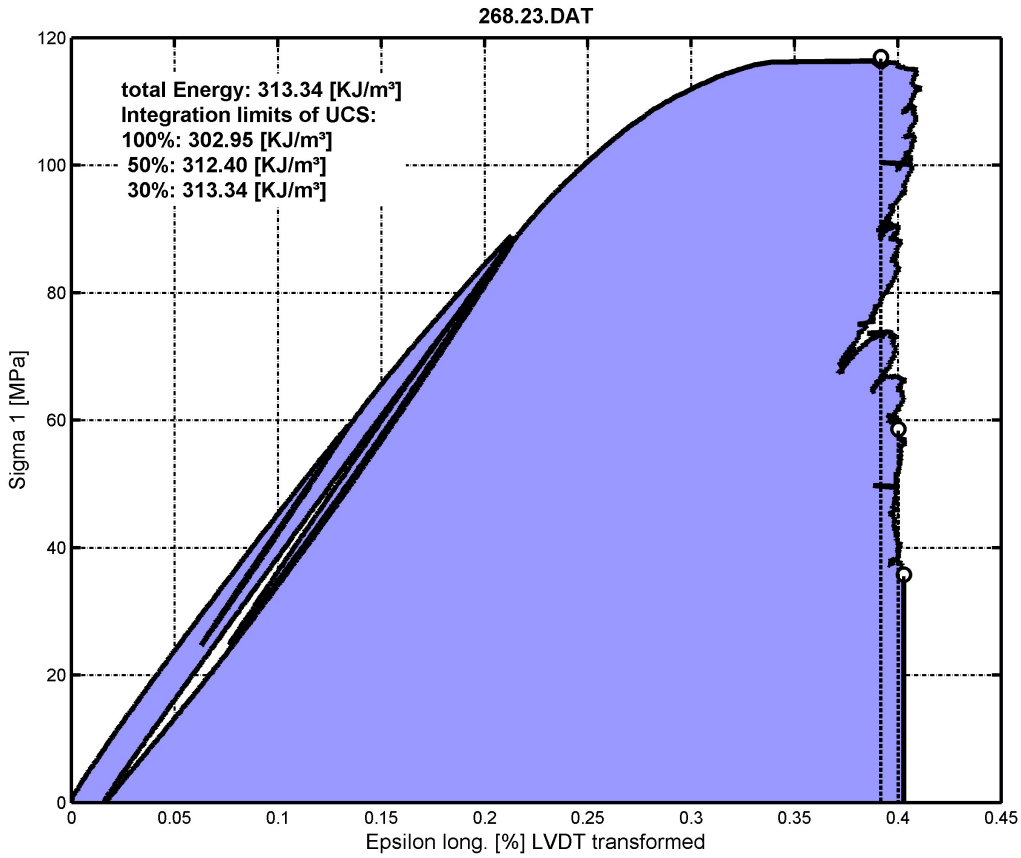

Gruppe **G**eotechnik **G**raz
TU-Graz
Labor für Felsmechanik und Tunnelbau

Rechbauerstraße 12, A-8010 Graz
Tel: ++43-316/873-8114
Fax: ++43-316/873-8618
e-mail: tunnel@tugraz.at

Projekt: Versuche Angelika Überwimmer *GZ:* 95268

Auftraggeber: Institut für Felsmechanik

Labornr.:	268.24	*Dichte [kg/dm³]:*	2,45
Länge [mm]:	101,87	*Lithologie :*	
Durchmesser [mm]:	50,75		
Gewicht [g]:	505,4		

Versuchsanordnung: Einaxialer Druckversuch

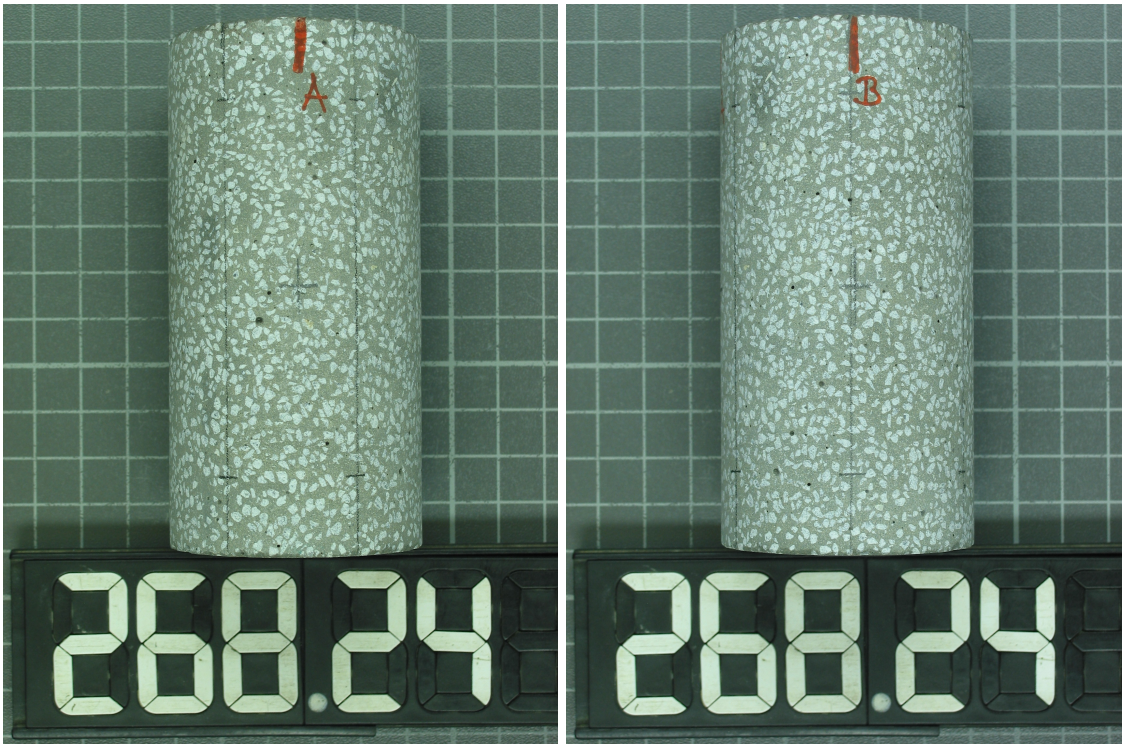

Abbildungen: Probe vor Versuch in Richtung A bzw. B

Gruppe **G**eotechnik **G**raz
TU-Graz
Labor für Felsmechanik und Tunnelbau

Rechbauerstraße 12, A-8010 Graz
Tel: ++43-316/873-8114
Fax: ++43-316/873-8618
e-mail: tunnel@tugraz.at

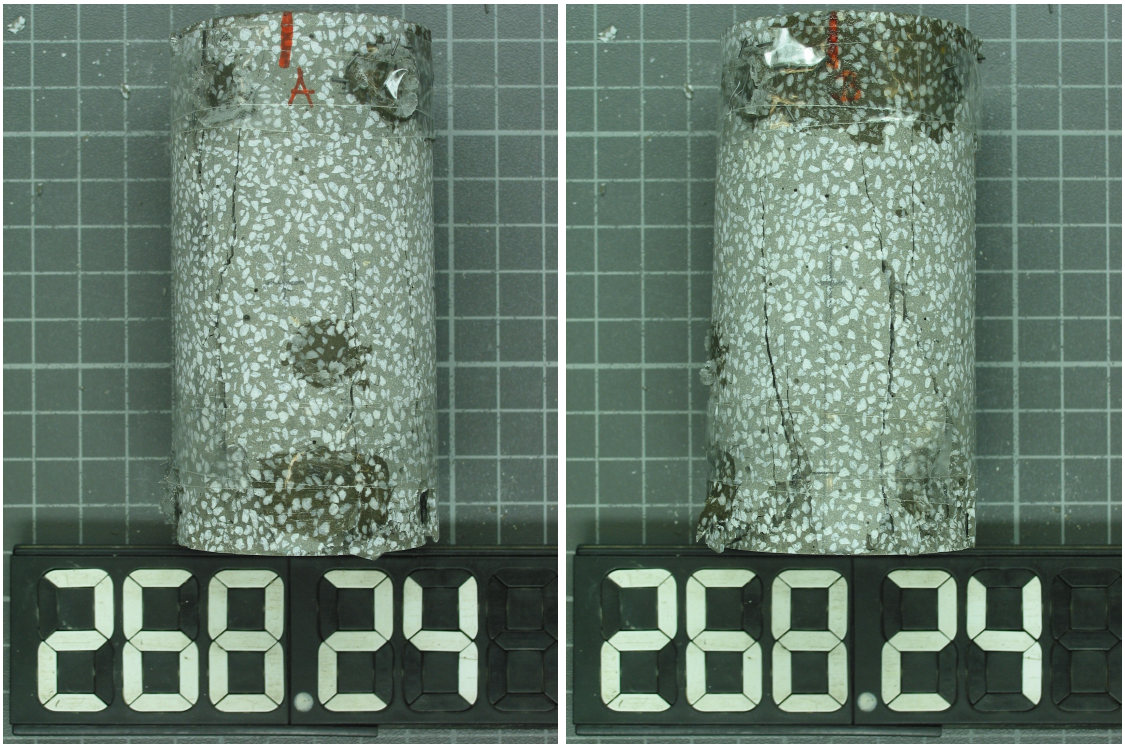

Abbildungen: Probe nach Versuch in Richtung A bzw. B

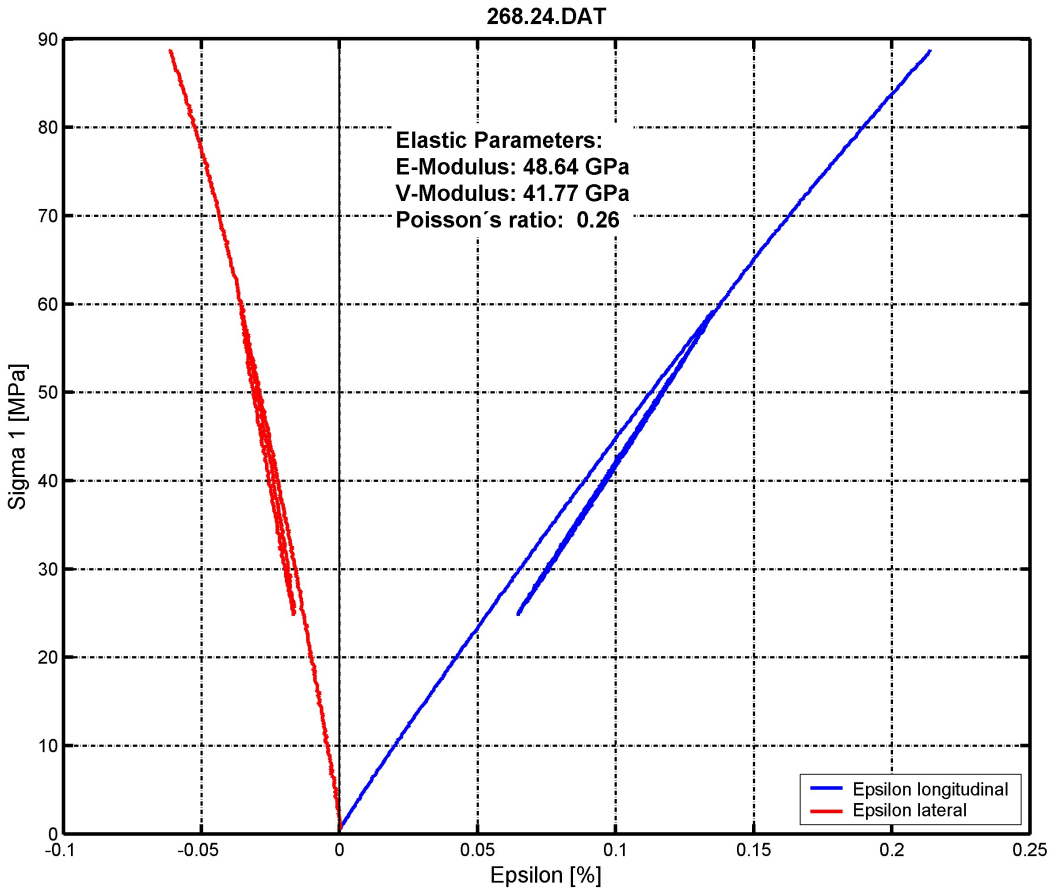

Gruppe **G**eotechnik **G**raz
TU-Graz
Labor für Felsmechanik und Tunnelbau

Rechbauerstraße 12, A-8010 Graz
Tel: ++43-316/873-8114
Fax: ++43-316/873-8618
e-mail: tunnel@tugraz.at

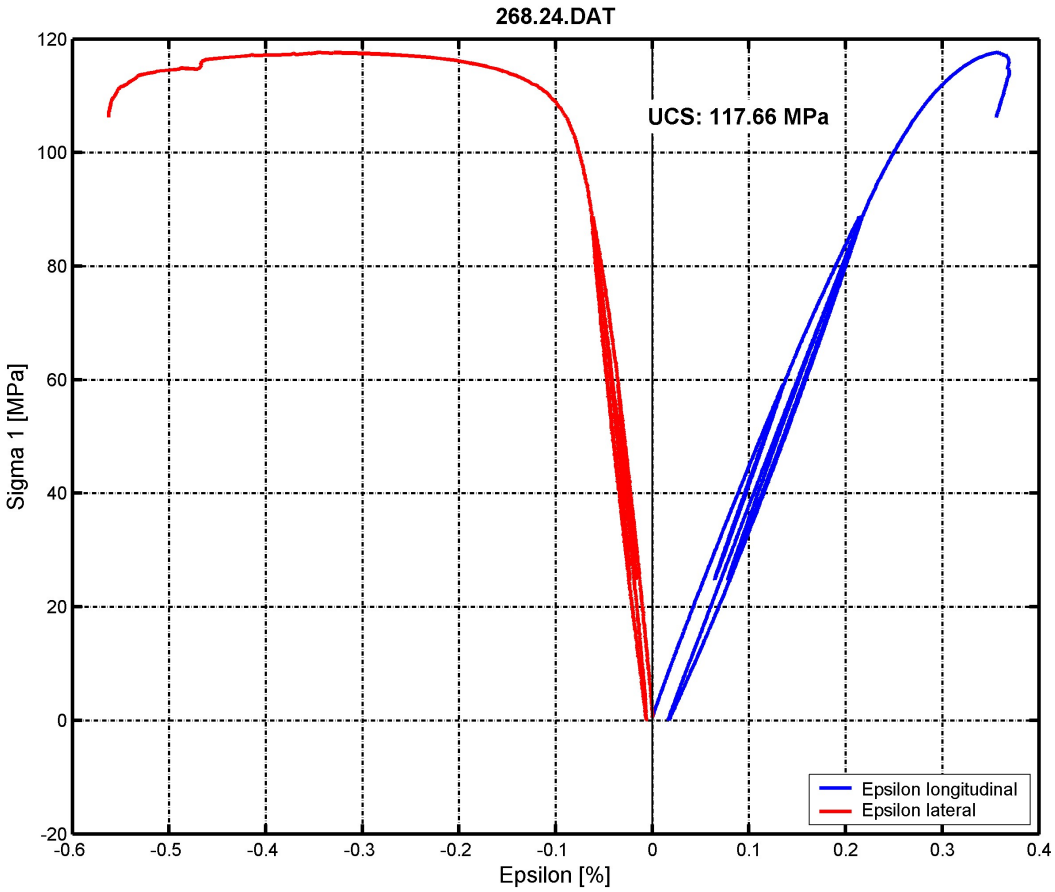

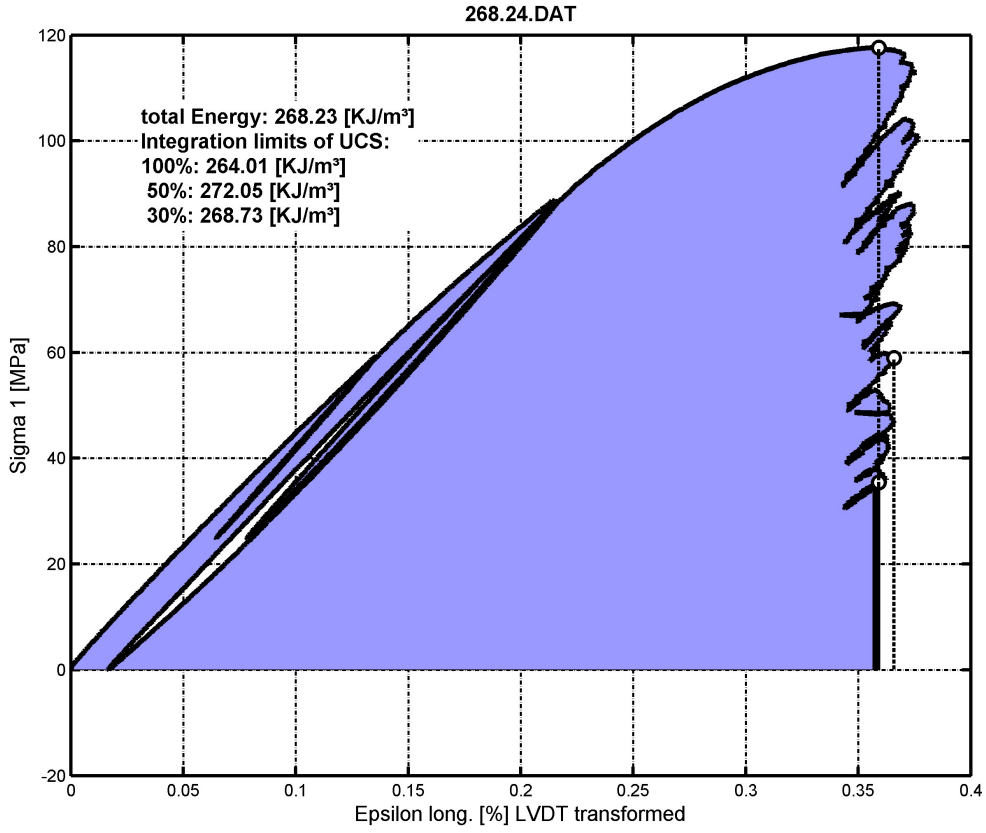

Gruppe **G**eotechnik **G**raz
TU-Graz
Labor für Felsmechanik und Tunnelbau

Rechbauerstraße 12, A-8010 Graz
Tel: ++43-316/873-8114
Fax: ++43-316/873-8618
e-mail: tunnel@tugraz.at

Projekt: Versuche Angelika Überwimmer *GZ:* 95268

Auftraggeber: Institut für Felsmechanik

Labornr.:	268.25	*Dichte [kg/dm³]:*	2,271
Länge [mm]:	102,7	*Lithologie :*	Kalkstein
Durchmesser [mm]:	51,3		
Gewicht [g]:	482,1		

Versuchsanordnung: Einaxialer Druckversuch

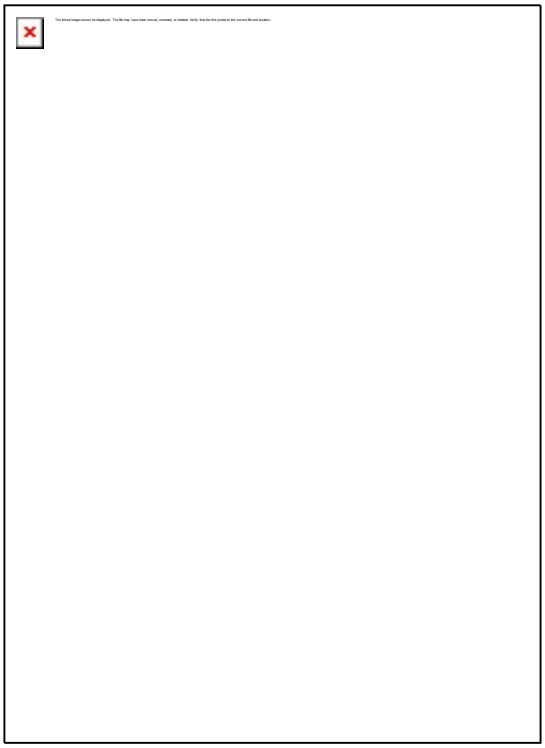

Abbildungen: Probe vor Versuch in Richtung A bzw. B

Gruppe **G**eotechnik **G**raz
TU-Graz
Labor für Felsmechanik und Tunnelbau

Rechbauerstraße 12, A-8010 Graz
Tel: ++43-316/873-8114
Fax: ++43-316/873-8618
e-mail: tunnel@tugraz.at

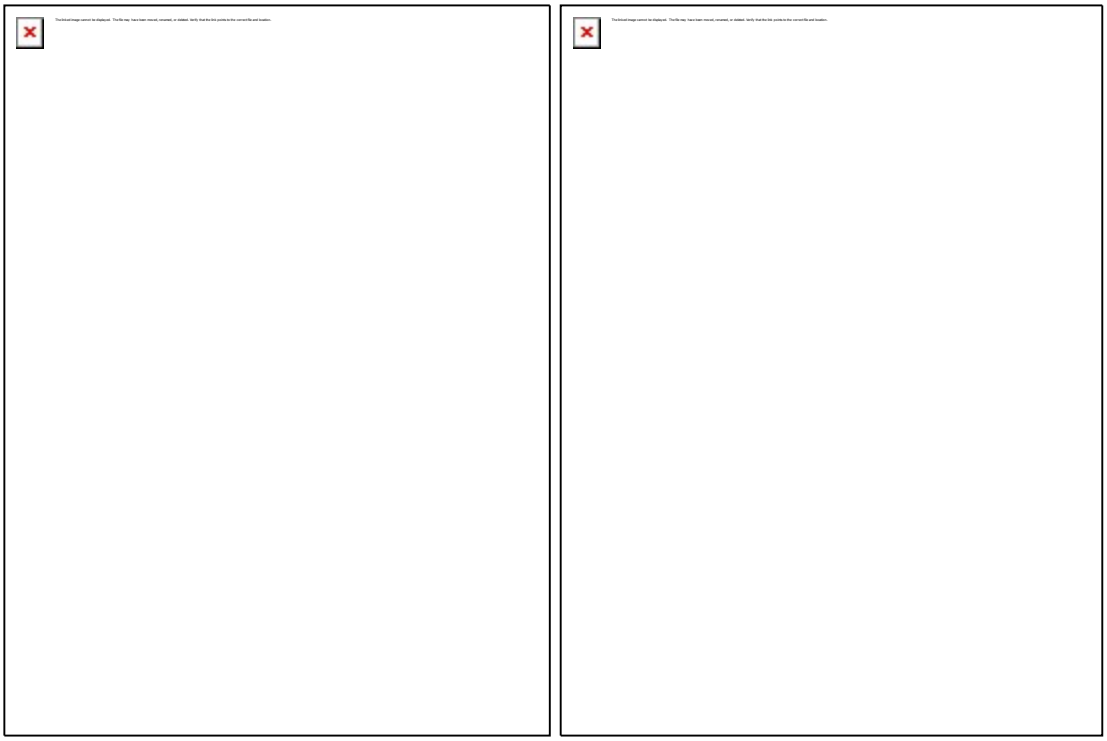

Abbildungen: Probe nach Versuch in Richtung A bzw. B

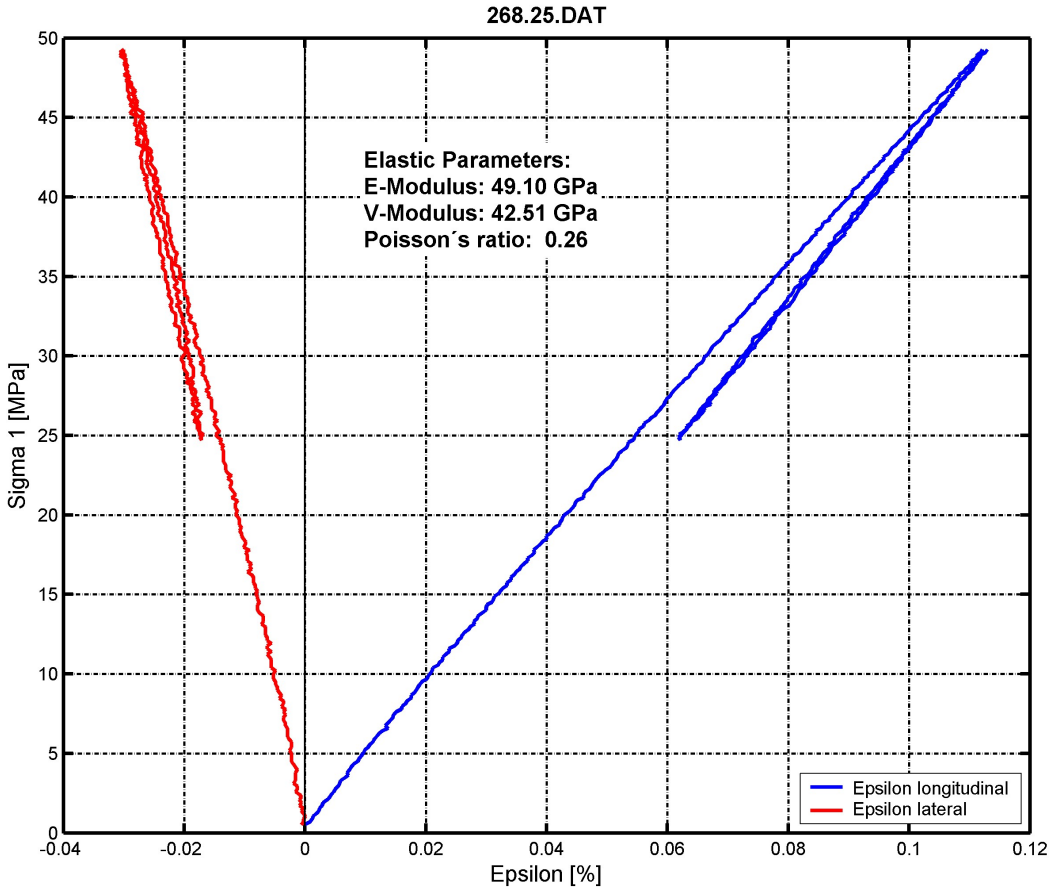

Gruppe **G**eotechnik **G**raz
TU-Graz
Labor für Felsmechanik und Tunnelbau

Rechbauerstraße 12, A-8010 Graz
Tel: ++43-316/873-8114
Fax: ++43-316/873-8618
e-mail: tunnel@tugraz.at

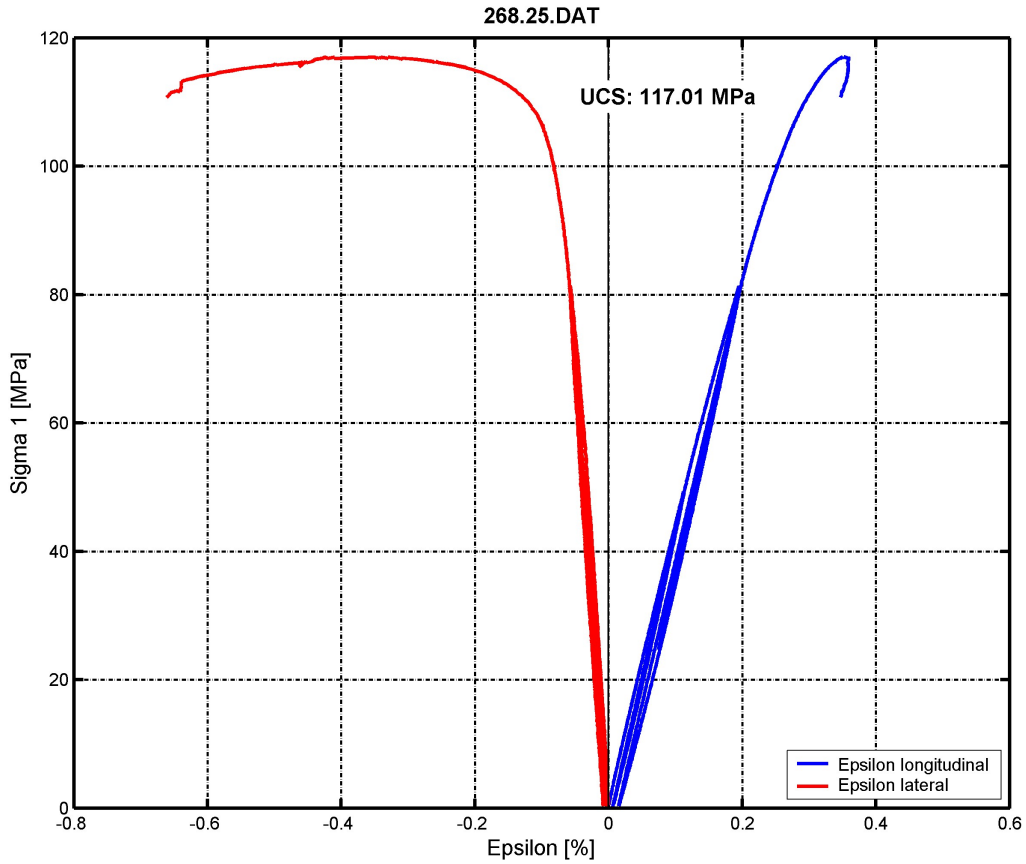

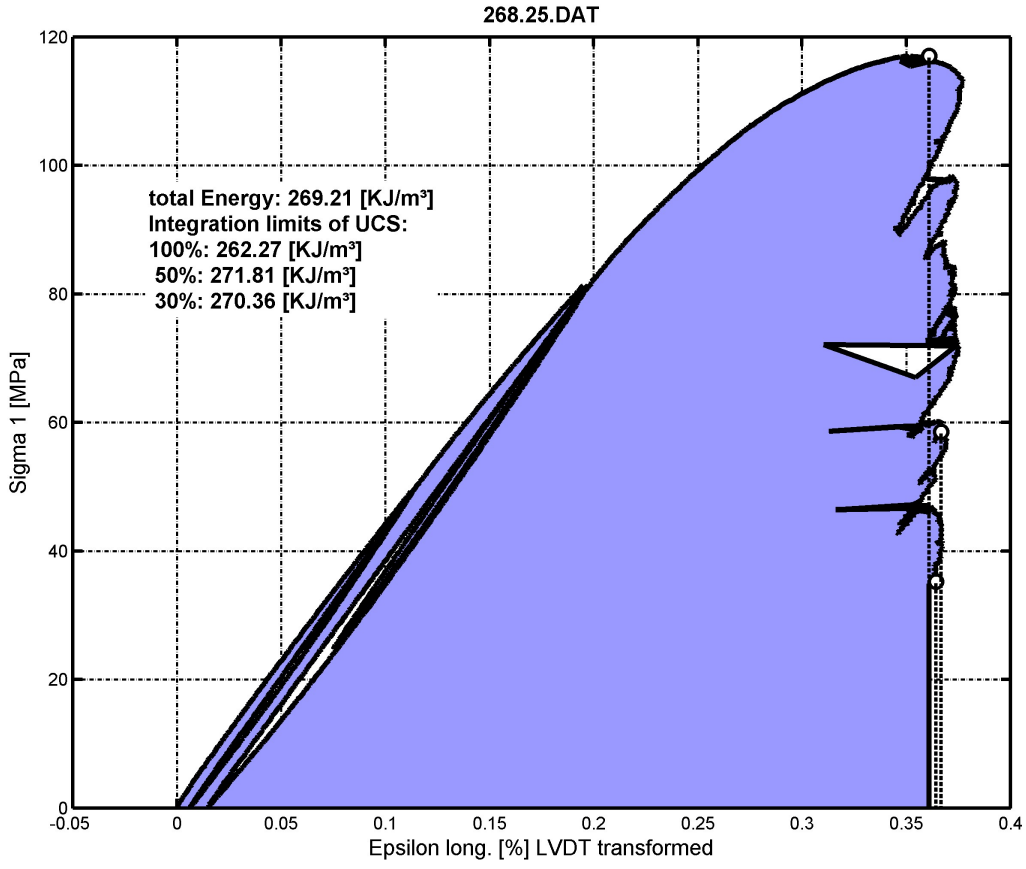

Gruppe **G**eotechnik **G**raz
TU-Graz
Labor für Felsmechanik und Tunnelbau

Rechbauerstraße 12, A-8010 Graz
Tel: ++43-316/873-8114
Fax: ++43-316/873-8618
e-mail: tunnel@tugraz.at

Projekt: Versuche Angelika Überwimmer *GZ:* 95268

Auftraggeber: Institut für Felsmechanik

Labornr.:	268.26	*Dichte [kg/dm³]:*	3,090
Länge [mm]:	102,7	*Lithologie :*	Plutonit
Durchmesser [mm]:	51,3		
Gewicht [g]:	655,9		

Versuchsanordnung: Einaxialer Druckversuch

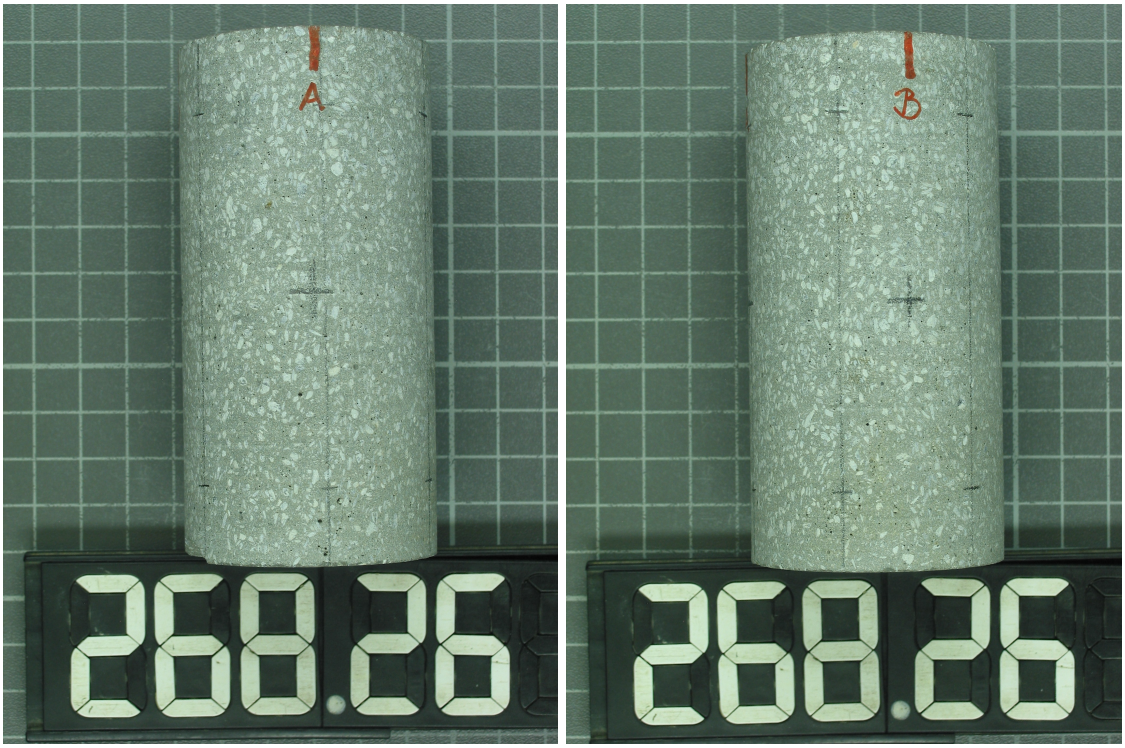

Abbildungen: Probe vor Versuch in Richtung A bzw. B

Gruppe **G**eotechnik **G**raz
TU-Graz
Labor für Felsmechanik und Tunnelbau

Rechbauerstraße 12, A-8010 Graz
Tel: ++43-316/873-8114
Fax: ++43-316/873-8618
e-mail: tunnel@tugraz.at

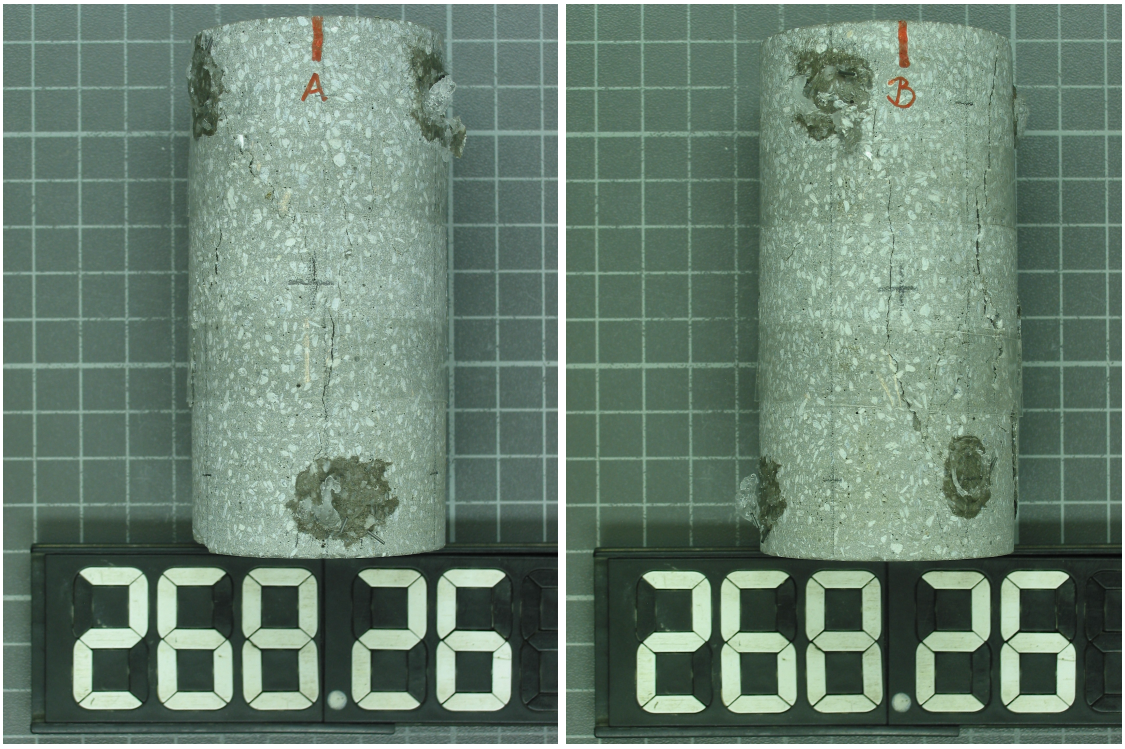

Abbildungen: Probe nach Versuch in Richtung A bzw. B

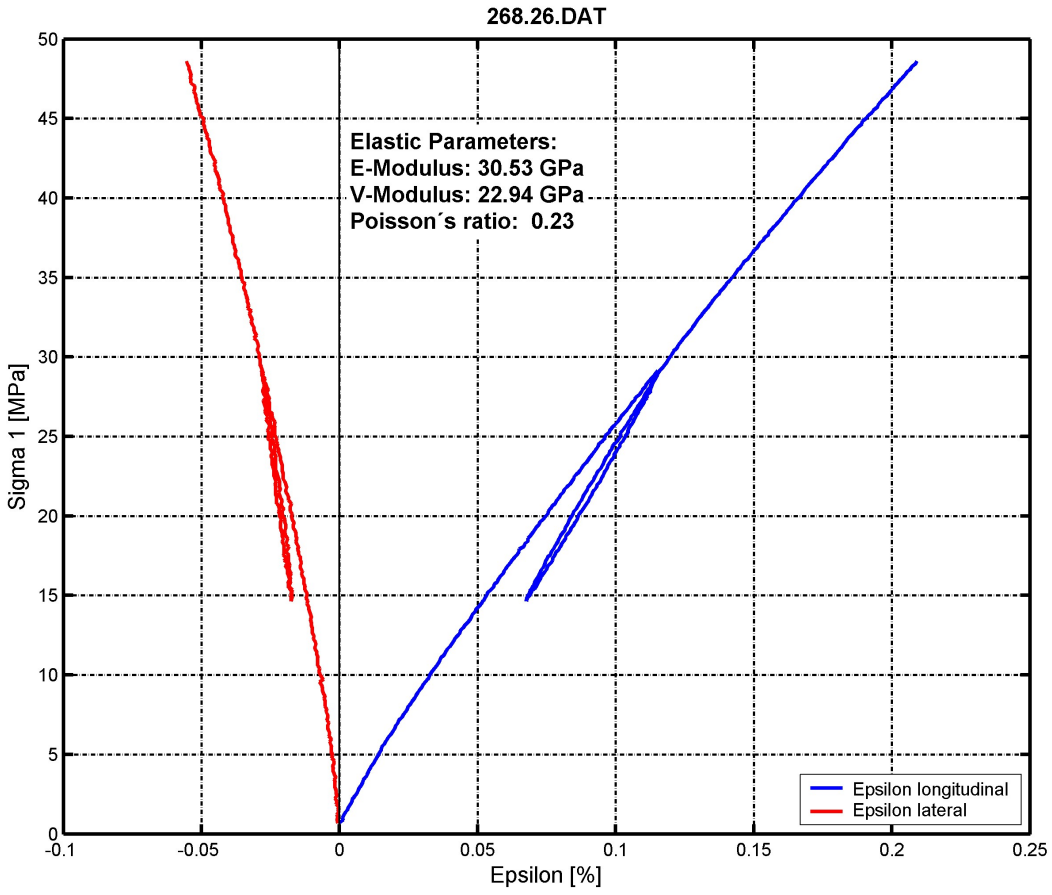

Gruppe **G**eotechnik **G**raz
TU-Graz
Labor für Felsmechanik und Tunnelbau

Rechbauerstraße 12, A-8010 Graz
Tel: ++43-316/873-8114
Fax: ++43-316/873-8618
e-mail: tunnel@tugraz.at

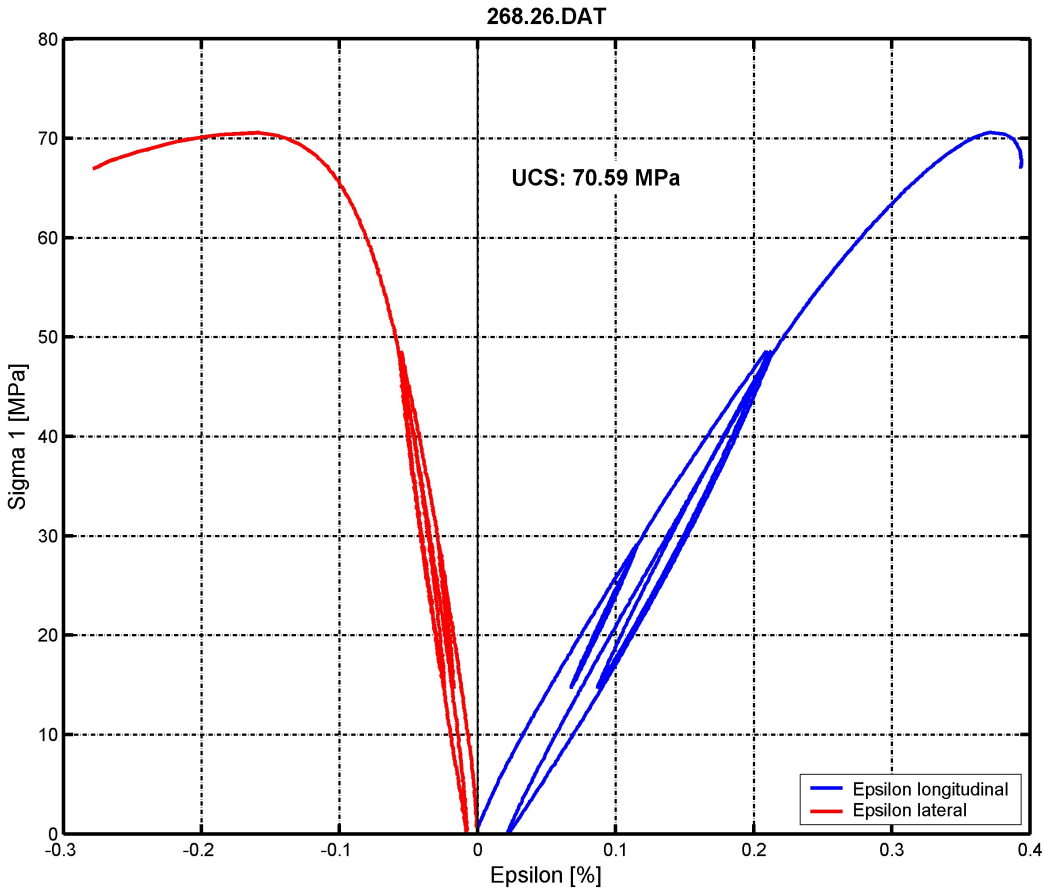

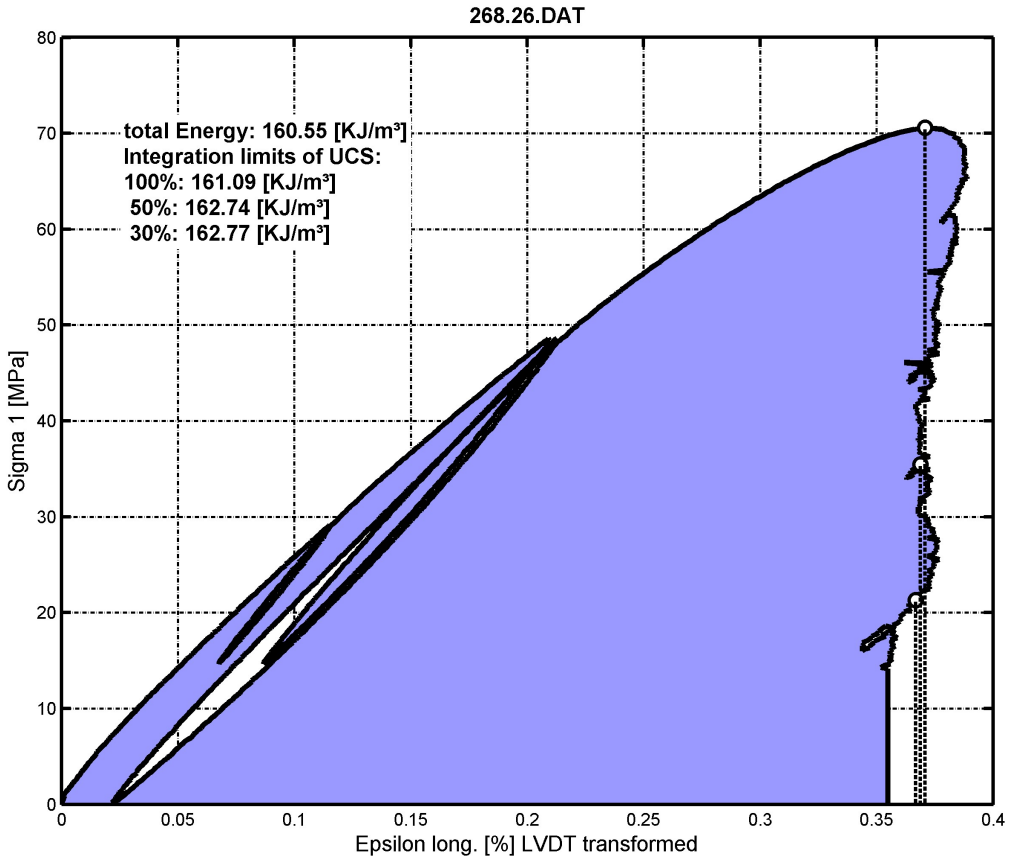

Gruppe **G**eotechnik **G**raz
TU-Graz
Labor für Felsmechanik und Tunnelbau

Rechbauerstraße 12, A-8010 Graz
Tel: ++43-316/873-8114
Fax: ++43-316/873-8618
e-mail: tunnel@tugraz.at

Projekt: Versuche Angelika Überwimmer *GZ:* 95268

Auftraggeber: Institut für Felsmechanik

Labornr.:	268.27	*Dichte [kg/dm³]:*	3,090
Länge [mm]:	102,8	*Lithologie :*	Plutonit
Durchmesser [mm]:	51,3		
Gewicht [g]:	656,6		

Versuchsanordnung: Einaxialer Druckversuch

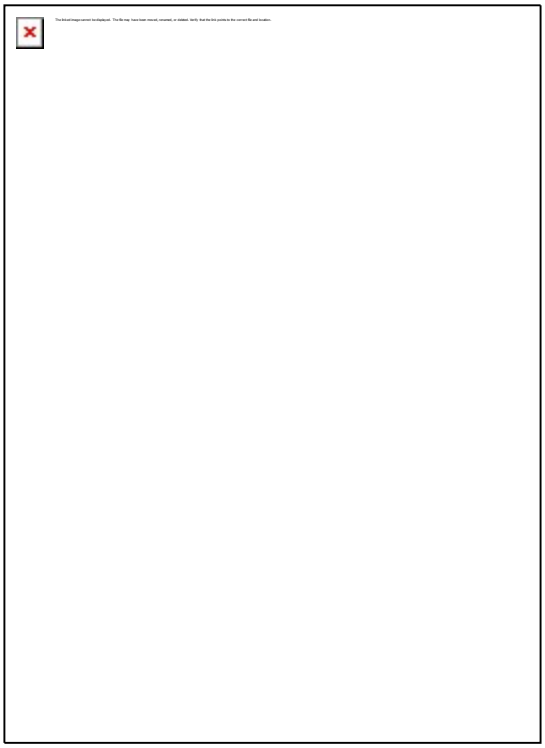

Abbildungen: Probe vor Versuch in Richtung A bzw. B

Gruppe **G**eotechnik **G**raz
TU-Graz
Labor für Felsmechanik und Tunnelbau

Rechbauerstraße 12, A-8010 Graz
Tel: ++43-316/873-8114
Fax: ++43-316/873-8618
e-mail: tunnel@tugraz.at

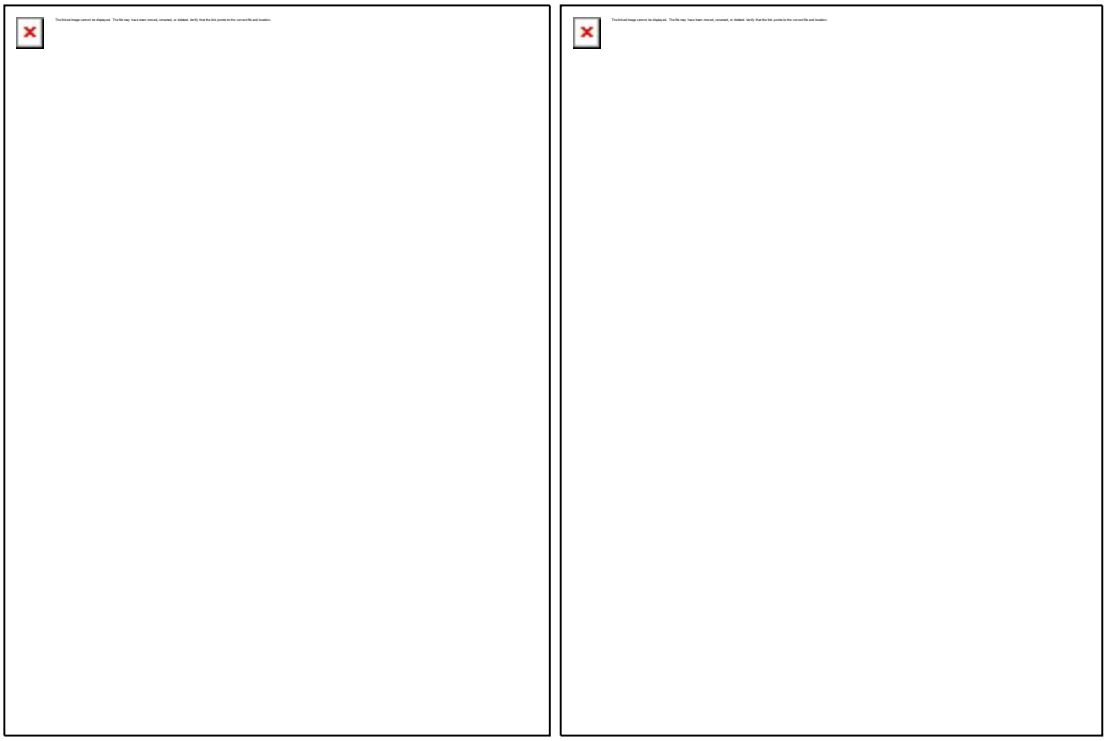

Abbildungen: Probe nach Versuch in Richtung A bzw. B

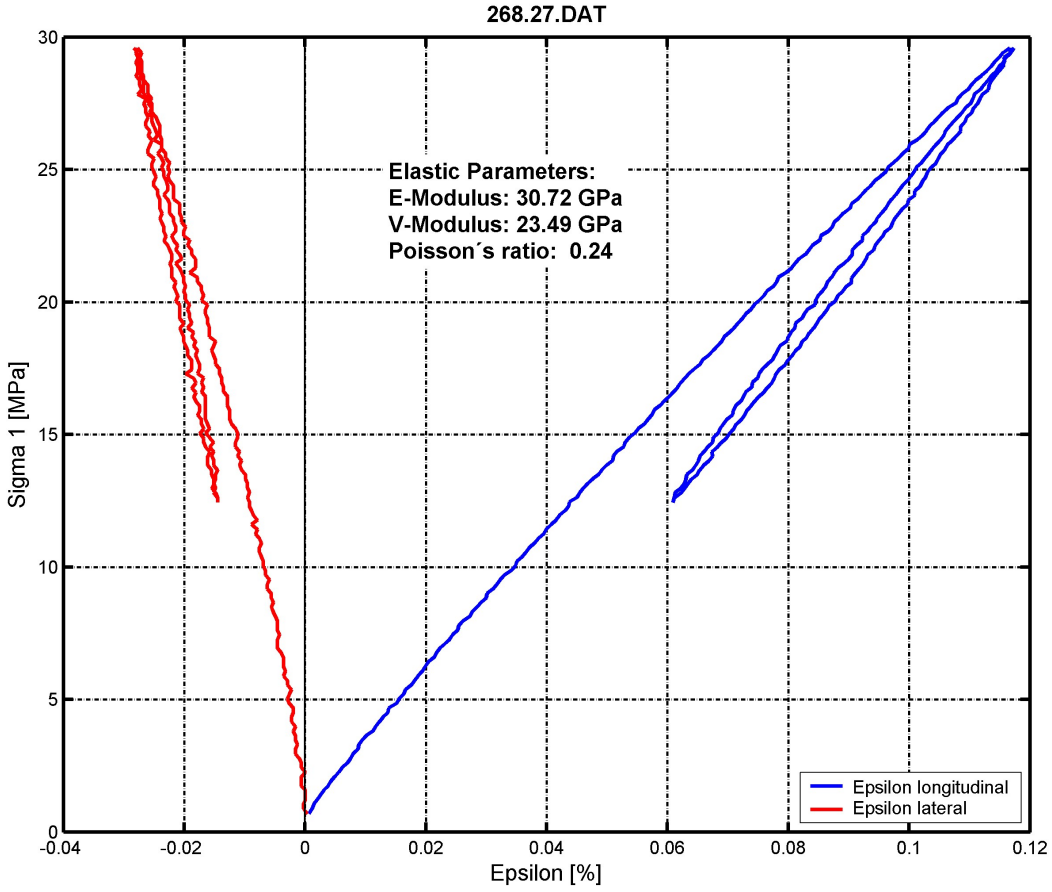

Gruppe Geotechnik Graz
TU-Graz
Labor für Felsmechanik und Tunnelbau

Rechbauerstraße 12, A-8010 Graz
Tel: ++43-316/873-8114
Fax: ++43-316/873-8618
e-mail: tunnel@tugraz.at

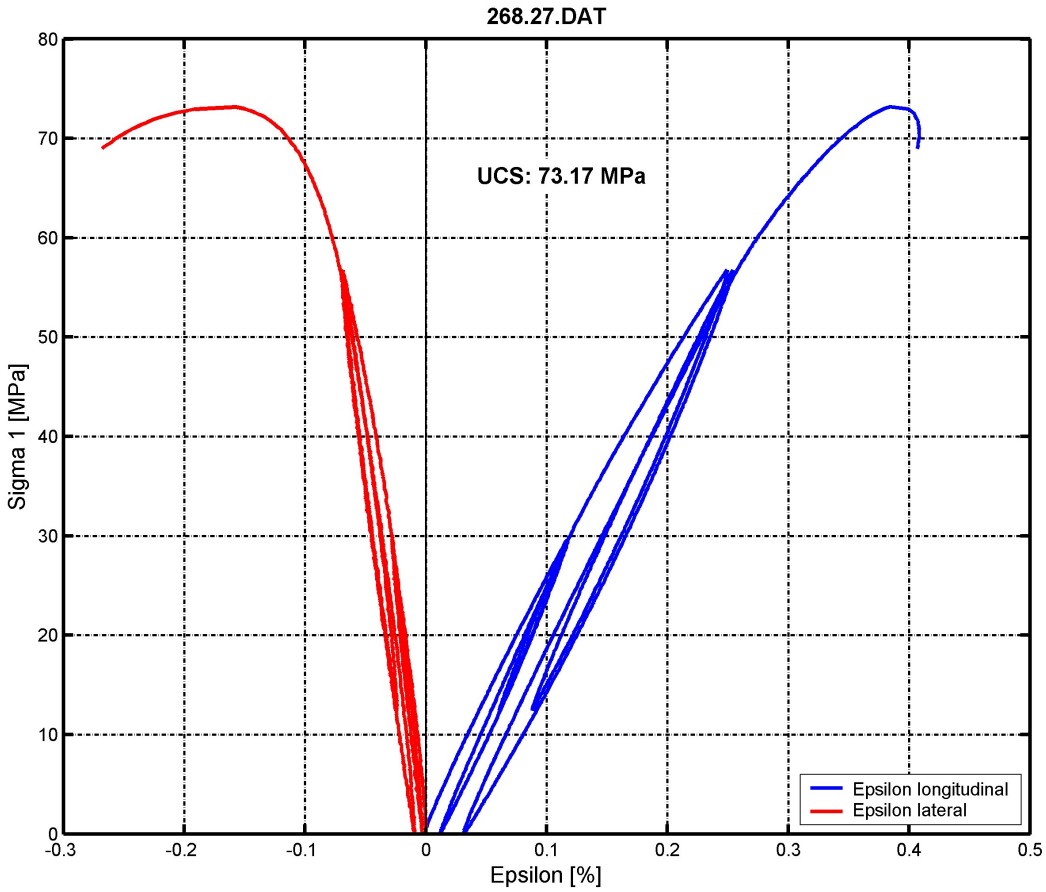

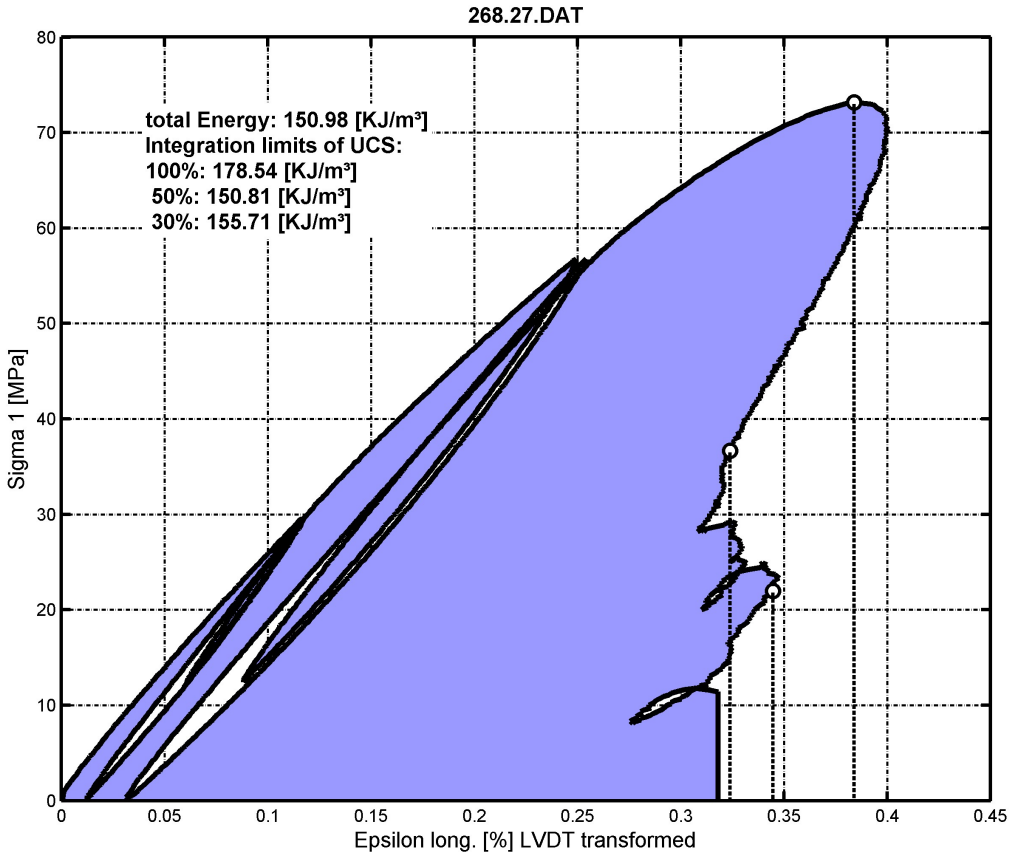

Gruppe **G**eotechnik **G**raz
TU-Graz
Labor für Felsmechanik und Tunnelbau

Rechbauerstraße 12, A-8010 Graz
Tel: ++43-316/873-8114
Fax: ++43-316/873-8618
e-mail: tunnel@tugraz.at